Seismic Attributes for Carbonates

Master thesis

Connie Lokøy Christiansen

Department of Earth Science

University of Bergen

Bergen, 2009

Abstract

Seismic attributes can reveal important information about rock properties, and rock physics modeling provide a link between geological and seismic parameters.

Carbonate rocks can have wide variations in properties due to their origin and susceptibility to post-depositional diagenetic processes. Thus, quantification of factors influencing seismic properties is important for seismic inversion. Porosity, pore shapes, depth and pressure, mineralogy, and fluid saturation are important factors affecting carbonate rock properties. Rock physics modeling can be used as a tool to study the seismic effects of such factors.

By exploring seismic velocities and amplitude versus offset (AVO) responses, in addition to utilizing rock physics templates (RTP) as an analytical tool, trends for different rock property factors have been observed for a synthetic carbonate model. Porosity and pore-shapes is observed to have a major importance for effective seismic responses, while mineralogy is less determent. Due to the fact that rocks with different properties may have similar seismic velocities, or comparable AVO responses, differentiation and quantification of various property-affecting factors is essential for inversion purposes. Comparison of responses viewed by different analytical methods enhances such differentiation and quantification.

The importance of evaluating AVO responses in accordance with background trend is demonstrated, and AVO analysis can serve as an important method for fluid detection.

Acknowledgements

I would like to thank my supervisor Tor Arne Johansen for guidance during the course of thesis. My co-supervisor Ivar Breivik is thanked for reading through parts of the thesis.

I would also like to thank Morten Jakobsen for his help to construct some programs in Matlab.

My fellow students are also thanked for ideas concerning different issues.

Finally, my gratitude is also given to my boyfriend, Jørgen, for enduring and supporting me the last hectic weeks of the project.

Connie Lokøy Christiansen
02. June 2009

Contents

Chapter 1: Introduction

1.1 Aim of Study

Seismic attributes can be defined as all information possible to directly or indirectly extract from seismic data, like P- and S-wave velocities and ratio between these, density, elastic moduli, and amplitude versus offset (AVO) responses. The scope of this project is to explore possible links between carbonate rock properties and seismic responses with the aid of rock physics modeling. Due to carbonates complexity, seismic responses from these rocks can have wide ranges in magnitudes. This project is aiming to reveal seismic trends for variations in different rock parameters, and to attempt to establish possible approaches on how to differentiate between seismic responses of various variables. Exploring fluid effects compared with effects of other factors on seismic responses from a carbonate-carbonate boundary is of particular interest.

Some important questions which serve as a basis for this study are:

- Is it possible to predict given rock properties from seismic responses?
- Can any attributes serve as indicators of certain properties?
- Can effects of different parameters be discriminated?
- Can saturating fluids be discriminated?
- Can other parameters inhibit fluid effects?

Carbonates are generally known to be more complex rocks than sandstones, which may complicate seismic modeling and seismic inversion for the properties of these rocks. Pore shapes are of major importance for seismic properties (e.g., Anselmetti and Eberli, 1993, 1997; Eberli et al., 2003; Wang 1997), and for carbonates there is a range of possible pore types. In addition to pore shapes, other intrinsic parameters like porosity, mineralogy, and fluid saturation, and extrinsic parameters like depth and pressure, can affect seismic properties for carbonate rocks. These parameters will be examined in this project. In addition to investigating seismic velocities and amplitude versus offset (AVO) responses, rock physics templates (RTP) will be used as a tool for investigation.

A synthetic carbonate model will be defined as input for the study, based on real measured rock properties. The model consists of different geologic facies representing different depositional environments. Variations of parameters will be studied in each facies. In addition 1D AVO studies will be carried out for two wells in the model. The construction and visualization of such a model, rather than simply defining rock properties in a more theoretical way, serves as a link between geology and geophysics by providing a geologic point of view concerning the different facies. Establishment of an understanding of the relations and origin of the facies, and of the geometry and structures to a geologic model as result of deposition environments and processes, is important when investigating relations between seismic and geological factors.

Many of the current seismic interpretation methods are originally developed for sandstones and shales, and may thus be less appropriate for carbonates, due to their complexities. For example, AVO analysis is often mentioned as a method to detect gas-sands (e.g., Box and Doss, 2008; Castagna and Swan, 1997). Thus, it is essential to evaluate such methods reliability and benefits for carbonate rocks.

Contents of the thesis

As an introduction to the world of carbonates, carbonate sediments and rocks will be described from a geological point of view in chapter 2, to obtain an understanding of these rocks' petrophysical properties in light of formation processes and environments, and post-depositional property-affecting processes. The important contribution from this chapter is to present an overlook on the variations which can differentiate one carbonate from another, and on the reasons for these variations. It is important to understand the link between geology and geophysics in order to fully understand geophysical responses, and to be able to predict such responses based on geologic knowledge.

Next a geophysical characterization is presented in chapter 3. To connect geologic and geophysical parameters, rock physics theories are needed. Some commonly used rock physics models, which will be used for later calculations, will be looked into and discussed, before values and ranges for some geophysical parameters, like seismic velocities, will be presented. Common variations in seismic rock properties due to geological and petrophysical variations will be mentioned.

Some basic seismic principles of relevance for the modeling are presented in

chapter 4. The topics are rock physics templates, amplitude versus offset analysis, and seismic resolution.

When an understanding of the link between geology and geophysics is established, a synthetic geological model can be created (chapter 5), with the purpose of exploring seismic effects of variations of rock properties (chapter 6).

Results will be discussed in chapter 7, and the main conclusions will be presented in chapter 8.

1.2 Calculations Prior to Modeling

Input values for modeling have been collected from two different sources of measurements (Soltveit (2007) and Fischer et al. (1996)), and consists of P- and S-wave velocities, densities, and porosities for different facies. The values assigned to facies 1, 3, and 5, are from saturated measurements, while values assigned for facies 2 and 4, are dry values. Thus, to calculate values not measured, two different approaches have to be used for saturated and dry facies.

For all facies, matrix properties have to be estimated, and in addition a saturation fluid is to be defined. Dry and saturated elastic moduli and densities have to be calculated from these parameters and the measured ones, to be able to calculate velocities and densities for all the facies for different saturation fluids, and for variation of different parameters like porosity or mineral composition.

Different approaches can be used for the calculations. Kumar and Han (2005) suggests that since the differential effective medium (DEM) approach (c.f. chapter 3) is asymmetric when calculating elastic moduli for saturated rocks (gives different results when starting with a solid matrix, and adding fluid inclusions, than when starting with a liquid matrix, adding solid inclusions, and when including larger pores first and then smaller ones, rather than staring with smaller pores and gradually including larger ones), this approach should be used for calculating dry moduli, while Gassmann (c.f. chapter 3) can be applied to calculate saturated moduli. However, this method is not straightforward to use for the calculations required in this project, since for the dry measurements, it is not needed since moduli can be calculated directly from the velocities and densities, and for the saturated measurements, if using the DEM approach to find dry moduli corresponding to the measured saturated values, the

asymmetry will be incorporated calculating the dry moduli. Thus, it seems more appropriate to use either the Gassmann or the DEM approach for calculations for all facies. Four methods for calculations of parameters necessary for modeling are described below; DEM approach for saturated and for dry measurements; and Gassmann approach for saturated and for dry measurements. The measured data for both dry and saturated measurements are P- and S-wave velocities, density, and porosity for each facies.

1.2.1 DEM – saturated input measurements

- Assuming a saturation fluid: Temperature and pore-pressure, in addition to salinity for fluids, and specific gravity for gas and oil, are required for calculation of bulk modulus and density of fluids (shear modulus is zero for fluids). General temperature and pore-pressure gradients for depth can be found in literature, and values for these and for salinity and specific gravity are chosen by assumptions. Assumptions have also been made for the volume fractions of gas and brine in the saturation fluid, and effective bulk moduli have been calculated using the Reuss equation (c.f. chapter 3).
- Knowing the saturated bulk rock measured density ρ_{eff}, the fluid density ρ_f, and the porosity φ, the matrix density ρ_m, can be calculated:

$$\rho_m = \frac{\rho_{eff} - \rho_f \varphi}{1 - \varphi} \ . \tag{1.1}$$

- Assumptions can be made about the matrix minerals according to this matrix density. A mineral composition giving this value (ρ_m) is chosen. Voigt-Reuss-Hill average (c.f. chapter 3) is used for calculations of effective composite matrix moduli.
- From the measurements of velocities (V_s, V_p) and density for given facies, shear and bulk moduli (μ and K, respectively) can be calculated directly:

$$\mu = V_s^2 \rho \ \ and \ \ K = \rho \left(V_p^2 + \frac{4}{3} V_s^2 \right) \ . \tag{1.2}$$

- Next step is to find a pore model (a set of aspect ratios) fitting the elastic moduli. Different models have been tested to find a model giving the same velocities and moduli as measured and calculated ones. The pore model giving the closest values to measured velocities and calculated moduli is chosen, and these velocities and elastic moduli are the ones used in the modeling rather than the original ones (the difference is minimal), to ensure most exact results.

For one of the initially saturated facies V_s is not given. This value has thus been calculated using a general equation relating V_s and V_p for limestones (Dvorkin, 2008), where velocity is in kilometers per second:

$$V_s = -0.055V_p^2 + 1.017V_p - 1.031\,. \tag{1.3}$$

1.2.2 DEM – dry input measurements

- For the dry measurements, the matrix composition is known from thin section analysis (c.f. Soltveit, 2007).
- Measured porosity and dry density (ρ_d) values have been modified slightly to fit the matrix density due to the formula:

$$\rho_d = \rho_m(1-\varphi)\,. \tag{1.4}$$

- The reason for this misfit between the measured values and observations from thin-sections is due to uncertainties in the measurements. If rather the matrix composition were to be modified, the fractions of the minerals would have to change significantly compared to the observed fractions. Thus the density and porosity of have been modified, since these modifications are minor.
- Elastic moduli for the dry rock are calculated directly from the velocities and densities.
- The pore model giving the velocities and elastic moduli closest to the measured ones is chosen for the given facies.
- Saturated values are then calculated by saturating the rocks with the same fluid as used for calculations for the saturated measurements.

When, after these steps, values for matrix, saturating fluid, and pore forms have been determined, all parameters needed for further calculations are collected, and variations of properties like saturation fluid, porosity, pore-shapes, or mineral composition, may be performed to evaluate the seismic effects of such variations.

In addition to these DEM calculations, the Gassmann equations have also been used, to compare the results from these two methods (chapter 5). Gassmann is used for fluid substitution purposes, and for the comparison the facies have been saturated with various fluids.

1.2.3 Gassmann – Saturated and dry input measurements

- The dry moduli are calculated from the saturated measurements using the Gassmann equations (equations 3.29 and 3.30). The shear module is the same for dry and saturated samples in this approach.
- The calculated and measured dry moduli are used in another Gassmann equation (equation 3.28, chapter 3) to find the moduli of the rocks when saturated with different fluid.

Basic theory and formulas of the Gassmann and DEM approaches, and seismic velocities, as well as discussion of pore forms can be found in chapter 3. All measured, calculated, and estimated initial values used for modeling are listed in chapter 5, and all original measurements are listed in Appendix.

Figure 1.1 illustrates the steps in building a rock model performed in this study.

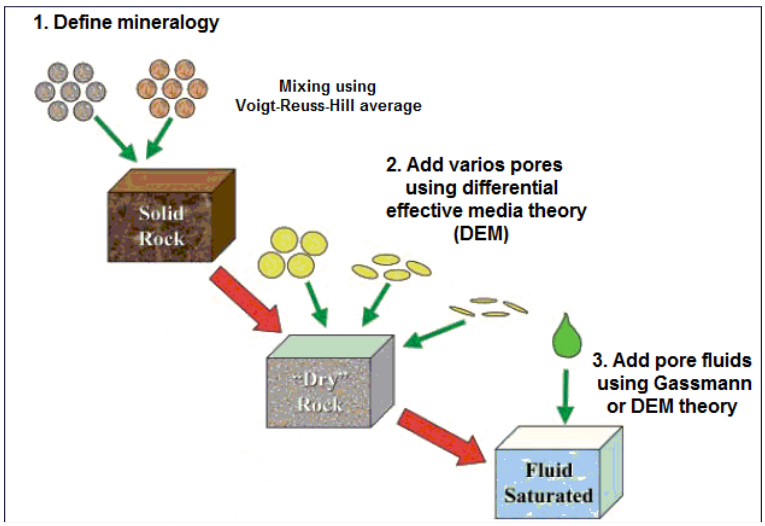

Figure 1.1 *Different steps for the building of a rock model. Modified from Shiyu and Pain (2009).*

1.2.4 Programs used for calculations, modeling and visualization

Calculations of rock properties for this study have mostly been performed in VelRock, which is a software from the NORSAR 2D and 3D seismic ray modeling package, while Gassmann calculations have been performed using Matlab software, which is a technical computing language for calculations and data visualization.

Fluid properties for various temperatures and pressures have been calculated in VelRock. Reuss average (c.f. chapter 3) has been aplied for fluid mixing, while matrix properties have been calculated according to Voigt-Reuss-Hill average in VelRock. Isotropic and homogenous rock properties are assumed.

AVO results have been created in the software Hampson-Russell from CGGVeritas, which uses ray-tracing to calculate the incidence angles, and the Zoeppritz equations (Appendix) to calculate the amplitudes. The Zoeppritz equations give angle-dependent reflection and transmission coefficients for elastic plane waves at a non-slip horizontal boundary between two semi-infinite isotropic elastic media. Only primary reflection events have been modeled.

Cross-plots of reflection coefficients versus offset are performed in the CREWES Zoeppritz explorer applet (version 2.0) from CREWES (Consortium for Research in Elastic Wave Exploration Seismology) available from internet.

All other plots are made in Matlab and in Microsoft Excel.

Chapter 2: Geology of Carbonates

Carbonates, in contrast to silisiclastic rocks, are formed mostly in situ by point sedimentation, rather than being composed of sediments transported by rivers and other transport mechanisms. These sediments are formed by geochemical or organic processes, and have higher variability in texture than silisiclastic rocks. Over 50 percent of all discovered petroleum reserves are located in carbonate reservoirs, and carbonates may also form seals or source rocks.

Much can be said about carbonate sediments and rocks, entire books are written about them, and there is increasingly ongoing research concerning rock physics modeling and seismic imaging of these rocks. In this chapter there will rather be given an introduction on these sediments and rocks, with the aim of describing the variety in textures and properties, and the reasons for these, with emphasis on reservoir properties. The most important aspects to look into to get a geological understanding of these rocks are their formation processes and environments, composition and classification, and diagenetic alteration of initial rock properties. These aspects are presented below. In addition a characterization of pore-types is given in the end, due to pore-types importance for seismic properties (will be described in chapter 3).

2.1 Formation and Depositional Environments

2.1.1 Formation of carbonate sediments

There are two ways in which carbonate sediments form. Carbonate can precipitate directly from seawater, or accumulate from skeletal debris from organisms (in situ processes). This means that these sediments can form by chemical or biological processes, and the formation thus depends on the type and amount of organisms in the sea, and the chemical composition of the water. In addition the waters temperature and pressure (depth dependent) are contributing factors.

The biogenic parts of carbonate rocks are composed of skeletal remains of different organisms. When these get buried and compacted and lithifies, they make up carbonate rocks. The texture of such carbonate rocks thus to some degree depends on

the shapes of the skeletal parts from the organisms, although it will be altered by compaction, dissolution, cementation and other diagenetic processes (described in section 2.3). Texture is a term covering the size, shape, and arrangement of grains and particles in a rock. The different shapes and sizes of the skeletal debris also give rise to the range of different pore types in carbonates, which is characteristic for these rocks (sandstones have less variation in pore shapes), and which is a major topic for research concerning elastic moduli and velocities for carbonate rocks.

Inorganic or chemical precipitation of calcium carbonate directly from seawater demands clear, warm, and shallow water. This can be explained by the fact that $CaCO_3$ precipitates in warm water and under low pressures, hence in shallow water, while it is highly soluble in cool water and under high pressures. If the water is muddy in contrast to clear, the carbonate sediments will be diluted, and it will inhibit the photosynthetic processes because of the limited amount of penetrating sunlight. It is true that the calcite and aragonite shells precipitated by invertebrates are thicker in clear warm waters. In addition, many more calcareous algae thrive there, and reef-building corals are restricted to such environments (Wilson, 1975).

Evaporation concentrates sea waters in environments with limited amounts of water and influx, like lagoons, and this process force precipitation of calcium carbonate if the concentration in the water gets high enough.

2.1.2 Depositional environments and facies

Carbonate sediments are not uniformly distributed in the oceans. The distribution is a factor of the sediment supply rate and the preservation potential. Sediment supply rate are mostly controlled by the productivity of the organisms in the photic zone which produce $CaCO_3$. The photic zone is the zone where the influx of sun light allows photosynthesis to occur, and since algae are organisms which perform photosynthesis, they only live in this zone, as do organisms feeding on algae. The photic zone are generally defined to be less than 10-15 m, since algal growth (codiaceans and blue green algae) is most abundant over this depth, even though the total depth range of tropical marine algae is down to 100 m or more (Wilson, 1975).

Climate (temperature and salinity), sea level and geotectonics are controlling factors on carbonate sedimentation. As mentioned in the preceding subchapter, temperature controls the inorganic precipitation of calcium carbonate from seawater. Ooids and aggregates needs average temperatures higher than 18°C to form. Organic

precipitation does also depend on temperatures. Coral reefs are restricted to form in areas where the surface temperature of the water is above 15°C, and in addition they only tolerate salinities between 32-40 ‰ (Tucker and Wright, 1990). Other organisms secreting calcium carbonate are also temperature and salinity dependent, but not all of them needs high temperatures, molluscs and calcareous red algae can exist in high latitudes where the water temperature are low.

The presence of carbon dioxide (CO_2) in water affects the $CaCO_3$ accumulation through the following equilibrium process:

$$CaCO_3\ (solid) + CO_2\ (gas) + H_2O \leftrightarrow Ca^{2+}\ (aqueous) + 2HCO^{3-}\ (aqueous).$$

This means that in waters containing much CO_2, $CaCO_3$ will be dissolved, while removing the CO_2 content from the water will make $CaCO_3$ precipitation preferable. Photosynthesis is a CO_2-removing process.

Sea level stand is an important factor for carbonate sedimentation, since thicker and more widespread sequences are being deposited when the sea level is high.

Geotectonics is important because it determines the depositional setting, and thereby also the water depth, which is important both for production and preservation of carbonate sediments. Together with climate it also determines water currents, which can bring nutrient to living organisms, and adjust the water temperature and salinity.

In the literature, carbonate facies are generally divided into nine basic facies belts, which are independent of geologic time and setting. Facies can be defined as laterally equivalent bodies of sediments of a given depositional setting, with distinctive characteristics (Boggs Jr., 2006), or more detailed as “particular sets of sediment attributes: characteristic lithologies, textures, suites of sedimentary structures, fossil content, color, etc.” (Tucker and Wright, 1990).

What are most interesting from this facies description, when evaluating reservoir potential, are what kinds of rocks that will form, and their porosity and permeability. Organic content is important when estimating the source rock potential. These factors will therefore be the main focus in the following description of the basic carbonate facies, which are based on descriptions by Wilson (1975), Schlager (1992), and Wilson (1997), and are grouped into different parts of a profile across a model of a gently sloping shelf atop a platform with an abrupt shelf margin (Figure 2.1):

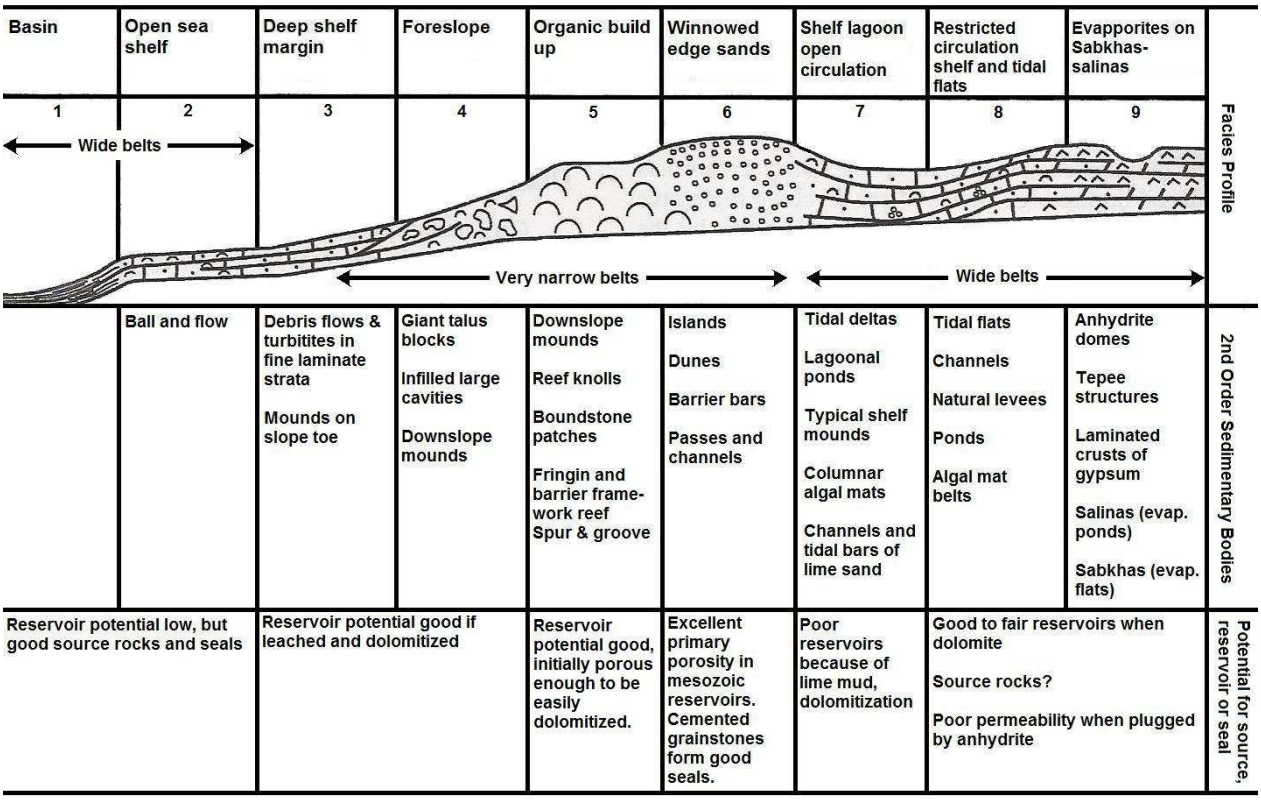

Figure 2.1 *Descriptive synopsis of idealized facies belts of a rimmed platform. Modified from Wilson (1975) and Wilson (1997).*

1. Basin facies (starved or filled basin)

This setting is below the wave base, and below the photic zone, so that no benthonic production of carbonates occurs. Sediments deposited in this zone can be all different types of deep-sea sediments, like pelagic clay, siliceous and carbonate ooze, and hemipelagic muds including turbidites. The biota in this zone is predominantly plankton, and rain of decaying plankton adds to the sediment deposits.

- *Dominating rock types:* Radiolarite, micrite, limestone, lime mudstone, grainstones, packstones, shale, or anhydrite.
- *Source rock potential:* Organic-rich black shaly lime mudstone may form in anoxic stagnant waters, and these are known to be petroleum source rocks (1-15 wt. % organic content).
- *Porosity:* Can be very dense, but can also make excellent reservoirs when they got some porosity and are overpressured, or if there is early oil migration, or fracturing, as in the Ekofisk Danian of the North Sea.

- *Permeability:* May be good if the rock is fractured or the porosity is high, but for shales or shaly lime mud, there is no permeability, which makes these rocks good seals.

2. Deep shelf facies

This setting is higher up in the profile than the first one, but is still below fair-weather wave base, although above storm wave base, and the water depth can be tens to a few hundred of meters. The zone is within or just below the photic zone, and the water is generally oxygenated, and of normal marine salinity. The current circulation is good. The biota consists of diverse shelly fauna, and minor plankton, and the sediments are mostly carbonate and marl, and some silica. They are well bioturbated and well bedded.

- *Dominating rock types:* Very fossiliferous limestone interbedded with marl.
- *Source rock potential:* May be good source rocks.
- *Porosity:* Generally low, but may be enhanced by dolomitization, leaching, or fracturing.
- *Permeability:* Generally low, but may be enhanced by same factors as porosity.

3. Basin margin or deep shelf margin facies

The setting of this facies belt is about the same as for facies group 2, with respect to depth, and wave base and oxygen level conditions. This zone is formed at the toe of the shelf slope, and the sediments are lime mud (somewhat siliceous), with intercalations of debris flows and turbidites. The biota consists of benthos and some plankton.

- *Dominating rock types:* Fine-grained limestone, which may be cherty.
- *Source rock potential:* May be layers of pelagic microorganisms and in situ buildups, but is not a general source rock producing facies.
- *Porosity:* May be porous if voids between clasts of debris flow and grain flow deposits are not fully cemented, or if preferential solution and dolomitization of the lower portions of slope deposits occur.
- *Permeability:* May have good permeability when porous.

4. Foreslope facies

This slope setting is strongly inclined, commonly as steep as 30°, and reaches from below to above fair-weather wave base. The water is oxygenated and the biota consists of benthos and some plankton. The sediments are unstable debris that varies greatly in size, and it is mostly pure carbonates, with a large amount of aragonite (unstable mineral).

- *Dominating rock types:* Variable types of limestone, lime muds and sands, boundstone, and sedimentary breccia.
- *Source rock potential:* Significant amounts of fossil debris, but is not a general source rock producing facies.
- *Porosity:* Already existing interparticle porosity may be enhanced by meteoric solution and dolomitization.
- *Permeability:* May be enhanced by meteoric solution and dolomitizaion.

5. Organic reef of platform margin

This setting is variable and depends among other things on the steepness of the slope, the wave energy and the organic productivity. Three different settings can be described; mounds of accumulated carbonate mud and organic debris; ramps of knoll reefs and skeletal debris; or reef rims. The biota consists of almost exclusively benthos, and the sediments are almost pure carbonate of very variable grain size.

- *Dominating rock types:* Massive limestone and dolomite, which in some places can consist solely of organism remains. Much bioclastic debris.
- *Source rock potential:* Not a general source rock producing facies.
- *Porosity:* May be very high or low. Reefs are initially porous, and may get their porosity enhanced in the meteoric regime since they commonly are composed of aragonite, and also by dolomitization. In addition they are prone to fracturing instead of taking stress along bedding planes like bedded rocks. In contrast the pore space also may fill with cement or lime mud and make the reef completely dense.
- *Permeability:* High when pores are not cemented.

6. Winnowed platform edge sands

The setting can be beaches, sand bars, elongate shoals, or dune islands, and this zone lies above the fair-weather wave base and within the photic zone, and is strongly influenced by tidal currents. Because of the shifting substrate there is little marine life in this zone, except from biota from reefs and associated environments. The sediments are clean lime sands, which may contain quartz occasionally.

- *Dominating rock types:* Cross-bedded calcareous or dolomitic lime sand.
- *Source rock potential:* Little organic production.
- *Porosity:* Great range of porosities depending on cementation in the different regimes. Initially porosity (~40%) may be enhanced or reduced.
- *Permeability:* Varies as the cementation varies, but may be significantly enhanced by dolomitization. May form good seals if cemented sufficiently.

7. Open marine platform facies

This setting is located behind the outer platform edge and it can include strait, lagoon, or bay environments. The water depth can reach up to a few tens of meters, but are normally shallow, and the salinity can be normal marine or variable. Biota in this zone is benthos, and the sediments can be lime mud or sand, and terrigenous sediments if the platform is attached to land.

- *Dominating rock types:* Variable limestones, and in cases lenses and thin beds of land-derived clastics.
- *Source rock potential:* Not a general source rock producing facies.
- *Porosity:* Generally low, but may be enhanced by dolomitization, leaching, or fracturing.
- *Permeability:* Generally low, but may be enhanced by the same factors as porosity.

8. Platform interior facies (restricted circulation)

The setting is closely the same as for facies 7, but it is less well connected with open sea, which may give great variations in salinity and temperature. The whole complex of tidal flat environment, channels, local beaches, cut-off ponds or lagoons can be present in this zone. The shallow-water biota that lives in this setting is reduced in diversity. Deposited sediments are mostly lime mud and muddy sand, and early

diagenetic cementation is common.

- *Dominating rock types:* Generally lime muddy sediment with much dolomite.
- *Source rock potential:* Not a general source rock producing facies.
- *Porosity:* May be high. A number of reservoirs are present in dolomitized cyclic tidal flat strata. Best dolomite reservoirs are found in strata that were originally of coarse textures, like channels, bars, beaches, and bays.
- *Permeability:* High in dolomitized strata, but lower in strata of finer grains, or where plugged by anhydrite.

9. Platform evaporite facies

The setting is the same as for facies 7 and 8 except that this environment has an arid climate, and only sporadic influx of marine waters. Sabkha, salinas and salt flats are typical features. This evaporitic setting gives rise to formation of gypsum and anhydrite, in addition to lime mud or dolomite mud. There is little biota in this zone.

- *Dominating rock types:* Nodular or wavy anhydrite, or gypsum interlaminated with dolomite. Commonly associated with redbeds.
- *Source rock potential:* Not a general source rock producing facies. Biota is essentially lacking.
- *Porosity:* Low. Generally no reservoirs exist in such sediments.
- *Permeability:* Low. When evaporites are well-developed, they form excellent seals.

2.1.3 Preservation of carbonate sediments

The degree of preservation are controlled by the waters chemistry, temperature, and pressure, and thereby depth, and the chemical composition of the sediments. The accumulation of carbonate rocks do also depend on the supply of terrigenous sediments, since a large volume of these will dilute the carbonate components. Carbonate sediments are generally restricted to warm shallow areas and are not found in deep ocean basins, since $CaCO_3$ are highly soluble in cool water and under high pressures, which are characteristic for the deep sea. The depth at which the carbonate skeletal dissolution starts is called the lysocline (Figure 2.2) (James, 2005). Below this depth the dissolution rate is increasing downwards. The depth at which the proportion of carbonate skeletal material is less than 20 % of the total sediment amount is called

the carbonate compensation depth (CCD) (Figure 2.2) (James, 2005). These two depths vary at different locations and are affected by temperature and the chemical composition of seawater. As mentioned, large amounts of CO_2 in waters will make $CaCO_3$ dissolve. The Pacific Ocean contains more CO_2 than the Atlantic due to thermohaline circulation patterns, and therefore has lower depths for both the lysocline and the CCD.

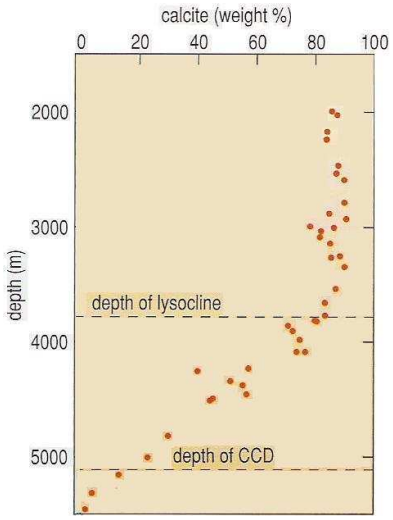

Figure 2.2 *Calcite content (in weight %) of depth-distributed modern sediment samples in the eastern equatorial Indian Ocean region. Depth of the lysocline occurs in the water column at a depth of 3800 m. Depth of the CCD occurs at approximately 5000 m water depth; below this depth, the percentage of calcite in the sediments is less than 20%. Modified from James (2005).*

Distribution of modern marine carbonate sediments in shallow water is showed in Figure 2.3, while Table 2.1 sums up the effects of water condition on $CaCO_3$ solubility and precipitation.

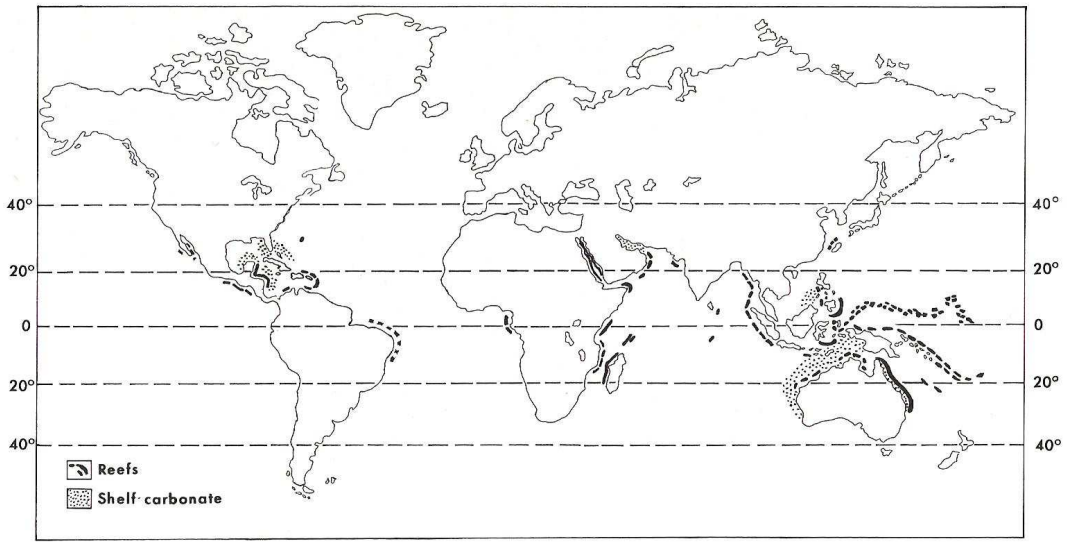

Figure 2.3 *Distribution of modern marine carbonate sediments in shallow water. From Wilson (1975).*

Table 2.1 *Principal factors that affect solubility and inorganic precipitation of $CaCO_3$ in seawater or freshwater.*

**Decrease in $CaCO_3$ solubility = increase in tendency to precipitate. From Boggs Jr. (2006).*

Water condition	Direction of change	Direct effect	Effect on $CaCO_3$ solubility	Kind of $CaCO_3$ precipitated
Temperature	Increase	Loss of CO_2, increase in pH	Decrease*	Micrite or ooids
Pressure	Decrease	Loss of CO_2, increase in pH	Decrease	Micrite or ooids
Salinity	Decrease	Decrease in activity of "foreign" cations	Decrease	Micrite or ooids

2.2 Composition and Classification

All carbonates are composed of the CO_3^{2-} anionic group. Combined with Ca^{2+} it forms $CaCO^3$, which can either be calcium carbonate (calcite) or aragonite. In the modern seas aragonite is the common mineral of these two, precipitating from the seawater and secreted by organisms, but calcium carbonate is the most chemically stable, so that aragonite sediments will over time convert to form calcium carbonate. In addition, some of the Ca^{2+} can be replaced by Mg^{2+}, which makes up high-magnesium calcite. If more than half of the calcium ions of the crystal lattice are replaced by magnesium ions the mineral is called dolomite. Dolomite may form by the chemical alteration of calcite. This mineral is common in many ancient rocks, even though they are uncommon in modern marine environments (Stanley, 2005).

As already stated, carbonate sediments can be chemically precipitated from seawater, or be formed by organisms. The biogenic parts of carbonate sediments are composed of skeletal remains of different organisms, mostly coccolithophores, foraminiferans and petropods. The hard skeletal parts of these vary in size, shape and chemical stability, and may therefore form carbonate rocks with different properties and preservation potentials (James, 2005). In addition the organisms producing calcium carbonate have been evolutionary varied throughout the geologic history (Phanerozoic).

The carbonate rocks that are built from these carbonate sediments are limestones and dolomites. Even though the mineral is called dolomite, many authors also use the same name for the rock consisting of this mineral, while others call it dolostone. Davies and Smith Jr. (2006) claims that "dolomite" in its original usage described the rock, not the mineral. Carbonate sediments can also be mixed with other

sediments and make other rock types, for instance with silisiclastic minerals, which can form chert.

The texture of dolomite is largely crystalline, while for limestone the calcite can be present in at least three distinct textural forms, which are carbonate grains (silt-size or larger aggregates of calcite crystals), microcrystalline calcite (extremely fine size crystals), or sparry calcite (coarser grained crystals) (Boggs Jr., 2006). Ooids and peloids are common carbonate grains. Ooids are formed in waters of high energy and high calcium bicarbonate saturation, where a shell fragment or some kind of grain gets coated by fine calcite or aragonite crystals. Their size can be up to 2 mm. Peloids are smaller (generally 0.03-0.1 mm), and are carbonate grains that are composed of microcrystalline or cryptocrystalline calcite or aragonite which do not have any distinctive internal structures (Boggs Jr., 2006). Peloids may form by organisms that ingest calcium carbonate muds and extrude undigested mud as pellets, or by micritization of small ooids or rounded skeletal fragments.

Many different classifications have been made for carbonate rocks, and they are usually based on the types of carbonate grains or allochems and the grain/micrite ratio. Allochems are defined by Folk (1959) as aggregate particles or grains that may have undergone mechanical transport before deposition, in contrast to normal chemical precipitates. Folk's (1959, 1962) classifications are of the most known ones (Table 2.2) and classifies carbonate rocks based on the relative amount of three major types of constituents, which are carbonate grains or allochems, micrite (microcrystalline carbonate mud), and sparry calcite cement. A schematic representation of the constituents that form the basis for Folk's classification in Table 2.2 is given in Figure 2.4, and a textural classification of carbonate sediments on the basis of relative abundance of lime mud matrix and sparry calcite cement and on the abundance and sorting of carbonate grains or allochems, are given in Figure 2.5.

Table 2.2 *Classification of carbonate rocks. After Folk (1962). Note: Names and symbols in the body of the table refer to limestones. If the rock contains more than 10 percent replacement dolomite, prefix the term "dolomitized" to the rock name. The upper name in each box refers to calcirudites (median allochems size larger than 1.0 mm); the lower name refers to all rocks with median allochems size smaller than 1.0 mm. Grain size and quantity of ooze matrix, cements, or terrigenous grains are ignored. *Designates rare rock types.*

					Limestones, partly dolomitized limestones						Replacement dolomites	
					>10% Allochems Allochemical rocks		<10% Allochems Microcrystalline rocks					
					Sparry calcite cement > micro-crystalline ooze matrix Sparry allo-chemical rocks	Microcrystalline ooze matrix > sparry calcite cement Microcrystalline allochemical rocks	1%-10% Allochems	<1% Allochems	Undis-turbed bioherm rocks	Allochem ghosts	No allochem ghosts
Volumetric allochem composition				>25% Intra-clasts	Intrasparrudite Intrasparite	Intramicrudite* Intramicrite*	Most abundant allochem	Intraclasts: intraclast-bearing micrite* Ooids: ooid-bearing micrite* Fossils: fossiliferous micrite Pellets: pelletiferous micrite	Micrite, if disturbed, dismicrite; if primary, dolomite, dolomicrite	Biolithite	Evident allochem	Finely crystalline intraclastic dolomite, etc. Coarsely crystal-line oolitic dolomite, etc. Aphanocrystalline biogenic dolomite, etc. Very finely crys-talline pellet dolomite, etc.	Medium crystalline dolomite Finely crystalline dolomite etc.
	<25% Intraclasts	>25% Ooids			Oosparrudite Oosparite	Oomicrudite* Oomicrite*						
		<25% Ooids	Volume ratio of fossils to pellets	>3:1	Biosparrudite Biosparite	Biomicrudite Biomicrite						
				3:1-1:3	Biopelsparite	Biopelmicrite						
				<1:3	Pelsparite	Pelmicrite						

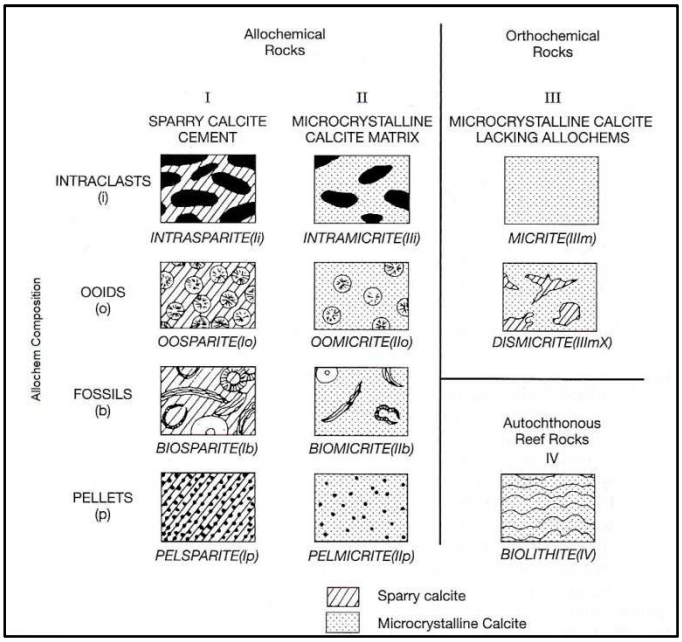

Figure 2.4 *Schematic representation of the constituents that form the basis for Folk's classification of carbonate rocks (Table 2.2). After Folk (1962).*

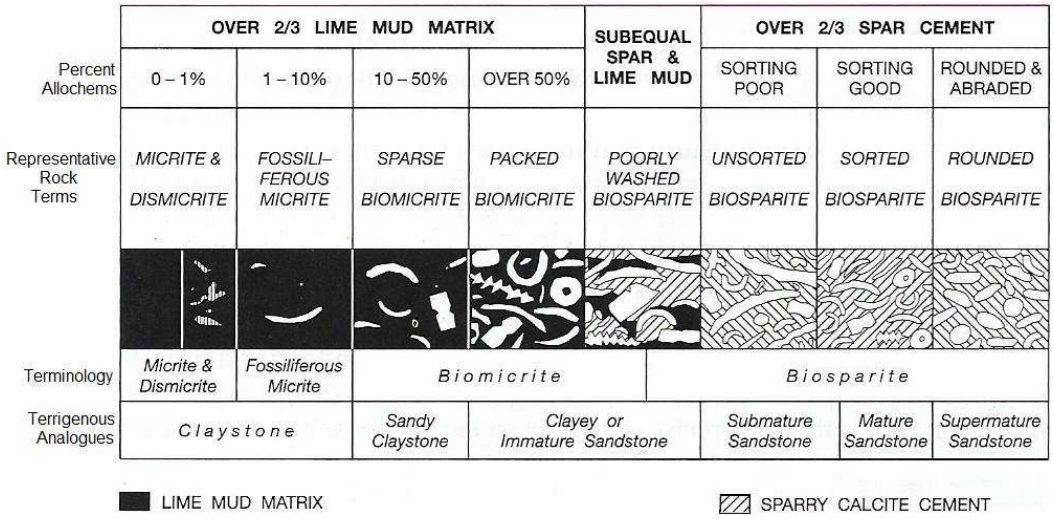

Figure 2.5 *Textural classification of carbonate sediments on the basis of the relative abundance of lime mud matrix and sparry calcite cement, and on the abundance and sorting of carbonate grains (allochems). After Folk (1962).*

Another widely known classification scheme is that of Dunham (1962) (Table 2.3), which are based on the constituents, their fractions, and which of them are the supporting material.

Table 2.3 *Carbonate textural classification of Embry and Klovan (1971), amplifying Dunham's (1962) classification. From Wilson (1997).*

ALLOCHTHONOUS LIMESTONES ORIGINAL COMPONENTS NOT ORGANICALLY BOUND DURING DEPOSITION						AUTOCHTHONOUS LIMESTONES ORIGINAL COMPONENTS ORGANICALLY BOUND DURING DEPOSITION		
LESS THAN 10% > 2mm COMPONENTS				GREATER THAN 10% > 2mm COMPONENTS		BY ORGANISMS WHICH ACT AS BAFFLES	BY ORGANISMS WHICH ENCRUST AND BIND	BY ORGANISMS WHICH BUILD A RIGID FRAMEWORK
CONTAINS LIME MUD (<.03mm)		NO LIME MUD		MATRIX SUPPORTED	> 2mm COMPONENT SUPPORTED			
MUD SUPPORTED		GRAIN SUPPORTED						
LESS THAN 10% GRAINS (>.03mm–< 2mm)	GREATER THAN 10% GRAINS							
MUD - STONE	WACKE - STONE	PACK - STONE	GRAIN - STONE	FLOAT - STONE	RUD - STONE	BAFFLE - STONE	BIND - STONE	FRAME - STONE

2.3 Diagenetic Alteration

Diagenetic alteration is a major factor affecting the texture and porosity of carbonate sediments. With respect to reservoir properties, diagenetic processes can either increase or reduce the initial porosity of the carbonate sediment. Diagenesis can be defined as “the chemical changes that occur within sediments, through interaction with pore waters, as they become compacted after burial and eventually lithified and recrystallized to form sedimentary rocks” (James, 2005). There are different stages of diagenesis, and it starts at deposition and continues until the first stages of lithification. It is affected by the compaction and burying of the sediments, which will change the pressure and temperature in the pore fluids and grains. There are different regimes for these processes, namely the marine, the meteoric, and the subsurface regimes. The marine regime is at the seafloor and slightly down in the subsurface beneath it, the meteoric regime is the zone where freshwater is present, or above the fresh water table, and the subsurface regime is the subsurface beneath the upper shallow zone where seawater or meteoric water penetrates the ground (Boggs Jr., 2006).

The different diagenetic processes are biogenic alteration, cementation, dissolution, neomorphism, and physical and chemical compaction. Neomorphism is a term Folk (1965) applied to cover the processes of replacement, recrystallization with some change in mineralogy, and inversion.

Replacement is the process of dissolution of one mineral and an almost simultaneous precipitation of another mineral (Boggs Jr., 2006).

Recrystallization is simply a process changing the size or shape of a crystal, without changing the mineralogy (Boggs Jr., 2006). But since many carbonate sediments originally consists of a mixture of aragonite and calcite, and the mineralogy therefore may change as a result of crystal size alteration, the recrystallization in carbonate sediments are termed a neomorphic process (Tucker and Wright, 1990). Most often the crystal size is increased (Boggs Jr., 2006).

Inversion changes one mineral to its polymorph (Boggs Jr., 2006). Polymorphs are different crystal structures of the same chemical compound. In contrast to replacement, this process only takes place in the solid or dry state, so when aragonite changes to calcite (mainly in the meteoric and in the subsurface regimes) this is a replacement process rather than an inversion process, since the diagenetic environments for limestones always are wet (Boggs Jr., 2006). The difference between

inversion and replacement is that when inversion occurs, the minerals do not dissolve to precipitate as a new mineral as in replacement, but they change without dissolving.

2.3.1 The marine regime

In the marine regime the diagenetic processes that take place are mainly bioturbation and thereby reorganization and modification of the sedimentary grains and original structures, cementation and some dissolution. Organism may make borings in the skeletal grains and carbonate substrate, and these can be filled by micrite (a term for very fine grained carbonate sediments). Cementation in this regime occurs particularly in warm areas, since carbonate minerals mainly dissolves in cool water, and precipitate in warm water, and the common cement is aragonite, although high-magnesian calcite also may occur. Cement does not only alter a rock by reducing its porosity and modify its mineralogy. In addition cementation processes may alter the texture of rocks, which may affect seismic properties. Thus a brief description of cement textures common in the different regimes, is included in this section. Figure 2.6 shows the different cement textures and cement geometry that can form. In the marine regime aragonite cement textures like a mesh of needles and micritic aragonite are common in intraskeletal and interskeletal cavities within silt-sized internal sediments. Needle-like crystals may also form an acicular fringe and make an isopachous geometry. Botryoids are isolated or coalescent mamelons, which consists of fans of elongate euhedral fibres (Tucker and Wright, 1990).

High-magnesium calcite cement can be bladed, equant, or peloidal. Peloids are a common feature of modern reef rocks, and also the bladed cements can be found in reefs and are most common isopachous (Tucker and Wright, 1990).

Meniscus cements can form on beaches when water is held by capillary forces as interstitial water drains during low tide. Dripstone geometry can form when drops of water are held beneath the grains on the beach, when the grains are not totally bathed in water (Boggs Jr., 2006). Acicular aragonite fringes may form on the seafloor when storms, waves and burrowing organisms disrupt the sediments and form intraclasts (Tucker and Wright, 1990).

Dolomite ($(Ca, Mg)CO_3$) may form on the seafloor when some of the calcium in calcium carbonate sediments dissolves and are replaced by magnesium (James, 2005). This is a replacement process (neomorphic).

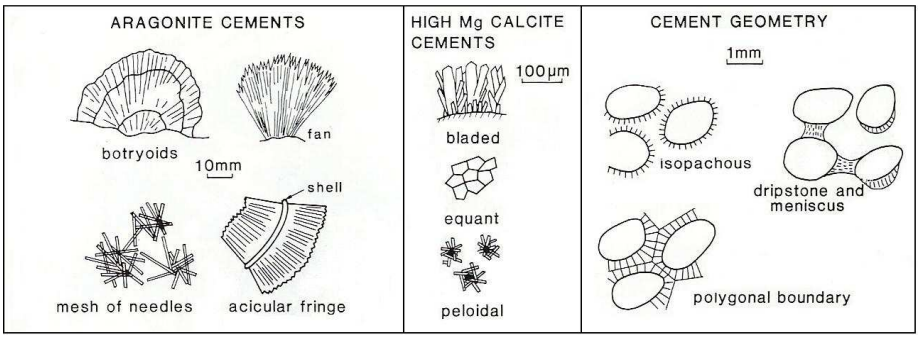

Figure 2.6 *Modern marine cements and their geometries. From Tucker and Wright (1990).*

2.3.2 The meteoric regime

To get into the meteoric regime the sediments have to be uplifted to get above the sea, or the sea level can fall, or a shallow basin can be filled. In this regime dissolution and cementation mainly take place, but some neomorphism may also occur. Dissolution of carbonates is most frequent in cool temperatures, and where acidic (low pH) pore waters are present. The meteoric water is typically acidic because it is charged with carbon dioxide (CO_2). Since aragonite and high-magnesian calcite are more soluble (unstable) than calcite, they are easily dissolved in this water, while calcite may precipitate and form cement.

The cements typically have dripstone or meniscus cement geometry in the unsaturated zone, while in the water-saturated zone they may be isopachous or make a polygonal boundary (Boggs Jr., 2006). But although cementation does occur in this regime, dissolution is the most important diagenetic process in the meteoric regime. Karstification is a dissolution process that takes place at the level of the water table. Karsts are carbonate rocks with caves, and these make good reservoirs because of the high porosity and permeability.

Neomorphic processes in this regime mainly consist of replacement, but recrystallization also occurs. Low-magnesian calcite typically replaces aragonite and high-magnesian calcite, as mentioned above. The replacement of aragonite by calcite is termed calcitization (Tucker and Wright, 1990). Aggrading neomorphism (recrystallization) may change fine-grained limestones to mosaics of microspar crystals and coarser pseudospar crystals (Tucker and Wright, 1990).

2.3.3 The subsurface regime

In the subsurface regime the temperature and pressure are increased. This causes compaction, both physical and chemical, and further cementation and chemical and

mineralogical changes (neomorphism), which all depend on the specific temperature, pressure, pore-fluid composition, and pH. Since the temperature and pressure are getting higher further down in the subsurface, there will be less dissolution and more cementation in this regime (carbonates in general dissolve in low temperatures and precipitate in high temperatures). In addition there are less unstable minerals (aragonite and high-magnesian calcite) in the subsurface than in the surface regimes, since most of these already have been dissolved. Actually the conditions that controls cementation in this regime is not well understood, but it is believed that the cementation are due to increase in temperature, decrease in CO_2 partial pressure, and pore waters that are highly oversaturated with calcium carbonate (Boggs Jr., 2006). High porosity and permeability will also contribute, since they enhance the fluid flow through the sediments. The cement may be derived from pressure solution of carbonate sediments in addition to be “delivered” from the streaming pore waters. Bladed and equant cements are common in the subsurface regime (Boggs Jr., 2006).

A common neomorphic process taking place in this regime is the coarsening of the crystals (recrystallization) called aggrading neomorphism.

The most obvious diagenetic process of this regime is compaction. The sediments are getting compacted because of the weight of the overlaying sediments and the water column. This will make the grains reorganize to a tighter packing, and they may also deform by brittle fracturing and breaking, and by ductile squeezing. Compaction has a major affect on porosities in carbonate sediments, since they initially have high porosities ranging from 40 to 80 percent. These initial porosities may decrease by 50 to 60 percent at only 100 m burial depth (Boggs, 2006 and references therein). The thicknesses of the beds are consequently reduced.

The chemical compaction is taking place at deeper depths, ranging from 200 to 1500 m (Boggs Jr., 2006). At this stage of compaction the grains are dissolved at the grain contacts because of the high pressure, and the dissolved minerals precipitate as cement. This process can form stylolite seams. In these seams fine-size non-carbonate minerals, as clay, accumulate as carbonate minerals dissolve. This type of pressure solution cause significant porosity loss, perhaps up to 30 percent of initial porosity (Boggs Jr., 2006).

The various diagenetic processes in the different regimes are illustrated in Figure 2.7.

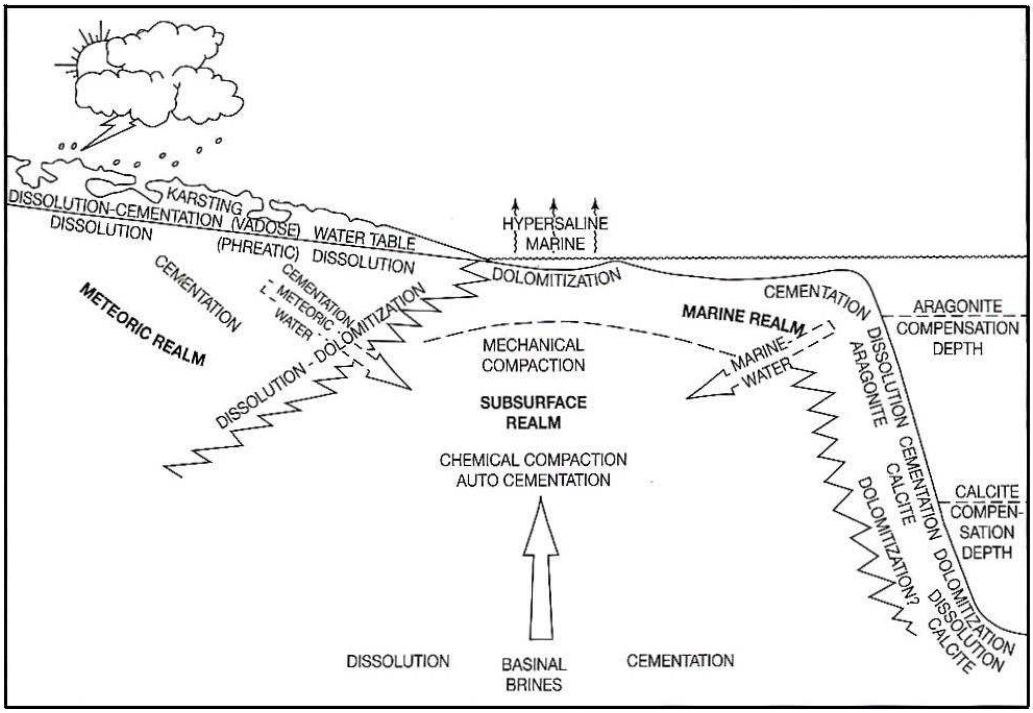

Figure 2.7 *The principal environments in which post-depositional modification of carbonate sediments occurs, with dominant diagenetic processes that occur in each of the major diagenetic realms indicated. From Moore (1989).*

2.4 Porosity and Pore Types

Porosity is obviously an important rock property when evaluating reservoir quality. The porosity and permeability have to be sufficient to store and transmit fluids. 5-15% is the common porosity range in carbonate reservoir rocks (Choquette and Pray, 1970). For carbonate rocks, in contrast to sandstones, the pore shapes is also of great importance. Since the fragments which make up carbonates are mostly produced in situ and do not get transported, they are not as rounded as sand grains, and the pore space can have a greater variety in shapes. For sandstones the pore sizes are closely related to sedimentary particle size and sorting, and the permeability-porosity interrelations are relatively consistent, and do also commonly depend on particle size and sorting. For carbonates both pore sizes and permeability-porosity interrelations are greatly varied and show little relation to sedimentary particle size and sorting (Choquette and Pray, 1970).

The pore form modifies the effective elastic moduli of the rock, and hence its seismic velocities (this effect will be discussed in detail in chapter 3). This is important

to keep in mind when dealing with seismic data from carbonate rocks. Many papers have been written concerning the relation between pore types and seismic velocities for carbonate rocks (e.g., Anselmetti and Eberli, 1993, 1997). In this section the different types and their origin will be described.

Pore types can be divided into two groups; primary and secondary pores. Primary pores are originally present in the sediment or rock, while secondary pores are formed by later diagenetic processes, fracturing, or decomposing of organic matter. Choquette and Pray (1970) describe 15 basic porosity types, which are listed in Figure 2.8, grouped by their relation to fabric. The most important and frequently observed ones of these are interparticle, intercrystal, moldic, vug, channel, intraparticle, fracture, and fenestral (Wang 1997) (Figure 2.8 and 2.9). The following description of these is based on Choquette and Pray's (1970) paper: "Geologic nomenclature and classification of porosity in sedimentary carbonates":

- *Interparticle porosity*

Porosity between particles. Generally primary, but can also be secondary due to selective solution of matrix or cement. In sediments this is generally the dominant porosity type, while for rocks it may or may not be of importance. Since particle has no lower size limit, neither have interparticle pores.

- *Intercrystal porosity*

Porosity between crystals, generally of equant and equal size. May be of primary or secondary origin. Dolomites may have this pore type.

- *Moldic porosity*

Porosity formed by selective removal of a former individual constituent of the sediment or rock, and thus of secondary origin. This removal is normally by solution, and various types of carbonate depositional particles may dissolve. In limestones molds are formed of aragonitic constituents, especially oolites and molluscan shells. In dolomites it is commonly either aragonite or calcite primary constituents that is selectively dissolved. In addition, moldic porosity may form by the decomposition of organic matter, like plant roots or soft parts of organisms. Moldic porosity is identified on the basis of shape, size, wall ornamentation, or relict features, and are extremely abundant in many carbonate rocks.

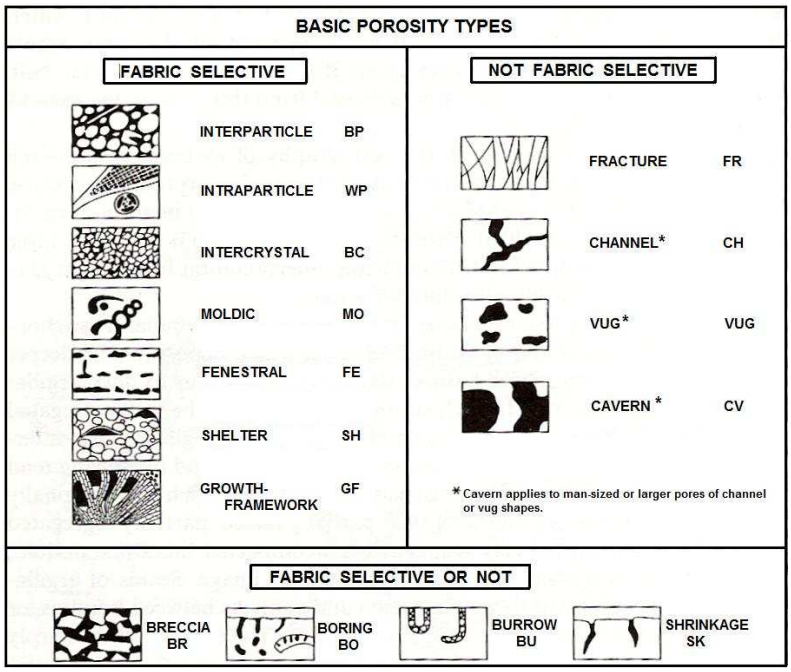

Figure 2.8 *Geologic classification of pores and pore systems in carbonate rocks. Porosity is colored black. From Choquette and Pray (1970).*

- *Vug porosity*

Vug is defined as a pore that is somewhat equant, or not markedly elongate, is large enough to be visible by eye (diameter greater than 1/16 mm), and that is not fabric selective. Vugs are dominantly formed by solution and may represent enlargement of fabric selective pores, like molds, to such an extent that they lose their original form.

- *Channel porosity*

Like vug porosity, but more elongated. The ratio of length to average cross-sectional diameter is more than 10:1. May form by solution enlargement of fractures.

- *Intraparticle porosity*

Porosity within individual particles or grains. This is a physical and positional, and not a genetic porosity type. It can be of primary or secondary origin. Primary intraparticle porosity is commonly internal chambers or other openings within skeletal organisms, but can also be pore space within individual nonskeletal grains, like ooids and pellets. Secondary intraparticle porosity forms mainly by solution and borings. This porosity type is abundant in carbonate sediments and may be an important part of the preserved porosity in carbonate rocks.

- *Fracture porosity*

Porosity formed by fracturing. In carbonates fracture porosity may form by collapse related to solution, slumping, or various kinds of tectonic deformation. With increasing dislocation or “chaos” this kind of porosity is called breccia porosity.

- *Fenestral porosity*

Primary or penecontemporaneous gap in rock framework, larger than grain-supported or mud-supported interstices. Fenestral pores are larger than normal interparticle pores, and have multigranular roofs, floors and other margins. Their shapes are somewhat rounded, spherical, lenticular, or more irregular. Even though these pores may be irregular or elongate in a vertical dimension, they are commonly somewhat flattened parallel with the lamina or bedding of the rock, which will give a greater horizontal than vertical permeability. Fenestral pores are often in close association, commonly along obscure partings or lamina in the rock. Most fenestral porosity forms by gas evolution and sediment distension shortly after deposition, and is thus of secondary origin. It may also form by decay of sediment-covered algal mats, or shrinkage during drying.

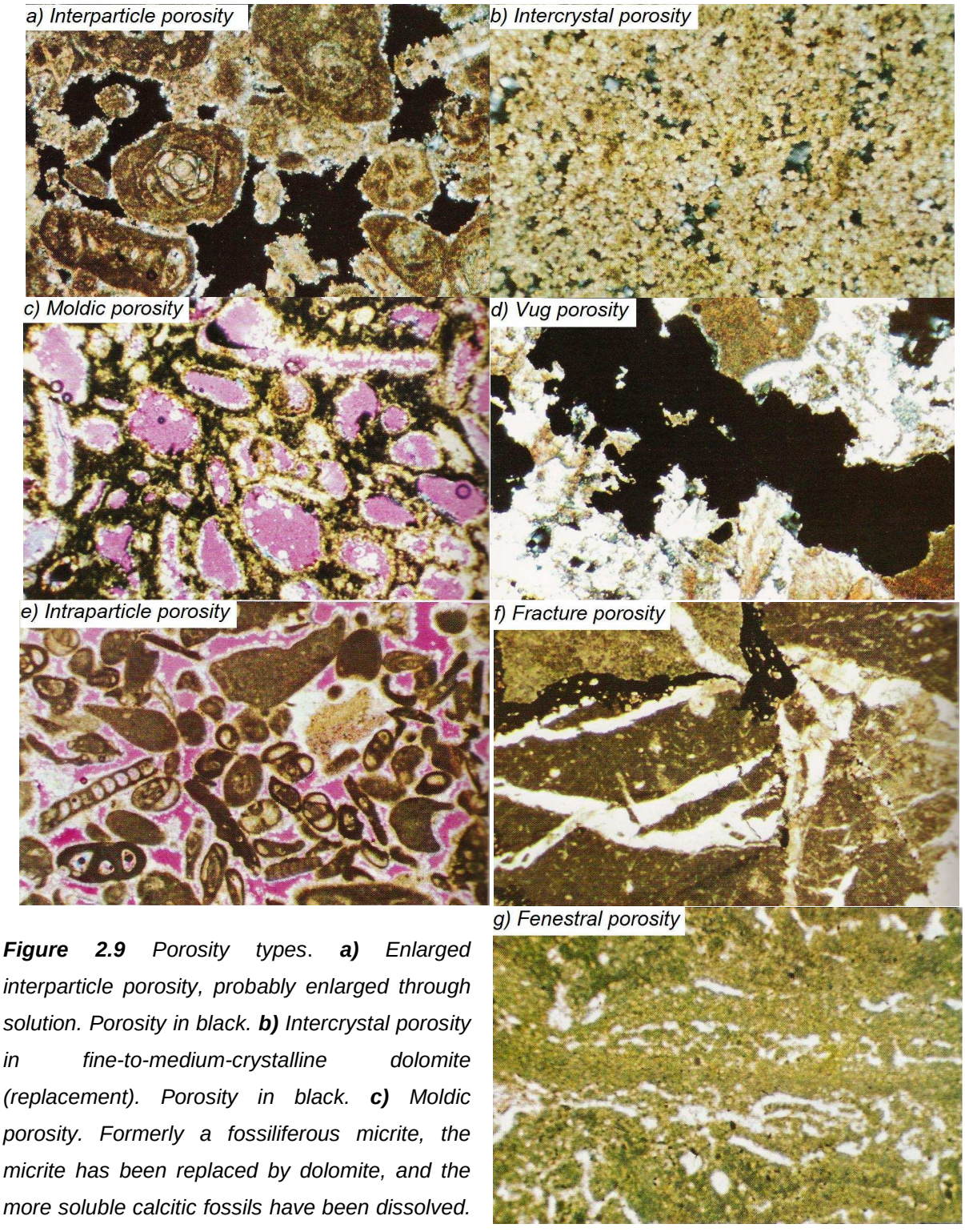

Figure 2.9 *Porosity types*. ***a)*** *Enlarged interparticle porosity, probably enlarged through solution. Porosity in black.* ***b)*** *Intercrystal porosity in fine-to-medium-crystalline dolomite (replacement). Porosity in black.* ***c)*** *Moldic porosity. Formerly a fossiliferous micrite, the micrite has been replaced by dolomite, and the more soluble calcitic fossils have been dissolved. Porosity in purple.* ***d)*** *Vug porosity, clearly enlarged and not fabric selective. Porosity in black.* ***e)*** *Reduced intraparticle porosity, and reduced interparticle porosity. Porosity in purple.* ***f)*** *Filled fracture porosity. Conjugate set of large fracture veins.* ***g)*** *Filled fenestral porosity in a blue-green algal biolithite. Porosity may be due to air spaces in crinkled mat sediments.* ***a)-c)*** *0.38 mm. From Scholle (1978).*

2.5 Summary

The significant difference between carbonate rocks and sandstones is mainly that carbonates generally are made up of more irregular particles than sandstones, and therefore may contain pores with a greater variety in shapes and sizes. In addition, carbonate minerals are less stable, and are more exposed to diagenetic alterations.

The formation of a good carbonate reservoir rock, depends on the original depositional setting (climate, tectonics, chemical composition of water, biota, etc.), and the later evolution of the sediments/rock, which include burial or uplifting, and the diagenetic processes these settings include. In a general shelf profile (Figure 2.1), the known reservoirs of highest qualities are found in deep shelf margins, winnowed platform edge sands, and platform interior. The initial porosities and permeabilities controlled by these depositional settings get altered by diagenesis. This alteration may increase or decrease initial porosity and permeability, mainly by the processes of dissolution and cementation, respectively. The most pronounced dissolution generally takes place in the meteoric regime, while cementation to a great extent occurs in the subsurface regime. Dolomitization is an important porosity enhancing process which may occur in waters of high magnesium saturation.

Chapter 3: Geophysics of Carbonates

As described in the previous chapter, carbonates are more complex rocks than siliciclastics due to the variety in these rocks as a result of formation processes and diagenetic alterations. For this reason they cannot be treated like siliciclastics when estimating and predicting rock property relations. In this chapter the relations between rock properties and seismic responses are the main objectives. Factors controlling these properties and the effects of variations in these will be described and illustrated, but first some rock physics models constructed to predict the elastic moduli of rocks resulting from different rock properties and saturations are introduced and discussed. Finally some common possible seismic problems concerning carbonate rocks are shortly mentioned.

3.1 Basic Principles for Seismic Reflection and Transmission

In seismic data, the signatures of a geologic model are seen as amplitudes of seismic traces. These are results of impedance contrasts in the subsurface. Acoustic impedance is defined as

$$AI = v \cdot \rho, \tag{3.1}$$

where *AI* is acoustic impedance, *v* is seismic velocity, and ρ is bulk density of the rock. The reflection coefficient *R*, which defines the signature to a trace as a response of crossing an interface between two different lithologies, for a normal incident wave, is defined as

$$R = \frac{A_1}{A_0} = \frac{AI_2 - AI_1}{AI_2 + AI_1}, \tag{3.2}$$

where A_1 is the amplitude of the reflected wave, A_0 is the amplitude of the incident wave, and AI_1 and AI_2 correspond to the acoustic impedances for the layer above and beneath the interface, respectively. This equation shows why changes in lithology (seismic velocity and bulk rock density) are observable in a seismogram, and is the basic principle for seismic imaging.

For transmitted waves, which travel through the interface and penetrate the layer below it, instead of getting reflected from it, the transmission coefficient *T* is defined as

$$T = \frac{A_2}{A_0} = \frac{2AI_1}{AI_2 + AI_1}, \tag{3.3}$$

where A_2 is the amplitude of the transmitted wave. This equation, like the reflection coefficient equation, is valid only for normal incident waves. When waves are incident with an angle, this angle needs to be incorporated into a more advanced formula.

3.2 Rock Physics Models - the Link Between Geology and Geophysics

Knowing that the reflection and transmission coefficients depend on seismic velocities and bulk densities of rocks, what then do these properties depend on? Seismic velocities for P- waves, V_p, (compressional) and S-waves, V_s, (shear) (Figure 3.1 a) and b)), are defined as

$$V_p = \sqrt{\frac{K + \frac{4}{3}\mu}{\rho}}, \tag{3.4}$$

and

$$V_s = \sqrt{\frac{\mu}{\rho}}, \tag{3.5}$$

respectively. *K* is bulk modulus, μ is shear modulus, and ρ is bulk density. *K* (equation 3.6) expresses the stress-strain ratio in the case of a simple hydrostatic pressure *P* applied to a cubic element of volume *v* (Figure 3.1 c)). *P* is then the stress, and the resultant volume strain (deformation) is the change of volume Δv divided by the original volume *v*.

In a similar manner the shear modulus μ (equation 3.7) is defined as the ratio of shearing stress τ to the resultant shear strain $tan\ \theta$ (Figure 3.1 d)).

$$K = \frac{volume\ stress\ P}{volume\ strain\ \Delta v/v}, \tag{3.6}$$

$$\mu = \frac{shear\ stress\ \tau}{shear\ strain\ tan\ \theta}\ . \tag{3.7}$$

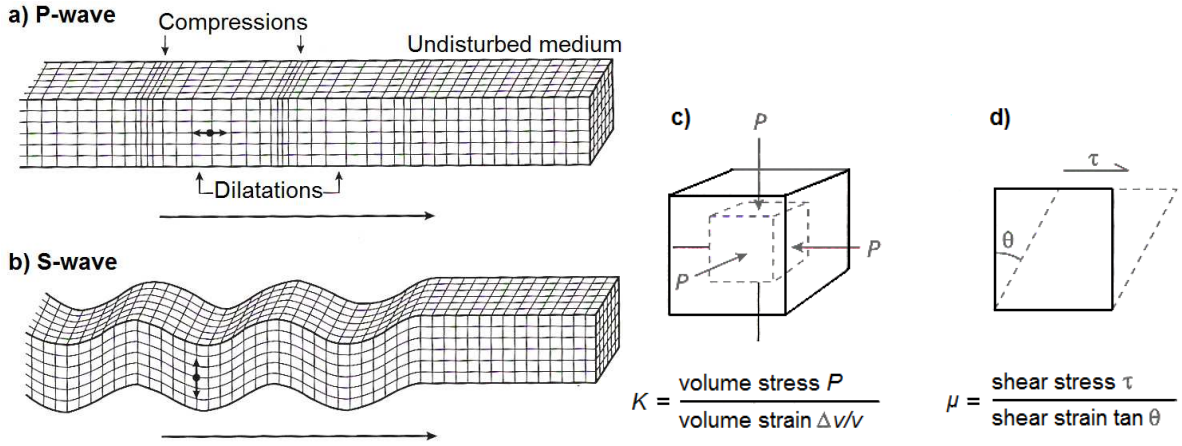

Figure 3.1 *Elastic deformations and ground particle motions associated with the passage of body waves for* ***a****) P-waves, and* ***b****) S-waves, and the elastic moduli:* ***c)*** *bulk modulus, and* ***d)*** *shear modulus. From Keary et al. (2002), and references therein.*

The elastic moduli are thus effects of stress (σ) and strain (ε). Stress is a force applied to a medium, while strain is the response of that force, which means the deformation of the medium as response to the applied force. For instance, if a rock gets buried and compacted, the pressure from the overburden is the stress, which forces the medium to deform by compaction, which is the strain. The relation between stress and strain is stated in Hooke's law:

$$M = \frac{\sigma}{\varepsilon}, \tag{3.8}$$

where M is any of the two elastic moduli. This implies that stress is proportional to strain, and that deformations are reversible. Hooke's law is valid for very small deformations, like the deformations caused by seismic waves passing through a rock. Stress and moduli have the units of pressure, while strain is dimensionless.

If a rock consists of two different phases, for instance solid grains (phase 1) and brine saturated pores (phase 2), and v_1 and v_2 represents the volume fractions of these two phases, respectively, and M_1 and M_2 are their elastic moduli, then average stress and strain are expressed as

$$\bar{\sigma} = \bar{\sigma}^{(1)} v_1 + \bar{\sigma}^{(2)} v_2, \tag{3.9}$$

and

$$\bar{\varepsilon} = \bar{\varepsilon}^{(1)} v_1 + \bar{\varepsilon}^{(2)} v_2. \tag{3.10}$$

respectively. *1* and *2* denotes the two phases, and bar denotes average values. An effective modulus is the average modulus of a medium consisting of more than one phase, or the multi-phase medium on a macroscopic scale. No rock is homogenous at a microscopic scale, but on a macroscopic scale they may be. The effective moduli can thus be representative for a rock that is homogenous on a macroscopic scale. The effective modulus of the brine saturated rock described above will be

$$M^* \equiv \frac{\bar{\sigma}}{\bar{\varepsilon}} = \frac{\bar{\sigma}^{(1)}}{\bar{\varepsilon}} v_1 + \frac{\bar{\sigma}^{(2)}}{\bar{\varepsilon}} v_2, \tag{3.11}$$

or

$$M^* = M_1 + (M_2 - M_1) \frac{\bar{\varepsilon}^{(2)}}{\bar{\varepsilon}} v_2, \tag{3.12}$$

where * denotes effective values (for derivation, see e.g., Gueguen and Palciauskas, 1994) . This formula can be used to calculate both the effective shear modulus and the effective bulk modulus since the effective modulus *M** can be either of them. The moduli of the single phases can be measured in a laboratory or found in the literature.

For small concentrations of spherical pores, when one can neglect the pore-interactions, the volume strain in equation (3.12) is defined as

$$\frac{\bar{\varepsilon}^{(2)}}{\bar{\varepsilon}} = \frac{(3K_1 + 4\mu_1)}{(3K_2 + 4\mu_1)}, \tag{3.13}$$

If the solid matrix or the saturating fluid consists of more than one constituent, effective values can be calculated for these, and then those effective matrix and fluid properties can be used to calculate the effective properties of the two-phase medium consisting of a matrix with fluid inclusions. For the calculation of an effective matrix, the following formula can be used:

$$M^* = \frac{M_V + M_R}{2}. \tag{3.14}$$

This is the Voigt-Reuss-Hill average (Hill, 1952), which is the average between Voigt's and Reuss' (1929) equations for the effective modulus of a phase. Voigt's equation is as follows:

$$M_V = \sum_{i=1}^{N} v_i M_i \ , \tag{3.15}$$

and Reuss' equation is

$$\frac{1}{M_R} = \sum_{i=1}^{N} \frac{v_i}{M_i} \ . \tag{3.16}$$

N is the number of constituents. These two end members, where Voigt's equation is the upper boundary and Reuss' equation the lower for the possible values of *M** according to possible orientations of the materials, correspond to the cases of iso-strain (all constituents have the same strain) and iso-stress (all constituents have the same stress), respectively. Most composite materials have effective moduli values in-between these boundaries, and thus the Voigt-Reuss-Hill average is often used for calculations of matrix moduli. Since liquids generally are incompressible while gases are very compressible, the iso-stress, rather than the iso-strain condition is appropriate for calculations of *M** for mixtures of fluids, and the Reuss' equation will give the exact effective bulk modulus for fluid mixtures where the shear modulus is zero (Mavko et al., 1998).

The densities of the matrix, fluid, and the effective medium are simply calculated as the sum of the densities of each component multiplied by the fraction of the total volume of those components:

$$\rho_t = \sum_{i=1}^{N} \rho_i \cdot v_i \, , \tag{3.17}$$

where ρ is the density, and *t* denotes the total value, either for one phase or for the effective medium.

This effective medium theory assumes that there are no pore-to-pore interactions, i.e. the pores are isolated. In addition different pore shapes are not considered, but all pores are assumed to be spherical. To calculate effective moduli in a more realistic

way, more complicated formulas are needed. Many such models exist, and of the most known ones are the models of Kuster and Toksöz (1974), and Gassmann (1951). In addition the method of the Differential Effective Medium theory (DEM), can improve the results.

3.2.1 Kuster and Toksöz model

The Kuster and Toksöz (K-T) model (1974) are constructed to calculate the elastic moduli of a two-phase composite medium (effective continuing matrix with inclusions of the other phase) given the properties, concentrations and shapes of the inclusions and the matrix material. The K-T formulas are based on first-order scattering of seismic waves, where the waves are much longer than the inclusions. Scattering is the internal reflections from the inclusions in the medium, when hit by a seismic wave. The K-T approach is restricted to first-order scattering, since for higher-order scattering to be considered, a complete statistical description of the distribution of the inclusions is required, and the relative location of all inclusions must also be known for the calculation of the sum of all scattered waves. The scattering are described in terms of displacement fields, expanded in series. A relation between the elastic moduli for the effective medium and those of the matrix and inclusions are provided by the coefficients of these series expansions (Kuster and Toksöz, 1974). The K-T formula can be used for calculations for both solid and liquid inclusions in a solid matrix, or for solid suspensions in a fluid matrix, and both spherical and oblate spheroidal inclusions are considered. Since only first-order scattering are incorporated into the model, the pores are non-interacting, and the porosity thus has to be sufficiently low.

For spherical pores the formulas used for calculations of effective properties are:

$$\frac{K^* - K_m}{3K^* + 4\mu_m} = c\frac{K' - K_m}{3K' + 4\mu_m}\,, \tag{3.18}$$

$$\frac{\mu^* - \mu_m}{6\mu^*(K_m + 2\mu_m) + \mu_m(9K_m + 8\mu_m)} = \frac{c(\mu' - \mu_m)}{6\mu'(K_m + 2\mu_m) + \mu_m(9K_m + 8\mu_m)}\,, \tag{3.19}$$

$$\rho^* - \rho_m = c(\rho' - \rho_m)\,, \tag{3.20}$$

where *m* denotes matrix properties, and ′ denotes inclusion properties, and *c* is the

inclusion volume concentration (or porosity) defined by:

$$c = \frac{1}{R^3}\sum_{j=1}^{N} r_j^3 \,, \tag{3.21}$$

where R is the radius of the spherical sample, r_j are the radiuses of the inclusions, and N is the number of inclusions in the sample. Derivations can be found in Kuster and Toksöz (1974).

For spheroidal inclusions the equations become (in a rewritten form from Wang, 1997):

$$K^* = \frac{3K_m(3K_m + 4\mu_m) + 4\mu_m\left(K_f - K_m\right)A}{3(3K_m + 4\mu_m) - 3\left(K_f - K_m\right)A} \,, \tag{3.22}$$

$$\mu^* = \frac{25\mu_m^2(3K_m + 4\mu_m) - \mu_m^2(9K_m + 8\mu_m)B}{25\mu_m(3K_m + 4\mu_m) + 6\mu_m(K_m + 2\mu_m)B} \,, \tag{3.23}$$

where f denotes inclusion fluid properties, and A and B are defined as:

$$A = \sum_{n=1}^{N} c(\alpha_n) T_{iijj}(\alpha_n) \,, \tag{3.24}$$

$$B = \sum_{n=1}^{N} c(\alpha_n)\left[T_{ijij}(\alpha_n) - \frac{1}{3}T_{iijj}(\alpha_n)\right], \tag{3.25}$$

where T_{ijjj} and T_{ijij} are tensor components (se Appendix for further definitions), α_n is the nth aspect ratio of the inclusions, and $c(\alpha_n)$ is the fractional concentration of α_n, and thus

$$\sum_{n=1}^{N} c(\alpha_n) = \varphi \,. \tag{3.26}$$

The effective density is defined as before (equations 3.17 and 3.20), but can be rewritten in the form:

$$\rho^* = \rho_m(1-c) + \rho_f c\,. \tag{3.27}$$

The Kuster-Toksöz model does consider scattering effects, and can be used for a medium with different pore-forms (aspect ratios), but it does not consider pore-interactions or pore-fluid flow, and assumes that pores are isolated rather than connected.

3.2.2 The Gassmann model

The Gassmann (1951) model (equations 3.28 and 3.29) can be used to calculate the effect of fluid substitution. The parameters used in this calculation are bulk modulus for the rock matrix (K_m), for the fluid (K_f), and for the dry rock (K_d), and the porosity (φ). The shear modulus is assumed to be the same for dry and wet rock since fluids have no shear strength.

$$K = K_d + \frac{\left(1-\frac{K_d}{K_m}\right)^2}{\frac{\varphi}{K_f} + \frac{1-\varphi}{K_m} - \frac{K_d}{K_m^2}}\,, \tag{3.28}$$

$$\mu = \mu_d\,. \tag{3.29}$$

These equations can be used when dry values are measured and one wants to predict the effect of saturation of different fluids, or when a saturated sample has been studied, and one wants to extract the effect of the fluid and calculate properties for saturation of another fluid. In the last case the Gassmann equation for the bulk modulus first has to be rewritten in the following form to find the dry bulk modulus:

$$K_d = K - \frac{K_f\left(1-\frac{K}{K_m}\right)^2}{\left(1-\frac{K_f}{K_m}\right)\varphi - \frac{K_f}{K_m}\left(1-\frac{K}{K_m}\right)}\,. \tag{3.30}$$

Using this formula to calculate the dry bulk modulus from the measurements of a wet rock sample with known fluid and matrix properties, the ordinary Gassmann equation (3.28) then can be used to calculate the modulus for the rock saturated with another fluid. These equations can only be used for fully saturated rocks, in a static condition

(i.e. frequency = 0 Hz), but has also approved to apply for low-frequency waves (Gelius and Johansen, 2007).

The Gassmann equation is widely used, but its validity for carbonate rocks are debated by many authors (e.g., Rossebø et al.,2005; Gomez et al., 2007; and Adam and Batzle, 2008). Rossebø et al. (2005) have questioned whether Gassmann is appropriate for carbonate rocks, due to the assumptions incorporated in this model. Two of the assumptions pointed out are the assumption that the pores are connected, and the assumption that the pore fluids do not interact with the solid rock. But generally, there is an isolated pore structure in carbonate rocks, and alterations of shear frame properties have been observed under several laboratory studies (Rossebø et.al, 2005, and references therein). Adam and Batzle (2008) states that the shear modulus has been observed to change compared to the dry shear modulus, especially for brine saturated carbonates. In their study they have observed an increase in shear modulus for high frequencies (0.8 MHz) relative to the dry modulus, which they explain as shear modulus dispersion with frequency. For low (seismic) frequencies (10 Hz), the observation is that the shear modulus decreases when the rock gets saturated. Adam and Batzle (2008) explain this effect as a possible result of a weakening of the solid matrix due to a fluid-matrix interaction, which possibly may be associated to the loss of surface energy and/or growth of sub critical cracks in compliant pores. Rossebø et al. (2005) which also have observed an apparent fluid control on the shear modulus for low-frequency measurements (from about 3 - 3000 Hz), suggest that this control may be due to the applied frequency.

In addition, the Gassmann equation does not give the possibility to define the pore forms in a material. Carbonates may have many different pore forms, as described in the previous chapter, and since these have lower aspect ratios, which are the ratios of the short axis to the long axis of the pores, than perfect spheres, they will be less stiff and reduce the bulk modulus of the rock compared to a rock of same properties with spherical pores. Since the Gassmann theory assumes that the pore fluids can easily flow and equalize the pore pressure gradients induced by the seismic waves, during a seismic period, the Gassmann equations may give erroneous values for rocks containing pores with very low aspect ratios, like cracks, since fluid flow through these require more time than through pores of higher aspect ratios.

There can be found many plots comparing real measured velocity values to calculated values from Gassmann model calculations. For example, Gomez et al.

(2007) state that Gassmann calculations are found to under-predict saturated bulk modulus, and Rossebø et al. (2005) have shown the failure of the Gassmann model to predict to the bulk modulus from dry to brine saturated conditions, and state that the Gassmann calculations overestimate the fluid effect on the bulk modulus for low porosities, and underestimate it for high porosities. However, this effect is more evident from high frequency measurements, which might indicate that the failure might be related to the applied frequency (Rossebø et al., 2005).

Rasolofosaon et al. (2008) suggest that it is not necessarily the Gassmann equations that are not appropriate for limestones, but it may be the velocity and drained moduli measurements that are questionable. They state that conventional measurement techniques for petroacoustics do not always perform adequately in carbonate rocks due to their heterogeneity, and common problems are: complex velocity-porosity relation; strong ultrasonic attenuation even under high-differential pressures; anomalous velocity dispersion; complex relation between P-wave velocity and air/water saturation (very variable results); violation of the Gassmann equation (gives too high bulk modulus compared to measured one); and difficulty in measuring S-waves in high-porosity limestones.

Measuring the velocity by the first-break technique, may lead to overestimation of the acoustic velocity in heterogeneous carbonate rocks, because some rays may follow a path which is not the fastest, so that some energy (second arrivals, codas, etc.) arrive after the “main energy packet”. Rasolofosaon et al. (2008) suggest possible approaches as solutions to improve the petroacoustical characterization of carbonate rocks, and states that the best way of minimizing the effects of heterogeneity is to measure the phase velocity using the phase spectral ratio method (e.g., Bourbié et al., 1987), but the result obtained depends on the quality of the spectra calculated. To avoid the attenuation that appears when using propagating ultrasonic waves, they suggest that sonic waves (1-10 kHz) can be used. However, this is expensive and long samples (~20 cm) are needed.

Finally Rasolofosaon et al. (2008) claim that problems with S-waves in high-porosity limestones seem to be a factor of the shape of the experimental setup, and it is possible that an experiment using a “pancake-shaped” sample could improve S-wave measurements. When these methods are used in their studies, the measured values are the same as predicted by the Gassmann equation, which support the

suggestion that it is not necessarily this Gassmann equation that is not suitable for carbonates, but the velocity and drained moduli measurements that is questionable.

3.2.3 Differential effective medium theory

The limitation of the Kuster-Toksöz model of not taking pore-to-pore interactions into consideration, since only first order scattering are considered, can be improved by performing the calculations according to the differential effective medium (DEM) theory. This method is a hybrid method, which incorporates pore interactions in the calculations. The way of doing this is to perform the K-T calculations in steps, by first embedding only a dilute concentration of the total pore-space within the matrix, and compute the effective elastic parameters of this composite medium. Then this is repeated, using the calculated effective moduli as the matrix moduli, and embedding more of the pore-space in more such steps, until the wanted porosity is reached. The elastic parameters calculated in the last step are the effective parameters (Gelius and Johansen, 2007). This method depends on in which direction the calculations are performed. Starting with a small porosity and gradually increasing it, will give a slightly different result than starting with total porosity and gradually decreasing it.

The DEM approach will incorporate higher order scattering in the calculations, since the first imbedded pores will alter the matrix properties, and thus affect the effect of later embedded pores on the matrix properties. In this way pore interactions are incorporated without breaking down the validity of the K-T model. However, these pore-interactions do not include fluid flow from one pore to another.

3.2.4 Limitations of rock physics models

In addition to the rock physics models described above, there exists many more. Some are developed for calculations concerning unconsolidated materials (e.g. Wood, 1955), and some for consolidated materials (e.g., Gassmann, Kuster-Toksöz), and in addition to the theoretical models, there exist many empirical models (e.g. Wyllie et al., 1958, and Han, 1986). Some models are simplified and easy to use, while others are more realistic, by incorporating more of the different aspects that influence the rock properties. However, the latter group often requires many input parameters, and may be too mathematical advanced to be of practical use. In addition, no mathematical model can possibly be able to describe a rock perfectly, and in lack of knowledge about all parameters, assumptions have to be made. Thus, no rock physics models will give

the absolutely correct values, but still many of them will give values that are very close to reality, when used within the boundaries of the assumptions incorporated in the given model.

Of the described models (Table 3.1), the Gassmann model is the easiest one to use, since it includes only a few short equations, and the only input parameters are bulk and shear moduli for the matrix, fluid, and the dry rock, and their densities, and porosity. But this model assumes connected pores with relatively high aspect ratios, no fluid flow, and no scattering.

The Kuster-Toksöz model does not require any dry-rock properties, but information about the pore shapes (aspect ratios) and the fractions of these different shapes of total porosity are needed. This model consists of more equations than the Gassmann model, but is still not too advanced to be useful. The K-T approach may be more appropriate for carbonates than Gassmann, since it assumes that pores are not connected, and carbonates generally have an isolated pore structure (Rossebø et al., 2005) In addition it can be used for all pore shapes, and first order scattering are considered.

The differential effective medium theory method can be used to make the K-T model incorporate pore interactions and higher order scattering. This does not require any more parameters than used in the K-T calculations.

Kumar and Han (2005) suggest an approach to avoid the path dependency of the DEM method. Their advice is to calculate dry rock moduli using DEM, since dry moduli are not asymmetric with respect to inclusion, and then use these moduli in the Gassmann equation and calculate for fluid substitution.

None of these methods allow for calculation of the effect of given frequencies on the behavior of a rock or the elastic moduli, but the Gassmann model will be appropriate for low (seismic) frequency calculations, while the two others are appropriate to use for high frequencies (Kumar and Han, 2005). In addition, since none of the models incorporate pore fluid flow, the damping effect caused by such flow is not considered either.

Table 3.1 *Some different rock physics models, and some of their assumptions and limitations.*

	Gassmann	Kuster-Toksöz	Differential Effective Medium
Pore shapes	Not suitable for fractures	Any	Any
Connected porosity	Yes	No	No
Pore interactions	No	No	Yes
Pore fluid flow	No	No	No
First order scattering	No	Yes	Yes
Higher order scattering	No	No	Yes

3.2.5 Calculation of pressure effects on pore shapes

Other effects may be incorporated in the previous discussed rock physics models. Pressure effects on the pore shapes can be included in the Kuster-Toksöz or DEM calculations. Flat pores and cracks will deform more easily than rounded pores, and cracks and fractures may close when sufficiently high pressures are applied. The following equation describes the crack aperture changes due to differential pressure *P*:

$$a = a_0 \left[1 - \frac{2(1-v)}{3\mu_0 \alpha} P\right]^{1/2}, \tag{3.31}$$

where *a* is pore aperture, the shortest of the axes in a pore, a_0 is the zero pressure aperture, *v* is Poisson's ratio, and α is pore aspect ratio (Walsh, 1965). Poisson's ratio is the ratio between the length and the cross-sectional dimensions in the matrix when it get stretched or compacted.

$$v = \frac{3K - 2\mu}{3K + \mu}. \tag{3.32}$$

Decreasing aspect ratios and possible closure of cracks, due to applied pressure, decrease the pore volume. Resulting pore volume can be calculated from the following equation:

$$V = (4/3)\pi\varepsilon\alpha, \tag{3.33}$$

where ***ε*** is crack (pore) density, defined as:

$$\varepsilon = \varepsilon_0 e^{-C_r P}, \tag{3.34}$$

where ε_0 is zero-pressure crack density, and

$$C_r = \frac{2(1-v)}{\pi\mu_{0\alpha}} . \quad (3.35)$$

3.3 Magnitudes of Rock Parameters, and Reasons for their Variations

There can be a great variety in carbonates from different locations due to variations in geologically determined properties like porosity and pore shapes, particle sizes, and mineral composition. These properties affect the seismic characterization. The magnitudes of reflection and refraction depends on bulk density and seismic velocity, which in turn depends on elastic moduli, which are directly affected by microstructure and petrophysical properties, pore pressure, and saturation fluid. Understanding why and how the geophysical parameters vary as effect of petrophysical properties, the range of velocities for carbonate rocks are not surprising. P-wave velocities may in fact range from 1700 to 6600 m/s, while S-wave velocities can vary between 600 to 3500 m/s (Eberli et al., 2003). Common magnitudes for elastic moduli and velocities for carbonate rocks, and variations of these due to differences in rock composition and microstructure, and different processes acting on the rock, are described below.

3.3.1 Elastic moduli, densities and velocities for minerals and rocks

Table 3.2 lists values for the elastic moduli and density for carbonate minerals, while Table 3.3 lists the P- and S-wave velocities and the ratio of these. These values are only valid for the minerals themselves. The bulk values of a rock (Table 3.4) will be different from the mineral values due to the pore space (amount, shape, and size) and the fluids these are filled with. Bulk density for the rock will be a result of the individual densities for minerals and fluids and the fractions of these in the rock sample (equation 3.17). Elastic moduli for the rock will be a result of the individual moduli for minerals and fluids (shear moduli for fluids are zero) and the fractions of these in the rock sample, and in addition it will depend on the microstructure. Both densities and moduli also vary with pressure and temperature. Seismic velocities (calculated from density and moduli) of rocks thus can have a range of values (Table 3.4) compared to the more or less constant velocities for minerals.

Table 3.2 *Elastic moduli and density for carbonate minerals.*

** and references therein.*

Mineral	Bulk modulus *(GPa)*	Shear modulus *(GPa)*	Density (g/cm^3)	Author
Calcite	70	29	2.71	Marion and Jizba, 1997*
Calcite	77	32	2.71	Marion and Jizba, 1997*
Calcite	76.8	32	2.71	Mavko et al., 1998, Sayers, 2008*
Dolomite	69	52	2.88	Marion and Jizba, 1997*
Dolomite	94.9	45	2.87	Mavko et al., 1998
Dolomite	76.4	49.7	2.87	Sayers, 2008*
Aragonite	45	39	2.92	Marion and Jizba, 1997*
Aragonite	44.8	38.8	2.92	Mavko et al., 1998

Table 3.3 *Velocities (km/s) for P- and S-waves, and their ratios, for carbonate minerals.*

** and references therein.*

*** calculated from the values in Table 3.2.*

Mineral	V_p *(Km/s)*	V_s *(Km/s)*	V_p/V_s	Author
Calcite	6.65	3.45	1.93	Gueguen and Palciauskas, 1994
Calcite	6.34	3.27	1.94	Marion and Jizba, 1997*
Calcite	6.64	3.44	1.93	Marion and Jizba, 1997*
Calcite	6.64**	3.44**	1.93**	Mavko et al.,1998, Sayers, 2008*
Dolomite	7.37	3.99	1.85	Gueguen and Palciauskas, 1994
Dolomite	6.93	4.23	1.64	Marion and Jizba, 1997*
Dolomite	7.35**	3.96**	1.86**	Mavko et al., 1998
Dolomite	7.05**	4.16**	1.69**	Sayers, 2008*
Aragonite	5.75	3.65	1.58	Marion and Jizba, 1997*
Aragonite	5.75**	3.65**	1.58**	Mavko et al., 1998

Table 3.4 *P-wave velocities for some rock types, and for air, water and petroleum. From Kearey et al., (2002).*

Material	V_p *(km/s)*
Limestones	2.0-6.0
Dolomites	2.5-6.5
Sandstones	2.0-6.0
Granite	5.5-6.0
Air	0.3
Water	1.4-1.5
Petroleum	1.3-1.4

3.3.2 Velocity variations due to porosity and saturation

Generally, for all rock types, velocity decreases as porosity increases. This is because the rocks will become less stiff and easier to deform, and hence the elastic moduli will decrease. Figure 3.2 a) shows a plot of velocity versus porosity for P- and S-waves for a simplified model of rocks consisting of different carbonate minerals and isolated pores. It is obvious from the figure that both mineralogy and porosity affects the velocity of a carbonate rock. The decrease in velocities for increasing porosity is approximately of same size for dolomite and calcite, but smaller for aragonite. In addition the decreases are slightly higher for P-waves than for S-waves. From zero to 25 % porosity, it can be seen that the porosity has a greater effect on the P-wave velocity (V_p) than mineralogy for dolomite and calcite, while the difference in velocity for aragonite and dolomite for any porosity (for the given range) is greater than the difference in aragonite velocity from 0-25 % porosity. For S-waves the mineralogy of calcite and aragonite gives very similar results, while dolomite gives a higher velocity, and porosity is seen to have a greater impact on velocities than mineralogy from 0-25 % porosity.

To differentiate between limestones and dolomites, the V_p/V_s relation can be useful (Rafavich et al., 1984), since even though a dolomite with a high porosity may have the same velocity as a limestone with low porosity, the relation between P- and S-wave velocities for each of them is usually different, and higher for dolomite than for limestone. This is clearly seen in Figure 3.3.

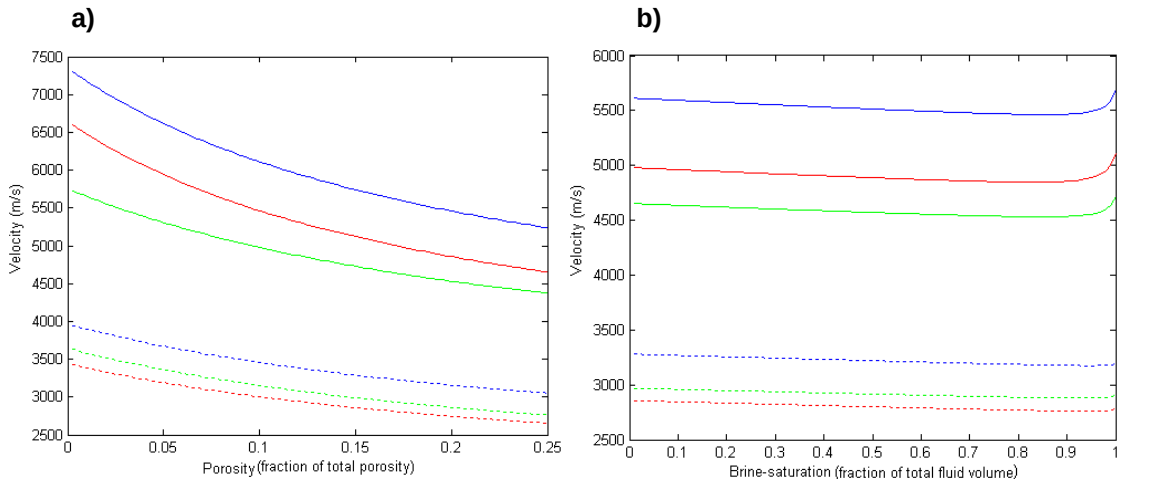

Figure 3.2 *P- and S-wave (dashed) velocities (m/s) versus porosity (**a**) and saturation (**b**) for different minerals. Calculated using the Kuster-Toksöz model, for **a)** 100 % brine saturation, and **b)** 20 % porosity.*

In Figure 3.2 b) it can be seen that the P- and S-wave velocities decrease for increasing water saturation (when the remaining pore-space is filled with gas) for P- and S-waves for all three carbonate minerals. However, for P-waves, velocities increase from about 90-100 % water saturation. For S-waves, since fluids have no shear strength, the only parameter that differs in the equation for shear wave velocity (equation 3.5) when water saturation increases, is the bulk density of the rock sample, which increases since water has higher density than gas, and thus, obviously, the velocity will decrease. For P-waves the velocity will depend on both the bulk modulus and the density of the fluid when saturation is varied. Whether the velocity increases or decreases, is thus determined by the one of the two parameters, affecting the effective values, having the greatest impact on the velocity. Increasing effective density will decrease the velocity when the elastic moduli are kept constant, while increasing the bulk modulus will increase the velocity for constant shear modulus and density.

Figure 3.2 implies that the saturation of gas and water is less important for the velocities than porosity and mineralogy of a rock.

The V_p/V_s ratios for different minerals are quite similar when varying porosity for a constant saturation, and when varying saturation for a constant porosity, and it is clearly highest for calcite, and lowest for aragonite (Figure 3.3). Thus it can be useful to study this ratio to get an idea of the mineral composition of a rock. One difference in the two plots (Figure 3.3) is seen in the V_p/V_s ratio for calcite. When varying the porosity towards higher values, the ratio for aragonite and dolomite increases, while for calcite it decreases. When varying the saturation towards higher water content for a constant porosity, the V_p/V_s ratio increases for all three minerals. Thus the V_p/V_s ratio for calcite is clearly different than for dolomite and aragonite, both because of the larger value, and because it reacts differently for variation of porosity and saturation, while for dolomite and aragonite, the result will be almost similar when reducing porosity and when reducing saturation, when starting with 20 % porosity and 100% gas saturation.

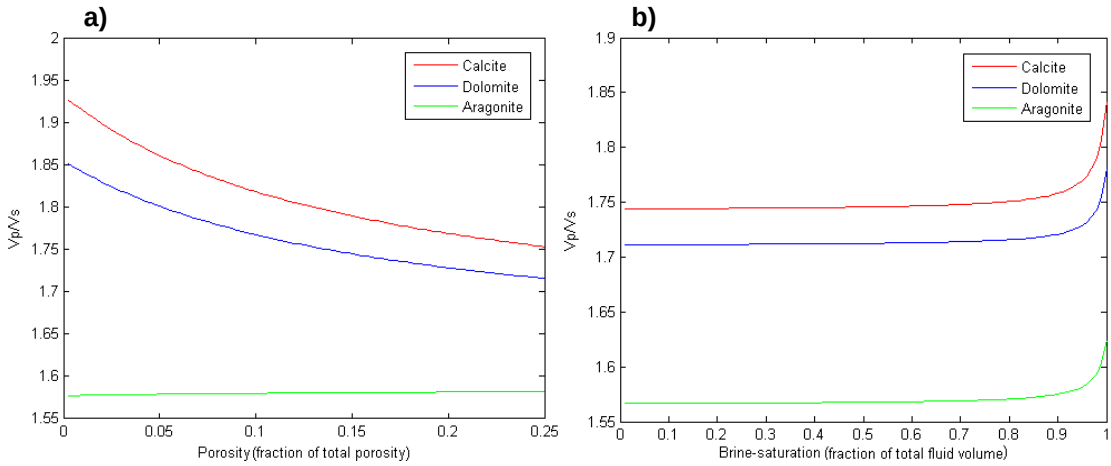

Figure 3.3 *V_p/V_s ratio for calcite (red), dolomite (blue) and aragonite (green), for variation of porosity (**a**) (100% water saturation), and variation of saturation (**b**) (20 % porosity).*

3.3.3 Velocity variations due to diagenesis

Different ranges of velocity for different rocks (Table 3.4) are as mentioned due to porosity, microstructure, mineral composition, pressure, and fluid saturation. These are values that differ due to the geologic evolution of the sediments and rocks. Compaction, cementation dissolution and dolomitization are parts of the differing evolutions (Figure 3.5). Each process affects the seismic velocity and porosity of a rock in a characteristic direction; compaction and cementation decrease the porosity and increase velocity; dolomitization may increase porosity and decrease velocity. But the timing and succession of the different processes are also important factors determining the properties of the rock. Dissolution increases the porosity, but can have only a minor effect on the velocity and acoustic impedance. This is due to preservation of elastic properties by selective dissolution, which causes the rock to maintain a framework with relatively high elastic stiffness (Anselmetti and Eberli, 1993, 1997). All the described diagenetic processes happen much faster than compaction, and this is the reason why carbonates generally show no clear correlation between seismic velocities and burial depth (Anselmetti and Eberli, 1993, 1997).

Dissolution and cementation create and destroy pore space, respectively, and may in extreme cases reverse the pore distribution, so that the minerals get dissolved and cemented in the pore space, and new pores are formed where the minerals originally existed. These diagenetic processes may also totally change the mineralogy of the rock, from calcite or aragonite to dolomite (Eberli et al., 2003). Dolomitization

may in fact increase or decrease the porosity of a rock, even though it is generally assumed to be a porosity increasing process because porosity is commonly observed to be preferentially associated with dolomite in carbonate reservoirs. In theory, approximately 12 % porosity will be created if (Mg, Ca)CO_3 replaces $CaCO_3$ mole-for-mole. This is due to the higher density of dolomite compared to calcite. However, no existing data can demonstrate that this process occurs in such a manner. If, on the other side, the dolomitization process proceeds with a net addition of CO_3, it may reduce the porosity (Lucia and Major, 1993).

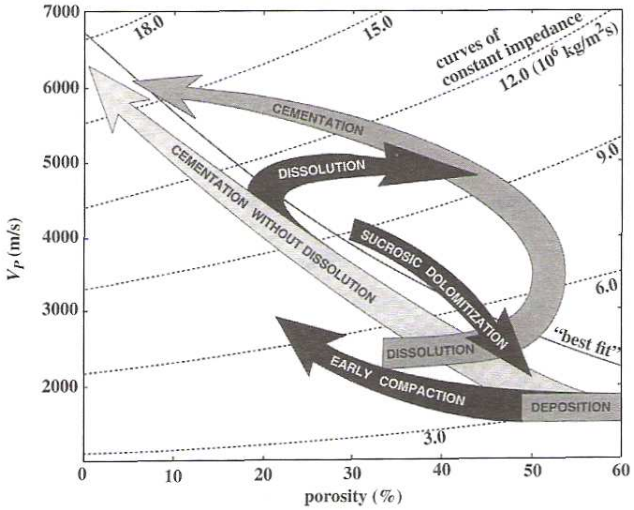

Figure 3.4 *Velocity-porosity paths of various diagenetic processes in carbonate sediments. The paths starts at deposition, and any given process may have a different position in the diagram depending on the timing of the diagenetic events, but the trend should be the same. The solid line is the exponential best-fit through all data points measured in the study (256 discrete samples from modern carbonate mud from Florida Bay, Cenozoic cores from deep drillholes of the great Bahama Bank, and Mesozoic-Cenozoic outcrops from an exhumed carbonate platform margin in central Italy); dashed curves are lines of equal impedance (calculated using the density of calcite). From Anselmetti and Eberli (1993, 1997).*

The diagenetic processes may vary as function of geological environment and setting, like for instance different facies belts of a platform (c.f. chapter 2.1.2), due to different sediment's diagenetic potential, and the different processes acting in the different settings. An example of a plot of velocities for different facies are given below (Figure 3.5), and it can be seen that velocity inversions are common in both of the two drillholes in the figure, which imply that diagenetic alterations and sediment type have a greater effect on the velocities than the burial depth. In addition, the velocities for shallow-water settings (shaded areas on the graphs) are more variable and higher than for the deeper water settings.

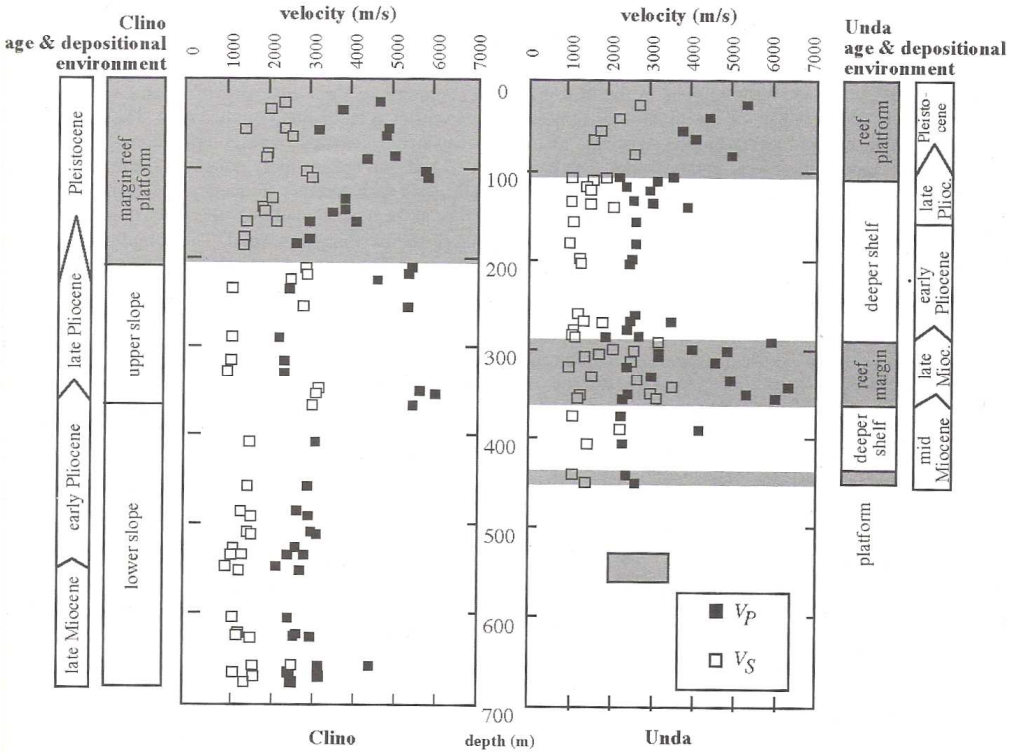

Figure 3.5 *Correlation of V_p and V_s (at 8 MPa effective pressure) with depth, depositional environment, and age of the drilled sediments from the drillholes Unda and Clino on the Great Bahama Bank. From Anselmetti and Eberli (1993, 1997).*

3.3.4 Velocity variations due to pore shapes and pressure

Even though porosity is the main controlling factor for velocities in rocks (Wang, 1997), in carbonates the pore shapes are of almost equal importance (Anselmetti and Eberli, 1993, 1997). The relation between seismic velocity and pore shapes (Figure 3.6) is due to the effects of different pore shapes on the stiffness of a rock. Flat, thin pores (cracks) are easy to deform, and rocks containing this type of pores, thus have lower velocities, while rocks containing more spherical (or moldic) pores have higher velocities because these pores are harder to deform (Wang, 1997). This fact is the reason why carbonate rocks of the same porosity and mineralogy may have great variations in seismic velocities. For example, even at porosities of less than 10 % the velocity can vary about 2000 m/s for rocks with the same chemicall composition (Eberli et al., 2003).

Pressure is an important factor affecting velocities, due to the difference in pores sensitivities to deform. Thin pores and cracks/fractures can be closed if the pressure gets sufficiently high and is applied parallel to the short axis of the crack, and thus increase the velocity. In addition, increasing pore pressure will make the pores stiffer and harder to deform, and sufficiently high pressures may fracture a rock.

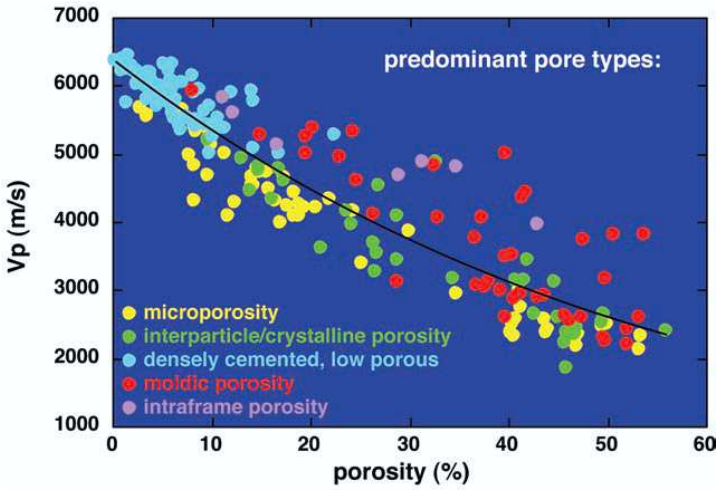

Figure 3.6 *Graph of velocity (at 8 MPa effective pressure) versus porosity of various pore types of carbonates, with an exponential best fit curve through the data for reference. The scattering of velocity at equal porosity seems to be caused by the specific pore type and their resultant elastic property. From Eberli et al. (2003).*

In Figure 3.6 it can be seen that rocks with moldic or intraframe porosity, generally have higher velocities than rocks with microporosity or interparticle porosity. Intercrystalline and intraparticle pores are usually irregular and angular in shape, and have high internal surface area (Wang, 1997), and where these pore types exist there is little or no cement or matrix (Eberli et al., 2003). These characteristics cause rocks with such pore shapes to have low seismic velocities, which are strongly dependent on the effective pressure, since increasing pressure creates better grain contacts, and makes the rock become stiffer, and thus increasing the velocity. However, this pressure effect is larger on the bulk modulus than on the shear modulus, so that the V_p/V_s ratio increases with increasing pressure. Rocks of fenestral porosity behave similarly to those of intercrystalline porosity (Wang, 1997).

A micropore has a size of approximately 10 micron, and microporosity gives a lower velocity than the general trend in a similar way as fine-grained interparticle porosity (Eberli et al., 2003).

Since moldic pores are created by dissolution of grains after or during cementation of interparticle pore-space, these pores are generally surrounded by a high amount of cement, and have regular shapes and low internal surface area (Wang, 1997), and thus rocks with moldic porosity have strong frames, and high elastic moduli and velocities. The strong frame makes the pores difficult to deform, and they are generally relatively insensitive to pressure changes. However the V_p/V_s ratio is showed to increase with increasing pressure in a gas-saturated sample, due to a lower V_s dependence on pressure (Wang, 1997).

Intraparticle or intraframe porosity is embedded in the particles or solid frame of the rock, and rocks with this porosity type show a similar velocity-porosity pattern like rocks of coarse moldic porosity (Eberli et al., 2003).

Rocks with vuggy pores have strong frames and low internal surface area to porosity ratios, and behave similarly to rocks with moldic pores; the velocities are relatively high, and the ratios of P- and S-wave velocities are relatively insensitive to pressure changes (Wang 1997).

Since channel pores are elongated (low aspect ratios), they are easy to deform, and thus have relatively low velocities. V_p/V_s ratio can change with pressure due to closure of channels (Wang, 1997).

For rocks with fracture porosity, the velocities depend on the direction of wave propagation relative to the orientation of fractures, since the fractures are easiest deformed when hit by a wave of direction perpendicular to the fracture. This kind of pores contributes little to the total porosity, but still they can decrease velocities significantly because of their high compliance. In addition, fractures can be closed when pressure increases, resulting in increasing velocities. However, most thin fractures are probably closed in rocks deeper than 1.5 km (Wang, 1997).

3.3.5 Velocity variations due to cements

Cementation stiffens a rock and increases the elastic moduli, but it is not only the amount of cement, but also the type, that affects seismic velocities in carbonate rocks. Actually experiments show that the amount of early cement in a rock does not correlate well with velocity, but different cement types affect the elastic properties of such young rocks differently. Cements may form only at the grain contacts, or along the entire grain toward the interparticle pore space either as blocky calcite or as fine aragonite needles. Such needle-like acicular cement is less efficient in building a rigid frame, than micritic or sparitic cement at grain contacts. For example only small amounts of bridging cement at grain contacts are needed to stiffen sediments enough to reach a velocity of 4500 m/s, while acicular cement that binds the grains by interlocking of crystals will not be able to make the same changes of the elastic behavior of the rock (Eberli et al., 2003).

3.4 Possible Seismic Problems for Carbonates

The main objective for exploring seismic velocity variations in rocks is the need to establish relations between different rock parameters and the velocities of the rocks, which can make us able to invert important information about the rock from velocities, such as porosity and saturation fluid, which is the main goal when exploring for hydrocarbon reservoirs. Rock physic models are constructed with the aim to enhance the correlation between internal rock properties and rock's seismic velocities. They are a tool for prediction of the velocities of a rock of given properties, and may in the inverse way help finding the properties of a rock from velocities and densities estimated from seismic data. Synthetic seismic studies can be helpful for estimation of the velocities and densities giving rise to the impedance contrasts and reflections seen in real seismic studies. Thus, if the effect of certain rock parameters on seismic properties of a rock is not well understood, this can lead to mispredictions in seismic data analysis. Eberli et al. (2003) state that most of the current theoretical rock physics equations do not, or insufficiently, account for the modification of the elastic behavior of carbonate rocks by the pore type, and consequently seismic inversion, AVO analysis, and calculations of pore volumes that are based on these equations are prone to large uncertainties in these rocks.

Some common seismic problems for carbonates have been listed by Palaz and Marfurt (1997). One problem is strong multiples from the sea bottom, when made up of a high-velocity carbonate rock. Such multiples may especially make it hard to recognize reflections from boundaries between two different carbonate layers, since the strong multiples may overwhelm the weak carbonate-on-carbonate reflections. Another problem arises from carbonates sensitivity to diagenetic alterations. This may cause lateral velocity variations in rock layers. When karsting is the result of the diagenetic processes, seismic waves passing through the karsted rock may lose much energy due to scattering, and it can be hard to recognize the lower boundary of the karsted layer and reflections below it. Yet another problem is the resolution problem caused by the high velocities and thus long wave lengths in carbonates compared to siliciclastics, since the wavelength is the result of the seismic velocity divided by frequency, and vertical resolution is simply defined as the wavelength divided by four. Thus, for a constant frequency, higher velocity will give larger wavelength and poorer resolution.

3.5 Summary

Seismic data are the visual result of reflections from rock boundaries in the subsurface. Reflection strength depends on the acoustic impedance, which is the product of seismic velocities and densities, of the rocks making the boundaries. Seismic velocities are determined by the elastic moduli and density of rocks. The densities are simply the sum of the densities for all constituents multiplied by their fractions. The elastic moduli, on the other hand, have more complicated origins. They are a result of many rock properties, like porosity, mineralogy, pore fluid type, pore form and cement type. Among these, porosity and pore form are the most significant for carbonates. Increasing porosity, results in decreasing velocities. Of the pore forms, moldic, intraframe or intercrystalline, and vuggy porosity generally give higher velocities than rocks consisting of intraframe, channel, or fracture porosity.

In addition the elastic moduli depend on pressure and temperature. Increasing pressure will increase the velocities, especially when cracks are closed.

Carbonate rocks are very sensitive to diagenetic processes which can alter their elastic properties greatly, and enhance or reduce the porosity (and density). Cementation generally makes the seismic velocities increase, while dissolution increases the porosity and decreases velocities. Diagenetic alterations are more important than burial depth for carbonates, and thus carbonates are more varied than siliciclastics, and need more advanced rock physics models to predict the relation between rock properties and velocities. The Gassmann model is easy to use, but the use of this model for carbonates is widely debated. One of the reasons for this is that low-aspect-ratio pore shapes are not handled well. Thus the Kuster-Toksöz model may be more appropriate for carbonate rocks. To consider higher-order scattering from the pores, the differential effective medium theory can be used.

It is important to keep in mind the complexity of carbonates to avoid erroneous predictions. In addition there are some common seismic problems related to these rocks, like low resolution because of the high velocities, poor imaging of karsted zones and beneath them, and strong sea bottom multiples when the seabed is carbonate.

Chapter 4: Seismic Data

Seismic data contain information about a given geologic model/field and the petrophysical parameters for this model. However, this information is not straightforward to derive. The geophysical data need to be “translated” into geological information. Many seismic attributes can be studied to derive information about the properties of rocks studied. For example, amplitude versus offset (AVO) studies are widely used for fluid detection purposes, and rock physics templates (RTP’s) can be used as a tool for prediction of lithology, porosity, and fluid type. The advantages of synthetic seismic studies are described below, as well as the utility of RTP and AVO studies. In addition, seismic data quality is briefly discussed.

4.1 Direct and Inverse Problems

Related to geophysics there are two main problems; the direct problem, and the inverse problem. The direct problem can be described as having a known geological model, and predict geophysical data related to the model (forward seismic modeling). The inverse problem is the opposite, trying to describe the geological model from seismic data (inverse seismic modeling). Seismic data are collected over an area which makes up the geological model. The rocks in the subsurface change the incident seismic waves by transmissions and reflections, giving them a specific signature, which give specific seismic responses for the specific region. This is the general case, seismic data are collected and processed, and they are to be interpreted, to get information about the geology. To guide this interpretation, one can make a synthetic geologic model based on assumptions about the real model, and perform a synthetic seismic survey over this model, and investigate the synthetic seismic data this will give. In this case the geology is known (assumed), so that the seismic results observed, directly can be traced back to the petrophysical parameters. This is useful to compare with the real seismic data in order to better understand the connection between geological features and seismic responses. With this approach one can change the synthetic model until it gives synthetic data which is approximately similar to the real data, and in thus find the true geological model.

In cases where no real survey is performed, creating synthetic seismic data can still be valuable, even though the aim is not to directly compare them with specific real data. Synthetic data can be studied aiming to better understand the connection between geologic and petrophysical parameters and seismic responses, attempting to make some general statements about this connection for different cases.

4.2 Rock Physics Templates

A rock physics template can be used as a tool for predicting different properties of rocks, like mineralogy, porosity, and saturation fluid. Such templates commonly refer to cross-plots of V_p/V_s ratio versus acoustic impedance. Estimations of these parameters are among typical outputs from elastic inversion of seismic data. Trends have to be established from data from laboratory measurements, log data, and rock physics calculations. These trends can then be utilized as basis for predicting lithology and saturation of seismic survey data.

Figure 4.1 shows an RTP including trends for various geologic parameters in sandstones and shales. Similar well-defined templates for carbonates are hard to find from published literature, and due to carbonates more prominent complexity one should not assume that they would create the same trends as observed from sandstones and shales.

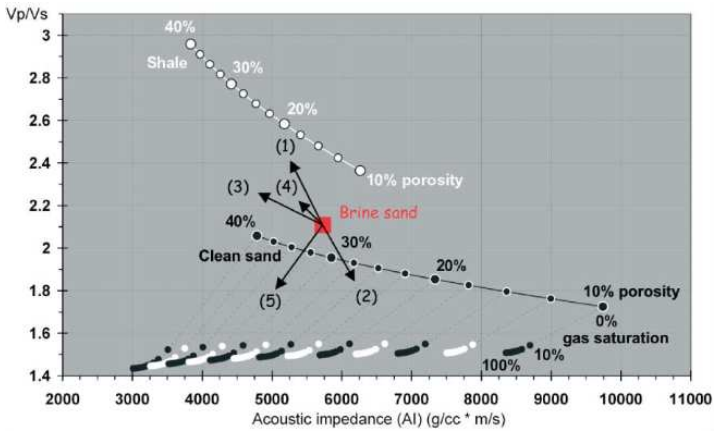

Figure 4.1 *Rock physics template in V_p/V_s versus Z cross-plot domain, which includes porosity trends for different lithologies, and increasing gas saturation for sands (assuming uniform saturation). The black arrows show the following geologic trends:* ***1)*** *increasing shaliness,* ***2)*** *increasing cement volume,* ***3)*** *increasing porosity,* ***4)*** *decreasing effective pressure, and* ***5)*** *increasing gas saturation. From Ødegaard and Avseth (2004).*

4.3 Amplitude versus Offset Analysis

As mentioned in chapter 3, the given equation for the reflection coefficient (equation 3.2) is only valid for normal incident waves. This is because different incident angles have different effects on this coefficient. Amplitude versus offset (AVO), or amplitude versus angle (AVA), is caused by the angle dependency of the reflection coefficients, as described by the Zoeppritz equations (Appendix), and is dependent on the individual rock properties.

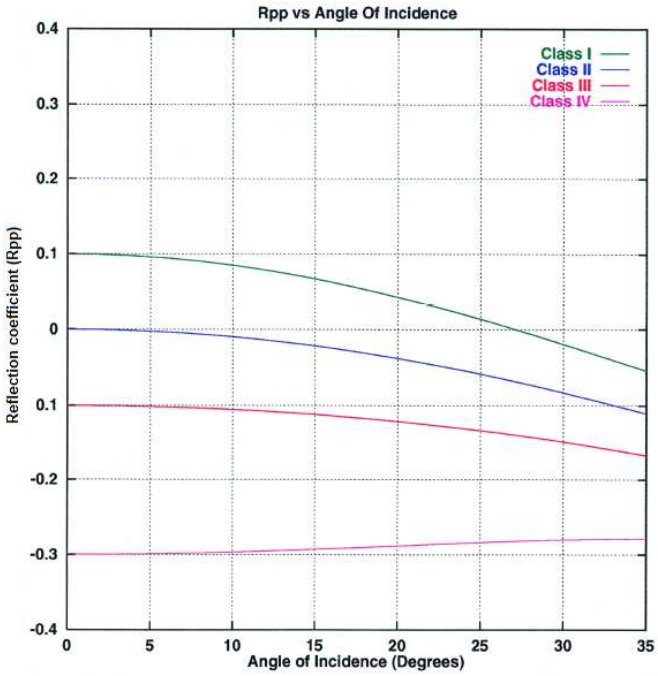

Figure 4.2 *The four basic AVO-classes. From Foster et al. (1997).*

AVO anomalies are responses which deviate from the “background” trend and they can be separated into different classes related to some specific characteristics. These classes can be separated in a reflection coefficient – offset plot (Figure 4.2), or in a gradient – reflection/intercept plot (Figure 4.3). The AVO intercept (*R*) is a measure of the normal incidence reflection coefficient, while the AVO gradient (*G*) is a measure of amplitude variation with offset. Table 4.1 lists the AVO-classes in a schematic way.

Originally Rutherford and Williams (1989) divided gas-sand reflections into three AVO classes. Class I responses have high-impedance and a positive reflection coefficient, *R*, at zero offset. The AVO gradient is negative, which means that the reflection coefficient and amplitude of reflections decrease with increasing offsets.

Class II implies close to zero impedance contrast responses, with a positive or negative zero-offset reflection coefficient, and a negative gradient. Thus the amplitude will decrease if zero-offset *R* is positive, and increase when it is negative. *R* may also change from positive to negative. Class III implies low-impedance (negative *R*) responses. The gradient for this class is also negative, meaning increasing amplitude for increasing offsets. In addition, a class IV AVO-response can be defined as consisting of responses with low-impedance and negative reflection coefficients at zero offset, but opposing to class III, the gradient is positive, which gives a less negative *R* and lower amplitude with increasing offsets. This fourth class is defined by Castagna and Swan (1997) by dividing Rutherford and Williams' class III into a class III and a class IV. Class IV responses may occur, for example, if a gas-sand is overlaid by shale with a lower S-wave velocity.

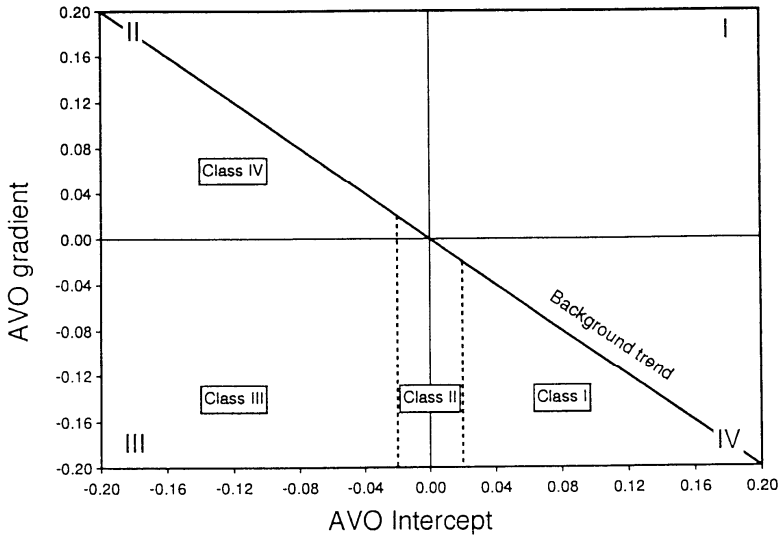

Figure 4.3 *AVO-classes defined in gradient – intercept plot. From Castagna and Swan (1997).*

Table 4.1 *AVO-classes. From Castagna and Swan (1997).*

Class	Relative Impedance	Quadrant	R	G	Amplitude vs. Offset
I	Higher than overlying unit	IV	+	-	Decreases
II	About the same as the overlying unit	II, III, or IV	+ or -	-	Increase or decrease; may change sign
III	Lower than overlying unit	III	-	-	Increases
IV	Lower than overlying unit	II	-	+	Decreases

Reflection as function of offset is dependent on *R* and *G*, and is given exact by the Zoeppritz equations (Appendix). The Zoeppritz equations give angle-dependent reflection and transmission coefficients for elastic plane waves at a non-slip horizontal boundary between two semi-infinite isotropic elastic media. However, these equations are complicated and without physical insight. A more insightful approximation (equation 4.1), which assumes small angles and V_p/V_s ratio = 2, is formed by Wiggens and published by Gelfand et al. (1986).

$$R(\theta) \approx R(0) + G \sin^2 \theta \,. \tag{4.1}$$

θ is incidence angle. The equations below define *A* and *B* for P-wave reflections:

$$R = \frac{1}{2}\left[\frac{\Delta V_p}{\bar{V}_p} + \frac{\Delta \rho}{\bar{\rho}}\right], \tag{4.2}$$

and

$$G = \frac{1}{2}\frac{\Delta V_p}{\bar{V}_p} - 2\left(\frac{\bar{V}_s}{\bar{V}_p}\right)^2 \left(2\frac{\Delta V_s}{\bar{V}_s} + \frac{\Delta \rho}{\bar{\rho}}\right). \tag{4.3}$$

ΔV_p and ΔV_s are the differences between velocities for lower and upper layer for P-waves and S-waves, respectively, and $\bar{V}_p$ and $\bar{V}_s$ is the average velocities for upper and lower layer for P-waves and S-waves, respectively.

4.3.1 Information from AVO analysis

Amplitude variations with offset are being analyzed with purpose to detect some characteristic feature or property of a rock layer with respect to lithology or saturating fluid. AVO interpretation is frequently used for fluid detection purposes since different saturation fluids affect the wave propagation through a rock differently for a range of offsets or incident angels. However, both hydrocarbon- and brine-saturated rocks may show increasing or decreasing AVO (Castagna and Swan, 1997).

Concerning carbonates, Li et al. (2003) claims that AVO variations are small for brine saturated reservoirs. In addition, the effects of different pore forms can be much stronger than the fluid effect on the wave propagation, and are also greater on the ultrasonic velocity changes than the effect of seismic dispersions. The same result is expected for seismic frequencies when pore structure variations are on a scale

comparable with seismic wavelength (Sun, 2004, and references therein). Due to this strong effect of pore structure on wave propagation, it may be impossible to detect fluid type from AVO analysis for carbonates with various pore structures, but for rocks with porosity consisting of micro-pores it may be quite possible to differentiate between water and gas saturation (Sun, 2004). However, different pore structures may give distinctive critical incidence angles (this angle is defined below). Thus, it could be possible to detect the pore structure type from AVO analysis, and this would be useful for porosity inversion and possibly to derive permeability from seismic data (Sun, 2004).

Li et al. (2003) have shown that all four AVO classes can be found in limestone/dolomite interfaces, and further they state that a class I AVO response represents a tight reservoir in carbonate, while class III and IV represent good reservoirs. They have also made an observation that a class III response at the base of a gas saturated reservoir changes to a weak class II response when the gas is substituted with brine. Further, Foster et al. (1997), claims that class I responses are easily generated at major lithology impedance boundaries.

4.4 Seismic Data Quality

4.4.1 Seismic resolution

“Resolution is the ability to separate two features that are very close together; the minimum separation of two bodies before their individual identities are lost” (Sheriff, 1991). Vertical resolution from a seismic perspective is thus the ability to for example separate two different layer interfacies, and is generally taken to be 1/4 of a wavelength. However, the detection limit can be as low as 1/30 (Sheriff, 1989). That is, two different reflectors can be separated if the spacing between them is no less than 1/4 of a wavelength, while one single layer can be detected when the layer thickness is above 1/30 of a wavelength. The wavelength (λ) is dependent on the frequency (f) of the wavelet and the seismic velocity (V) of the rock:

$$\lambda = \frac{V}{f} . \tag{4.4}$$

Thus, higher frequencies give better resolution. However, the energy loss is greater for higher frequencies, and the reflections will be weaker when there is less energy to reflect.

The seismic wave does not get reflected from an exact infinitesimal point on a reflector, but rather from a small zone, due to scattering of the ray in this zone. Horizontal resolution is the width of this reflection-zone, known as the Fresnel zone, from which energy is reflected. The width of the Fresnel zone is defined as:

$$w = \sqrt{2z\lambda} \ , \tag{4.5}$$

where z is the reflector depth.

As an example, if a reflector has a depth of 1000 m, and the overlying rock has a velocity of 4000 m/s, and a wavelet of 40 Hz is used, the vertical resolution will be 25 m, and the horizontal resolution will be 447 m. Thus geological features have to be larger than these sizes to be recognizable from seismic data.

In addition the horizontal resolution depends on the receiver spacing. The length of a reflector detected by any receiver spacing, for a flat reflector, is half the spacing length (Kearey et al. 2002).

4.4.2 Energy loss

A seismic wave's energy loss is caused by geometrical spreading and absorption. Geometrical spreading is the spherical spreading of the energy from the source, and the energy loss due to this is r^{-2}, where r is the radius of the wave-front. The amplitude of the wave decreases as r^{-1}.

Absorption of energy during transmission is due to internal frictional losses in the rock. The absorption per wavelength is constant, and thus the energy loss for a wave transmitted a certain distance is higher for higher frequencies (higher frequencies produce smaller wavelengths).

4.4.3 Critical angle

When a seismic ray hits an interface between two layers, or a reflector, it can get reflected, transmitted or refracted (Figure 4.4). Actually refraction means the changing of direction of a wave as it enters the medium below the interface. Thus, the transmitted wave is refracted except when the incident wave is normal. However, the

term “refracted ray”, is often used for the refraction that happens at critical angle of incidence (θ_c):

$$\theta_c = sin^{-1}(V_1/V_2) \ , \tag{4.6}$$

where V_1 and V_2 are the velocities of the layer above and below the interface, respectively, and the angle is measured between the incident ray and the normal to the layer (greater offsets give greater incident angles). At this incidence angle, the refracted wave travels along the boundary between the two layers and generates a head wave (Figure 4.4). This only happens when V_2 is greater than V_1. The head wave travels forward in the upper layer with velocity V_2, and may interfere with the reflected waves giving a result as in Figure 4.5.

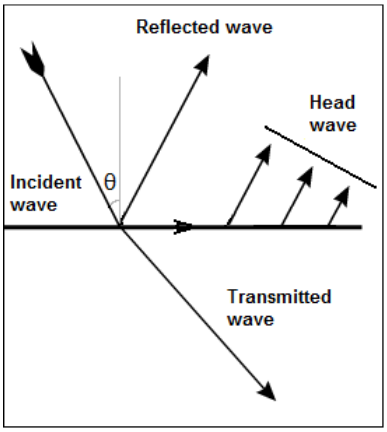

Figure 4.4 *Different possible ray paths for a ray hitting an interface between two layers. Modified from Mjelde (2009).*

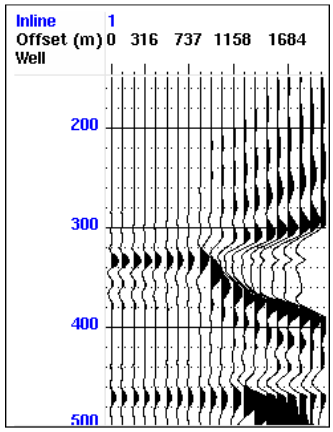

Figure 4.5 *Distortion of seismic traces due to head wave.*

Chapter 5: Model and Input Parameters

The geological model used as basis for synthetic seismic modeling is presented below, as well as the values used as input parameters. These values, as well as the limitations and assumptions incorporated in the model, will be discussed. Finally, there will be a discussion concerning the differing results achieved from DEM versus Gassmann calculations.

5.1 The Geological Model

The geological model used in this project is based on a model from Droste and Van Steenwinkel (2004), which is a north-south schematic geological cross section through the Cretaceous carbonate platform of Oman (Figure 5.1).

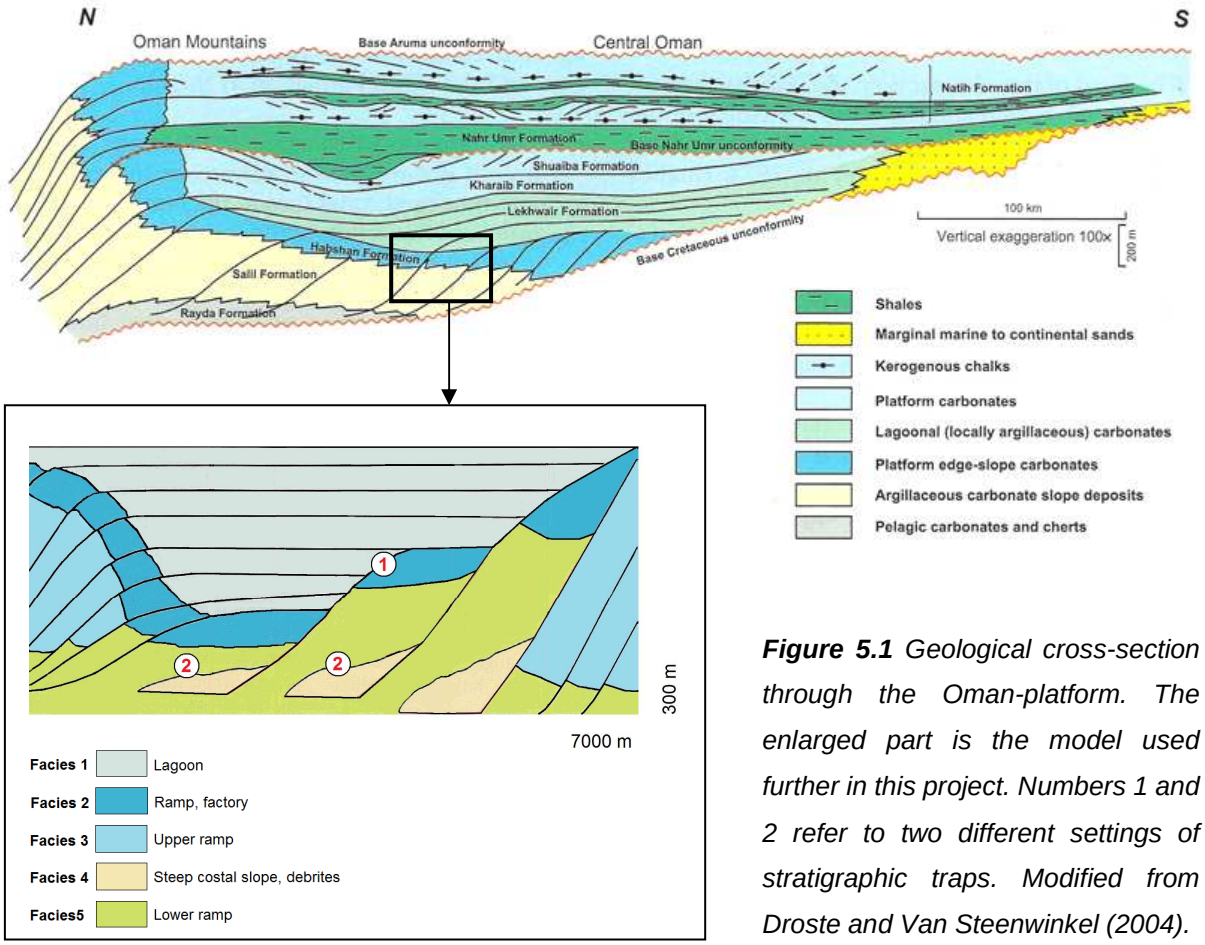

Figure 5.1 *Geological cross-section through the Oman-platform. The enlarged part is the model used further in this project. Numbers 1 and 2 refer to two different settings of stratigraphic traps. Modified from Droste and Van Steenwinkel (2004).*

The enlarged simplified part of the figure, consisting of five different facies, is the model used in this project. Two different settings of stratigraphic traps are marked as 1 and 2. 1 is ramp reservoir facies sealed by lagoon and lower ramp facies, while 2 are two cases of debrites sealed by lower ramp facies.

This model is chosen to be used for this project because it consists only of carbonate facies. It is only used to study seismic responses for different carbonate facies and petrophysical parameters. Thus, the aim is not to study this specific region, even though the model is a real geological model. The model has been simplified to ease the seismic modeling. There is no vertical or lateral velocity changes in any facies, and in addition the transition zones between facies of sediments deposited at the same time in one deposition cycle have been defined as interfacies between two different facies, for instance upper and lower ramp facies, instead of being gradual transitions between those two as they would be in a real setting. In addition ramp facies have been used in the model rather than platform facies, even though a ramp has a less steep incline than a platform. These simplifications and modifications will not have any important impact on the study, since the aim is to make a general analyze of the seismic responses between different carbonate facies, and not to study this specific geologic region.

Table 5.1 *Paleo-environments and lithologies for facies 1-5.*

Facies	Paleo-environment	Lithology
1	Lagoon	Mudstone
2	Ramp, factory	Grainstone/rudstone
3	Upper ramp	Grainstone-packstone-wackestone-mudstone
4	Steep costal slope, debrites	Matrix-supported conglomerate
5	Lower ramp	Mudstone-wackestone-packstone-grainstone

The simplified model consists of five different facies; lagoon; ramp, factory; upper ramp; steep costal slope, debrites; and lower ramp, which are termed facies 1-5, respectively. Their lithologies are listed in Table 5.1. Initial values for velocities, densities, elastic moduli, and porosities for the facies are listed in Table 5.2. These values are derived from measurements performed by Soltveit (2007) (facies 2 and 4) and Fischer et al. (1997) (facies 1, 3, and 5), which are used as guiding values, and

their original measurements are listed in Appendix. The values for facies 2 and 5 are measured in dry state.

Table 5.2 *Velocities, densities, elastic moduli, and porosities for facies 1-5.*
**dry values.*

	1	2	3	4	5
V_p (m/s)	5164	4144*	3616	3661*	5000
V_s (m/s)	2673	2559*	1902	2341*	2675
ρ (kg/m^3)	2650	2225*	2450	2344*	2470
K (GPa)	45.42	18.78*	20.21	14.28*	38.26
μ (GPa)	18.93	14.56*	8.87	12.85*	17.72
φ (%)	5.5	17.8	21.5	13.4	9.0

Soltveit (2007) has given an estimate of mineral composition from studying thin sections, and due to these estimates, facies 2 and 4 have been given a mineral composition consisting of 95 % calcite and 5 % quartz in. The mineralogies, and elastic moduli and densities for each facies' matrix, are listed in Table 5.3. Mineral compositions for facies 1, 3, and 5 have been estimated according to the measured values listed in Table 5.2 (details for these estimates are described in chapter 1).

Table 5.3 *Matrix properties for facies 1-5. Values for calcite and dolomite corresponds to the values listed in Table 3.2 from Mavko et al. (1998), while for quartz K = 37.00 GPa, μ = 44.00 GPa, ρ = 2650 kg/m^3, and for clay K = 13.43 GPa, μ = 5.9 GPa, ρ = 2457 kg/m^3. Letters indicate the following minerals:* ***C****: calcite;* ***D****: dolomite;* ***Q****: quartz; and* ***Cl****: clay.*

	1	2	3	4	5
Mineralogy	0.77 C	0.95 C	0.88 D	0.95 C	0.81 C
(volume fraction)	0.23 D	0.05 Q	0.12 C	0.05 Q	0.19 Cl
K_m (GPa)	80.64	73.85	92.55	73.85	52.63
μ_m (GPa)	34.63	32.52	43.20	32.52	22.21
ρ_m (kg/m^3)	2747	2707	2851	2707	2662

5.2 Saturated Model

To make synthetic seismic data from the model, the dry facies need to be populated with a saturating fluid. To simulate a burial depth of 2 km (which is roughly the depth of

the origin of facies 1, 3 and 5), the physical properties (like elastic modulus and density) of a fluid consisting of 95 % brine and 5 % gas were calculated according to this depth, using the model of Batzle and Wang (1992). For facies 5 the fluid consists of 50 % brine and 50 % gas in order to match the very low saturated density measured for this facies, and still have high enough elastic moduli to fit the measurements. However, this facies will be saturated with the same fluid as the other facies for the modeling in chapter 6, because the geological model geometry used in this project contains no trap structure supporting gas accumulation in facies 5.

The temperature used for calculation of fluid properties at 2 km depth is set to be 59 ℃, according to the average global geothermal g radient, which is about 2.6 ℃/100 m (Selley, 1998) (and assuming a surface temperature of 7 ℃). The pore pressure is set to be 20 MPa according to a gradient of 0.45 psi/ft for hydrostatic pressure for water with 5.5% dissolved salts (Selley, 1998). Figure 5.2 illustrates the relation between the concepts of hydrostatic pressure, lithostatic pressure, pore pressure, and overpressure. Hydrostatic pressure is the pressure at a given depth corresponding to the weight of an overlying water column. This is the same as the pore pressure if the pore space is open and the pore fluid is free to flow. The lithostatic pressure, or the overburden stress, is the pressure corresponding to the weight of overlaying lithology. If the pore fluid is not free to flow, e.g. in a sealed layer, there will become an overpressure in this layer, and the pore pressure will have a value between that of the hydrostatic pressure and the overburden stress. The magnitude of the overpressure is the value of the pore pressure minus hydrostatic pressure, while effective pressure is the value of the overburden stress minus the pore pressure.

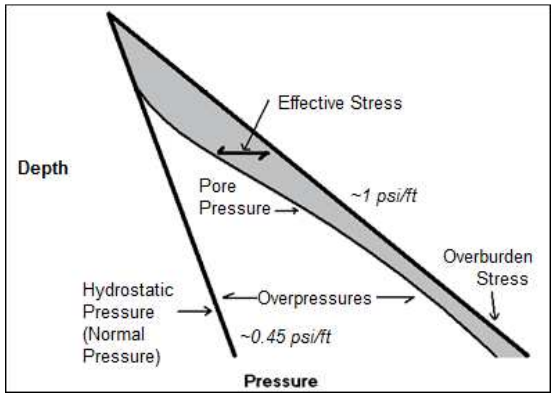

Figure 5.2 *Relations between hydrostatic pressure, pore pressure, overburden stress, effective stress, and overpressure. Modified from Bruce and Bowers (2002). Gradients derived from Selley (1998).*

Brine salinity is set to 5.5 % according to the gradient used for calculating hydrostatic pressure, and the specific gravity for gas is set to be 0.6. The density and bulk modulus of a fluid with these specifications of temperature, pressure, salinity, and specific gravity, and the given volume fractions of gas and brine, thus is 985.7 kg/m^3 and 0.64 GPa, respectively, calculated as Reuss' average.

Table 5.4 *Values for saturated facies 1-5, at 2 km depth (saturated with use of DEM).*

	1	2	3	4	5
V_p (m/s)	5164	4147	3616	4197	5000
V_s (m/s)	2673	2499	1902	2445	2675
ρ (kg/m^3)	2650	2400	2450	2480	2470
K (GPa)	45.42	21.30	20.21	23.89	38.26
μ (GPa)	18.93	14.99	8.87	14.80	17.72
V_p/V_s	1.93	1.66	1.90	1.72	1.87

Populating the dry facies with this fluid gives the values given in Table 5.4. These calculations are performed with the DEM approach. The highest P-wave velocity is in the lagoon facies (1), while the lowest is in upper ramp (3). From the table it can be seen that while saturation of facies 2 increases the P-wave velocity only with 3 m/s, saturation of facies 4 (same mineralogy as facies 2), increases V_p with 536 m/s. This can not only be explained by the higher porosity of facies 2 relative to facies 4, which causes a larger increase in density for facies 2. The additional explanation is the significantly greater increase in bulk modulus for facies 4 than for facies 2 (shear modulus for both facies have only slightly increased). This difference can be explained due to the different pore shapes assigned to these facies (Table 5.5). Facies 2 is the only facies which have no pores with aspect ratios lower than 0.1. This is the reason why the bulk modulus increase is only minimal when saturating the rock. Due to the fact that pores deform more easily when having lower aspect ratios, the pore fluid will increase the stiffness of such soft pores more than for more spherical pores, since these initially have greater stiffnesses. This is the reason why bulk modulus clearly increases less from dry to saturated state for facies 2 than for facies 4, even though this facies has a higher porosity than facies 4.

Table 5.5 *Pore forms, and their percentages of total porosity for facies 1-5.*

Pore-model	Percentage of total porosity	Aspect ratio
1	95 %	0.16
	5 %	0.00145
2	80 %	0.1
	20 %	1.0
3	61 %	1.0
	36 %	0.1
	3 %	0.00177
4	79 %	1.0
	21 %	0.016
5	99.8 %	1.0
	0.2 %	0.001

The pore forms assigned to every facies is derived by choosing the aspect ratios and the fractions of the total porosity of these which will give the same velocities and elastic moduli as the measured ones. Soltveit (2007) has described porosity types from thin sections in her study, and has stated that for the sample defined as facies 2 here, the predominant pore type is vuggy pores. From Figure 2.8 and 2.9 it is seen that vuggy pores may have relatively high aspect ratios (~0.1-1.0), thus the pore forms defined in Table 5 for facies 2 is consistent with the thin section observations. Soltveit (2007) has also stated that for the rock sample which facies 4 is derived from, interparticle pores are abundant. Such pores may be quite spherical in form (Figure 2.9), although irregular. Thus defining 79 % of the pore space in facies 4 to have aspect ratio 1.0 is fairly consistent with most of the pores being interparticle pores.

Porosity for facies 5 has been defined as mostly spherical pores and some cracks. Since this is the facies originating from the location most offshore, only small particles will settle here, compared to larger shell fragments in other facies, and thus the pores are defined as mostly spherical.

5.3 DEM versus Gassmann

As described in chapter 3, there are some basic differences between DEM and Gassmann methods. A short evaluation will be done here, comparing results from these two methods when substituting fluids in the 5 defined facies. Kumar and Han (2005) have suggested that DEM should be used when calculating dry moduli, and saturation of the rocks should be done using Gassmann calculations. An important difference between these two calculation methods is the fluid effect on shear moduli. Using DEM, fluids will affect shear moduli, while according to Gassmann theory it remains constant for saturation of all fluids and for dry rocks. Thus, since fluids have no

shear strength, it seems reasonable to use Gassmann for fluid substitution. The reason for this evaluation of the two methods is due to possible differences for the original saturated and the original dry facies, since DEM give a greater fluid effect than Gassmann (as seen below). While original dry facies can get saturated in one step, original saturated facies need two steps when using Gassmann, while one if DEM is used. When applying Gassmann for fluid substitution, dry moduli is needed as input. Thus, dry moduli must be calculated either by DEM calculations or from Gassmann equations. But, since DEM gives a greater fluid effect than Gassmann, it would not be appropriate using one method for the calculation of dry moduli from saturated values, and the other for saturation. Thus, only one of the methods should be used for both steps, and the same method should be used for the original dry facies. However, this could result in some differences between originally dry and originally wet facies if the methods under- or over-estimates the effects of fluid substitutions.

Figure 5.3 shows velocities and velocity ratios for saturation with different fluids of facies 1-5, in addition to dry values. It can be seen that most of the P-wave velocities are higher when calculated by DEM than by Gassmann equations. However, dry and gas-saturated values for facies 1 and 3 are clearly higher when calculated by Gassmann equations. Both of these facies originally have saturated input values with an assumed fluid composition of 95 % brine and 5 % gas. The observed deviations can thus be explained as DEM giving higher fluid effects than Gassmann. Thus, substituting the fluid with a less dens fluid or extracting the fluid, results in lower velocities applying DEM than Gassmann. Facies 5 is also an initially saturated facies, but shows no deviations like for facies 1 and 3. In fact, values for saturation of all fluids and dry values for facies 5 are approximately the same calculated by both methods. This can be explained by this facies low porosity and its pore-model, consisting almost entirely of spherical pores with high stiffnesses, which cause fluid effects to have little additional effects on rock stiffness.

Contrary, facies 1 and 3 have pore-models consisting of small, but significant, amounts of very low aspect ratio pores. Thus, saturating these with an incompressible fluid compared to dry or gas saturated pores, will have greater increase on rock stiffness than when saturating pores of higher aspect ratios, which have significantly higher dry stiffnesses.

As mentioned in chapter 3, Gassmann assumptions get violated when pores have low aspect ratios, like cracks, and thus this may also be a reason for deviations for facies 1 and 3 in Figure 5.3.

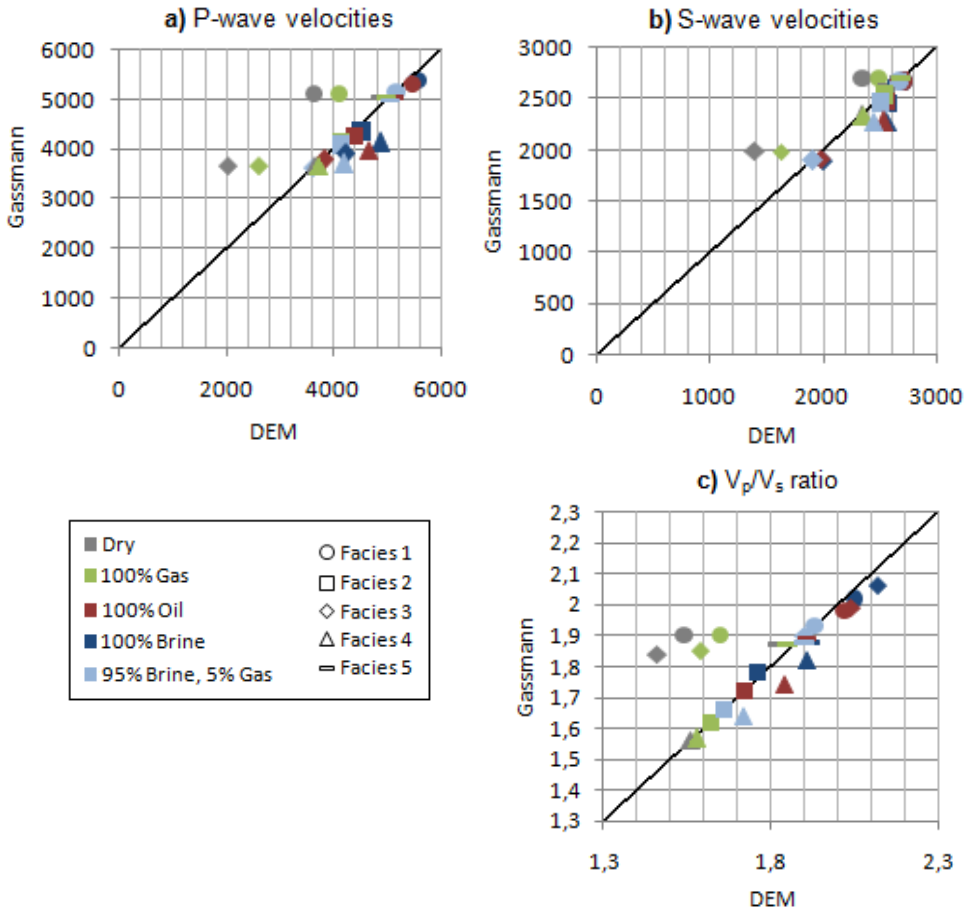

Figure 5.3 *Cross plots of Gassmann versus DEM calculated properties for facies 1-5 saturated with different fluids; gas; brine; oil; and a mixture consisting of 95 % brine and 5 % gas. In addition dry values are calculated. Velocities are in m/s.* ***a****) P-wave velocities,* ***b****) S-wave velocities, and* ***c****) velocity ratio. The line represents all points where data obtained from Gassmann and DEM are coincident. Points above this line have velocities that are higher from Gassmann than from DEM, and vice versa.*

Shear modulus remains unchanged for all saturations and dry rock according to Gassmann theory, thus only densities affect the S-wave velocities for variation of fluids, and denser fluids result in lower velocities. When using DEM for the same calculations, shear modulus, in addition to density, increase for denser fluids, thus giving higher, lower or similar velocities for different saturation fluids. The comparison of Gassmann and DEM calculated S-wave velocities (Figure 5.3 b), shows a quite

similar trend as P-wave velocities. All S-wave velocities are higher calculated by DEM than by Gassmann, except velocities for facies 1 and 3 saturated with gas and when dry. While the general trend for DEM calculated S-wave velocities, is increasing velocity as saturation fluids get denser, the opposite is true for Gassmann calculated velocities.

V_p/V_s ratio is an important relation for AVO outcome. In Figure 5.3 c) it can be seen that this ratio is quite similar for Gassmann and for DEM calculated results for varying saturation fluids. Again dry and gas saturated facies 1 and 3 get clearly higher values calculated by Gassmann equations than by DEM. For both calculation methods, the general observation is higher velocity ratio for denser saturation fluids.

Facies 4 shows deviations both when looking at velocities and V_p/V_s ratio, and gets slightly higher values from DEM calculations than from Gassmann, when saturated with denser fluids than gas. These deviations for this original dry facies can also be explained partly by the differing fluid effect from the two calculation methods, although results for the other originally dry facies (facies 2) is approximately the same for both methods. Again, the different results for these two facies, which have the same mineralogy, may be explained by pore shapes.

It is not possible from this comparison to say which method ensures the most correct results, but it it obvious that the general observation is that greater variations for saturation of different fluids are obtained by DEM than by Gassmann.

For calculations performed to reveal the results in the next chapter, DEM will for practical reasons be used for saturation when considering porosity, pore shapes, and mineralogy, while Gassmann will be used when considering saturation effects, and depth effects, since these studies include fluid substitutions. For all other calculations than those concerning fluid substitutions, a fluid consisting of 95 % brine and 5 % gas will be used as satutation fluid. Differences between Gassmann and DEM velocities for facies saturated with this fluid are seen to be small in Figure 5.3, and results from DEM are thus expected to be as reliable as Gassmann results.

The reason for choosing Gassmann theory for fluid substitution is that for DEM data, shear modulus is affected by fluid substitution, which contradicts the general assumption that fluids have no shear strength and thus do not affect effective shear modulus of the rock. As discussed in chapter 3, effective shear modulus has in some studies been observed to get altered by fluids, and thus shear wave velocities from DEM calculations are not necessarily erroneous in all cases. However, if such

fluid-rock interactions were to be incorporated in the calculations, it should be done in a controlled manner, rather than using DEM values, which simply gives higher effective shear modulus for denser fluids.

Chapter 6: Rock Physics Modeling Results and Analysis

In this chapter effects of variations of different parameters on seismic attributes and imaging are studied. The following subjects will be looked into:

- porosity and pore shape effects
- mineralogy effects
- fluid and saturation effects
- pressure and depth effects
- resolution

The main purpose is to explore the effects of intrinsic rock parameters like porosity, pore shapes and mineralogy on seismic responses. Since fluid detection generally is a main purpose for seismic exploration, fluid effects will be studied next. Of interest is then to reveal if fluid effects can be differentiated form the other factors, and how other factors may affect fluid responses. Thereafter effects of the extrinsic factors pressure and depth will be looked into. Finally, resolution issues will briefly be mentioned, but first of all, initial values and modeling aspects need to be specified.

6.1 Initial Values and Modeling Specifications

Velocity variations due to variations of the mentioned factors will be examined, as well as velocity ratios and acoustic impedances with the aid of rock physics templates. In addition effects on AVO responses will be studied. All acoustic impedances will be calculated for P-waves, and only P-wave AVO responses (not converted P-waves) will be considered.

When studying the effects of various parameters for the different facies defined, this will reveal possible effects of different lithologies on the results, and thus give a broader understanding of sensitivity of seismic responses for variations of different rock-affecting parameters, than if only looking at one defined lithology. Thus, all facies will be studied, although some will be studied in more detail for some parameters.

Two wells have been defined in the model presented in chapter 5, and are showed in Figure 6.1. Facies values calculated for 2 km burial depth and a saturation fluid consisting of 95 % brine and 5 % gas are referred to as original values and, unless stated otherwise, are the ones concerned. The carbonate model is buried beneath a homogenous sandstone (V_p: 3000 m/s, V_s: 1732 m/s, ρ: 2000 kg/m^3. At 4 km depth V_p: 4600 m/s, V_s: 2850 m/s, ρ: 2410 kg/m^3).

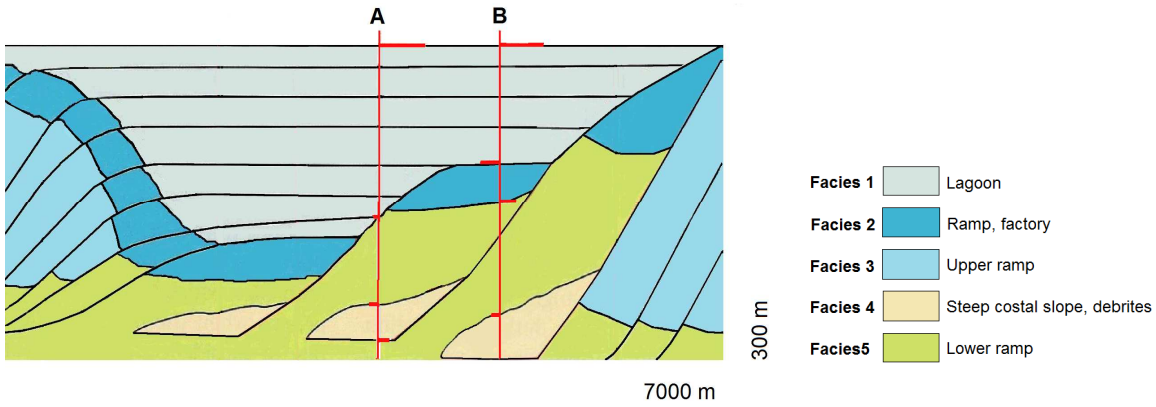

Figure 6.1 *Carbonate model with wells A and B, and their reflectivity logs. Modified from Droste and Van Steenwinkel (2004).*

Initial velocities and velocity ratios (saturated, 2km depth) for facies 1-5 are showed in Figure 6.2, plotted against porosities. Clearly there is a trend of decreasing velocities as porosity increases. This trend is more significant for P-waves than for S-waves. Thus, as seen, V_p/V_s ratio decreases for increasing porosity. However, results for facies 5 deviates from this trend.

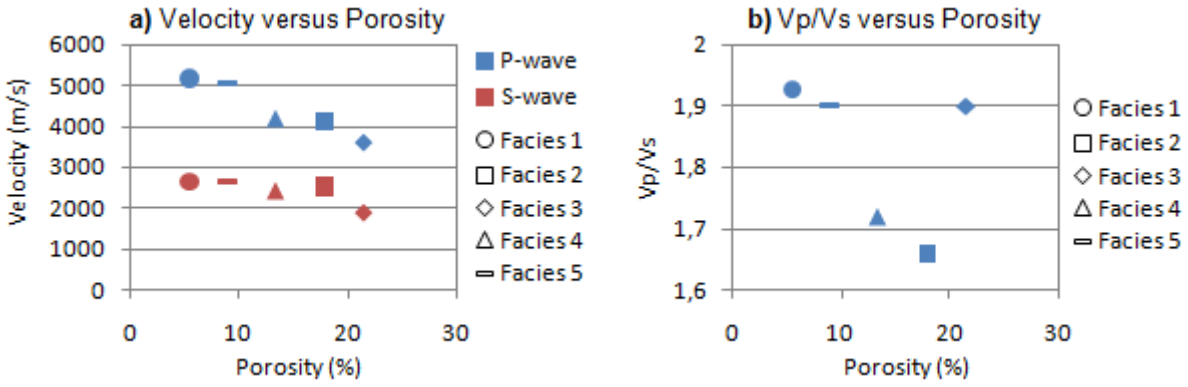

Figure 6.2 a*) Velocity, and* ***b****)* V_p/V_s *ratio versus porosity for saturated facies at 2 km depth.*

6.2 Porosity and Pore shapes

As stated in chapter 3, both porosity and pore shapes affect the P- and S-wave velocities of a porous rock, and it may be hard to estimate the porosity and pore-model from given velocities, since they both can affect the velocities in a quite similar range.

6.2.1 Velocities and acoustic impedances

To evaluate effects of porosities and pore-models individually, different pore-models (Table 6.1) are assigned to facies 4, keeping the porosity and mineralogy constant at the original values for 2 km depth (listed in Table 5.4, except for facies 5 which has the following values when saturated with the same fluid as the other facies: V_p = 5062 m/s, V_s = 2666 m/s, ρ = 2510), and next the porosity is varied while keeping the pore-model and mineralogy constant. Figure 6.3 a) and b) show the resulting P-wave velocities (V_p) and S-wave velocities (V_s) for variations of pore-models and porosity, respectively. The original pore-model for facies 4 (Table 5.5) is termed F-4. Variations in V_p due to pore-model changes are approximately as high as1500 m/s, while for V_s it is about 500 m/s. When varying porosity from 4-17% (original value is 13.4 %) similar velocity ranges can be observed, although variations are slightly higher: near 2000 m/s for P-waves, and 1000 m/s for S-waves. Velocities decrease as porosity increases.

Even though the velocity changes may be quite similar for porosity- and pore-model-variations, one difference between the two is the effects on density. Density remains unaltered when varying pore-models, while it varies when varying porosity. Thus, the acoustic impedance variations will only be due to velocity changes when varying pore-models, while when varying porosity the variations will in addition be caused by density changes.

Table 6.1 *Definitions of different pore-models according to their pore aspect ratios and fractions of these of total porosity.*

Pore-model	Percentage of total porosity	Aspect ratio
1	95 %	0.16
	5 %	0.00145
2	80 %	0.1
	20 %	1.0
3	61 %	1.0
	36 %	0.1
	3 %	0.00177
4	79 %	1.0
	21 %	0.016
5	99.8 %	1.0
	0.2 %	0.001

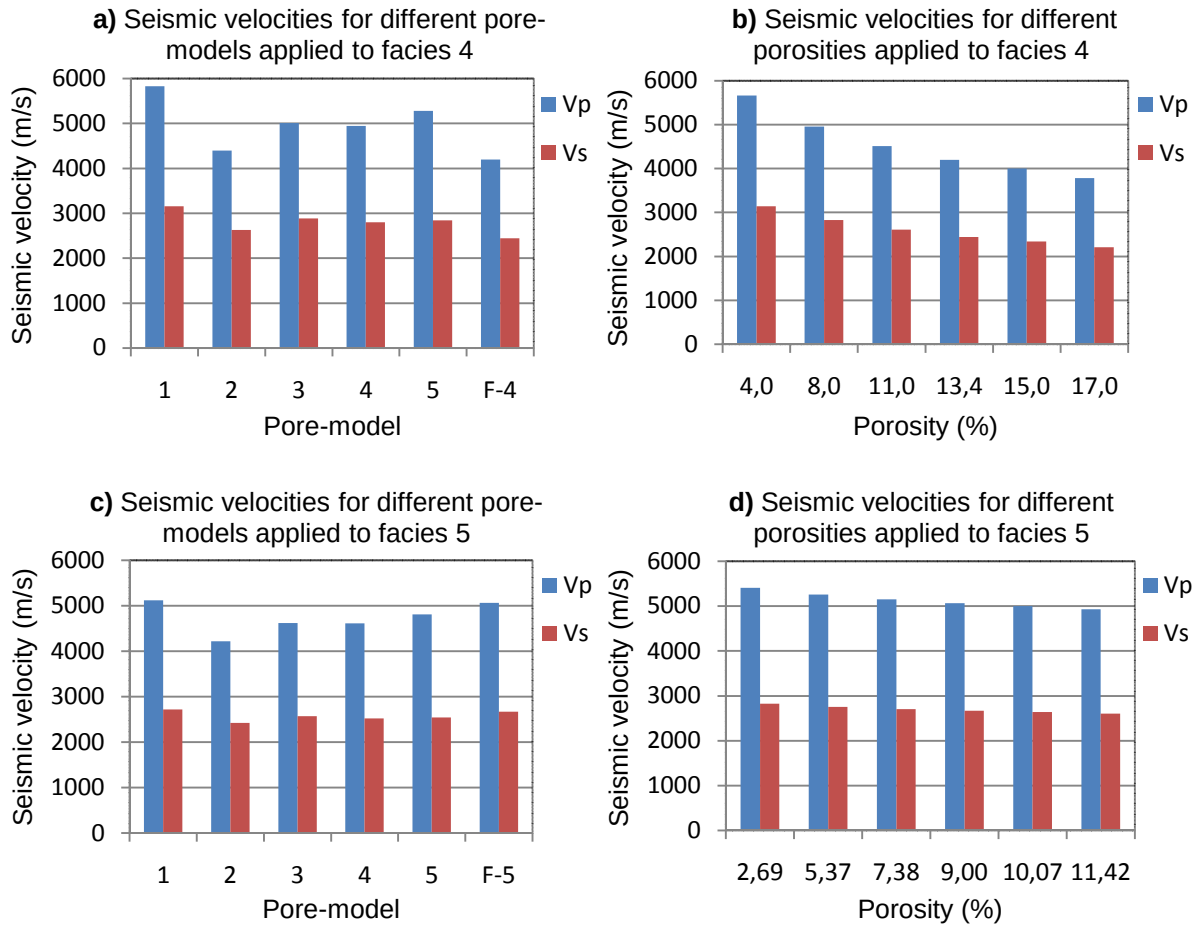

Figure 6.3 *Velocity variations for P- and S-waves due to variation of pore-models in* ***a****) facies 4, and* ***c****) facies 5, and due to variation of porosity in* ***b****) facies 4, and* ***d****) facies 5. Original pore-models for facies 4 and 5 are termed F-4 and F-5, respectively, and original porosities are 13.4 % for facies 4 and 9 % for facies 5. Pore-model specifications can be found in Table 6.1, and Table 5.5 (F-4 and F-5).*

From Figure 6.4 it can be observed that it is not straightforward to differentiate between porosity changes and pore-model changes in a rock physics template. The acoustic impedance (AI) and V_p/V_s ratio varies for both cases. As porosity increases, acoustic impedance and velocity ratio decrease. Changes in acoustic impedance are more prominent than V_p/V_s ratio variations. The defined pore-models result in values not too far from those for varying porosity. A trend cannot be defined for these pore-models due to their small number, and the lack of a gradual change from one model to the next. Nevertheless, it can be seen that pore-models containing significant amounts of spherical pores give velocity ratios above the trend-line for decreasing porosity. Highest V_p/V_s ratio is achieved for pore-model 5, the only model consisting of a fraction of 0.001 aspect ratio pores.

Next, the same variations are done for facies 5. Since facies 5 has a different

mineralogy than facies 4, comparing the results from these two facies will allow an evaluation of the consistency of the results for V_p and V_s, and the ratio of these, and AI, for variations of pore types and porosity, for different mineralogies. Porosities applied to facies 5 are not the same as those applied to facies 4, but rather of the same percentages of the original porosity as the porosities applied to facies 4.

The velocity variations in facies 5 are plotted in Figure 6.3 c) and d). From this figure the main observation is that the variations in velocities are about the same as for facies 4, both when varying pore-model and when varying porosity. However, one difference is that the velocity-decrease with increasing porosity is less significant for facies 5.

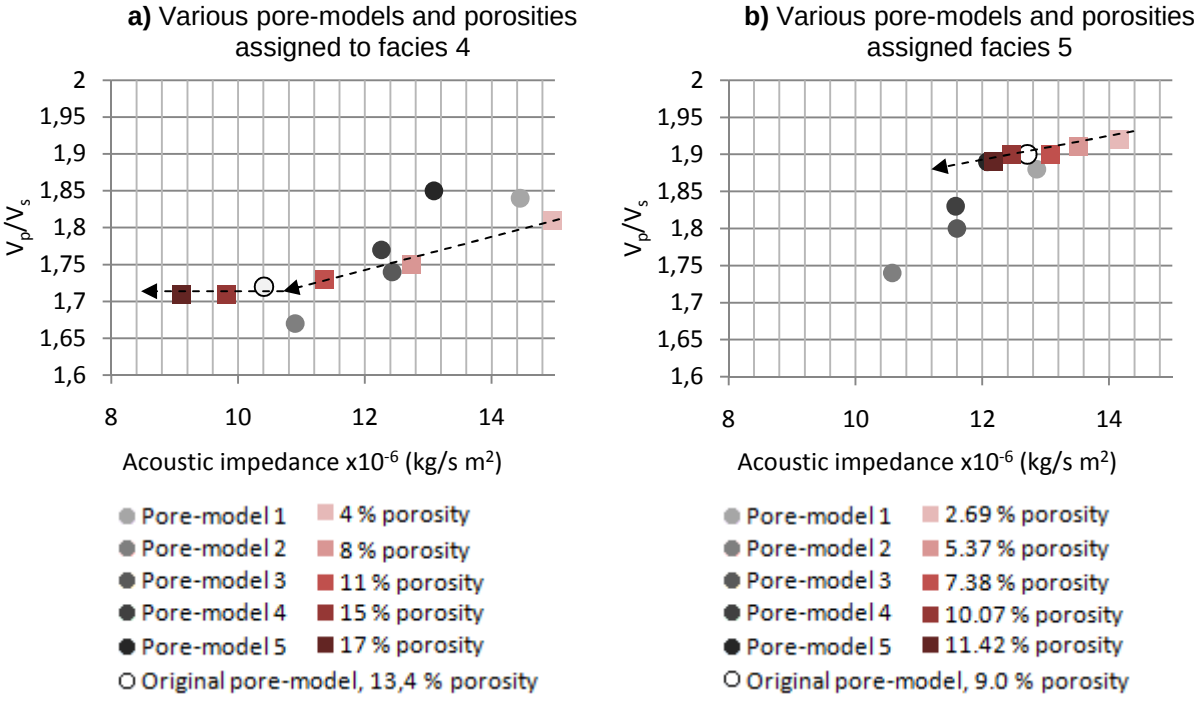

Figure 6.4 *V_p/V_s ratio versus acoustic impedance for varying pore-model and porosity in **a**) facies 4, and **b**) facies 5. Arrows correspond to increasing porosity.*

The original pore-model for facies 5 (Table 5.5), termed F-5, consists mainly of spherical pores. This gives high velocities compared to pore-models consisting mostly of pores of lower aspect ratios. This is observed in Figure 6.3 c). Comparing the results of different pore-models for facies 4 and 5, it is observed that the trend of velocity changes is approximately the same, although the exact velocities depend on the original velocities of the facies.

The results for facies 5 in a rock physics template (Figure 6.4 b)) differ slightly from the results for facies 4. The original pore model consists mostly of spherical

pores, and thus V_p/V_s ratios for different porosities are higher than for facies 4. In addition, the range of velocity ratios and impedances for variation of porosity is smaller for facies 5. Nevertheless, the general trend is the same as for facies 4, although variations of pore-models result in slightly smaller variations in acoustic impedance, than for facies 4. The range of V_p/V_s ratio variations is approximately the same for both facies.

It can be stated from these observations that a given pore-model affects seismic results for porosity variations, and vice versa. This concerns not only exact values, but also the range of variations.

Figure 6.5 expands and sums up the results discussed above. Velocities and acoustic impedances have been calculated for facies 4 given each of the pore-models listed in Table 6.1, in addition to models F-4 and F-5, and porosities ranging from 0-25 %. It can be seen that the velocity decrease due to increasing porosity is greater for P-waves than for S-waves (dashed lines) (Figure 6.5 a)). In addition, V_p for different pore-models differ with more than 1000 m/s at 25 % porosity. For S-waves the range is smaller, but still over 500 m/s. It can be seen that for P-waves, pore-model 1, which consists only of spherical pores, gives the highest velocity at all porosities, while pore-model 2, consisting only of pores with aspect ratios 0.1, gives the lowest velocity at all porosities. Further, it is seen that pore-model F-5 coincides with model 1 for P-waves. The results are the same for S-waves, except that lowest velocities is reached for pore-model F-4. The different effects on P- and S-wave velocities for the different pore-models result in different V_p/V_s ratios for each model. The ratio decreases with increasing porosity. However the gradients for the decrease vary significantly for different pore-models, and at 25 % porosity the ratio varies with almost 0.20. The greatest V_p/V_s ratio is resulting from pore-model 1, while the lowest is for pore-model 2.

The acoustic impedances for P-waves decrease as porosity increases, and the order of AI-magnitudes for the different pore-models, for increasing porosity, is the same as for P-wave velocities. At 25 % porosity the acoustic impedance has variations up to $3*10^6$ m/s*kg/m^3.

In Figure 6.5 d) the results for the different pore-models are plotted in a rock physics template. The porosity range is the same as in the other figures. Zero porosity is at the point where all curves meet, and it increases towards 25 % at the ends of each pore-model curve. It can be seen that even though the coincident observation for all

the models is increasing V_p/V_s ratio for increasing AI, there is a wide range in actual values.

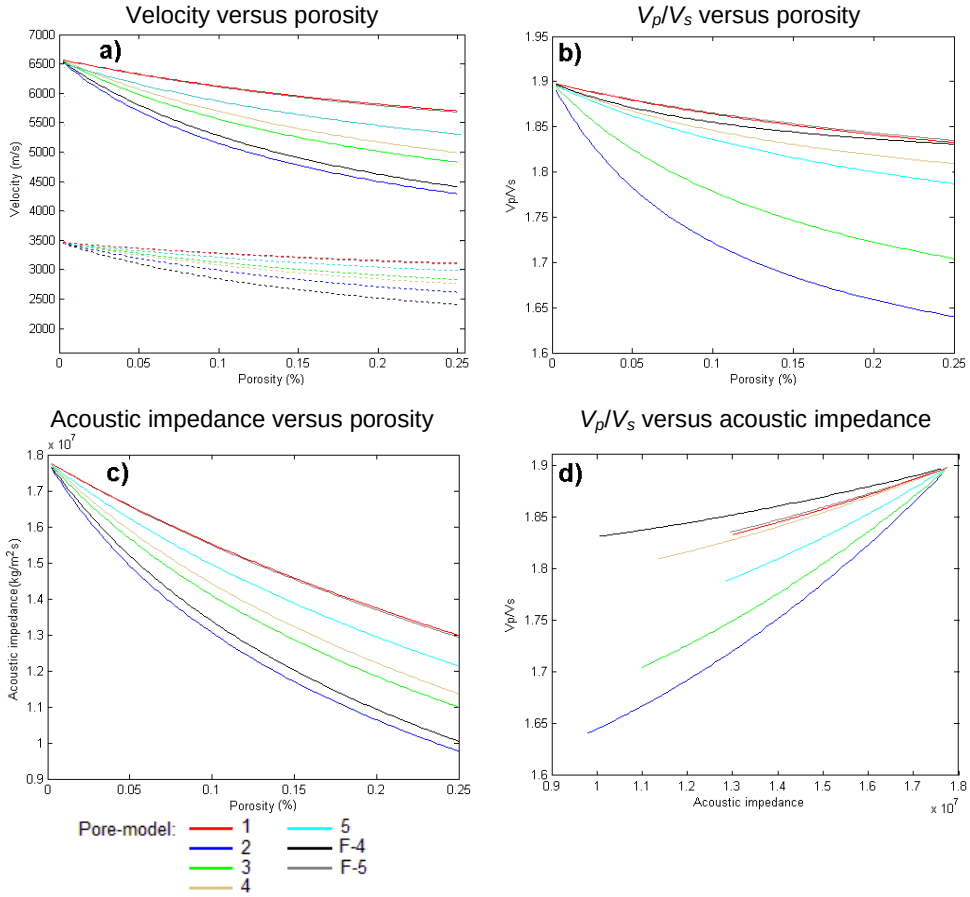

Figure 6.5 *Responses of different pore-models and porosities in plots of* ***a****) velocity versus porosity,* ***b****)* V_p/V_s *versus porosity,* ***c****) acoustic impedance versus porosity, and* ***d****)* V_p/V_s *versus acoustic impedance. Dashed lines refer to S-waves. Plots are made for facies 4. Pore-model specifications for models 1-5 can be found in Table 6.1. F-4 and F-5 corresponds to original pore-models assigned to facies 4 and 5 respectively (Table 5.5). The curve for F-5 is hard to see because it is approximately coincident with the curve for pore-model 1.*

The difference in porosity dependence for the velocities of facies 4 and 5, as seen in Figure 6.3 b) and d), can according to Figure 6.5 a) be explained by their respective pore-models. It is clearly seen that pore-model of facies 4 (F-4) creates a steeper decline in velocities, than pore-model of facies 5 (F-5) for increasing porosity.

The results above show that pore shapes may affect seismic properties considerably. The five pore-models applied differ greatly from each other, and are designed to get a clear overview on the magnitudes of variations that can be caused by pore shapes. To explore the effects of the exact pore shapes in detail, a set of

additional pore-models have been defined (Table 6.2). These are assigned to facies 4 in Figure 6.6.

Table 6.2 *Definitions of different pore-models according to their pore aspect ratios and fractions of these of total porosity.*

Pore-model	Percentage of total porosity	Aspect ratio	Pore-model	Percentage of total porosity	Aspect ratio
6	100 %	0.9	20	99 %	1.0
7	100 %	0.8		1 %	0.01
8	100 %	0.7	21	98 %	1.0
9	100 %	0.6		2 %	0.01
10	100 %	0.5	22	97 %	1.0
11	100 %	0.4		3 %	0.01
12	100 %	0.3	23	96 %	1.0
13	100 %	0.2		4 %	0.01
14	99.5 %	1.0	24	95 %	1.0
	0.5 %	0.001		5 %	0.01
15	99.4 %	1.0	25	95 %	1.0
	0.6 %	0.001		5 %	0.1
16	99.3 %	1.0	26	85 %	1.0
	0.7 %	0.001		15 %	0.1
17	99.2 %	1.0	27	75 %	1.0
	0.8 %	0.001		25 %	0.1
18	99.1 %	1.0	28	65 %	1.0
	0.9 %	0.001		35 %	0.1
19	99 %	1.0	29	55 %	1.0
	1 %	0.00.1		45 %	0.1

It can be seen that variation of different pore shapes makes separate trends in a rock physics template. When all pores have aspect ratios which decrease from 1.0 to 0.1 in steps of 0.1, both acoustic impedance and V_p/V_s ratio decrease (trend-line is denoted 3 in Figure 6.6). However, the decreases are small when pores have aspect ratios above 0.3. Below this value, the further decreases are significant.

When separately increasing the amounts of 0.1, and 0.01 pores in pore-models where all other pores are spherical, again AI and V_p/V_s ratio decrease (trend-lines 4 and 2, respectively). The V_p/V_s-AI gradient is steepest for increasing amount of 0.1 pores.

When pores with aspect ratios 0.001 are increased in amount, the resulting responses deviate from the previously described cases. While AI decreases, V_p/V_s ratio increases profoundly (trend-line 1) when adding only small fractions of these pores.

It can be seen from Figure 6.6 and Table 6.2 that smaller amounts of pores with

lower aspect ratios are needed to make comparable variations in magnitude as greater amounts of higher-aspect-ratio-pores.

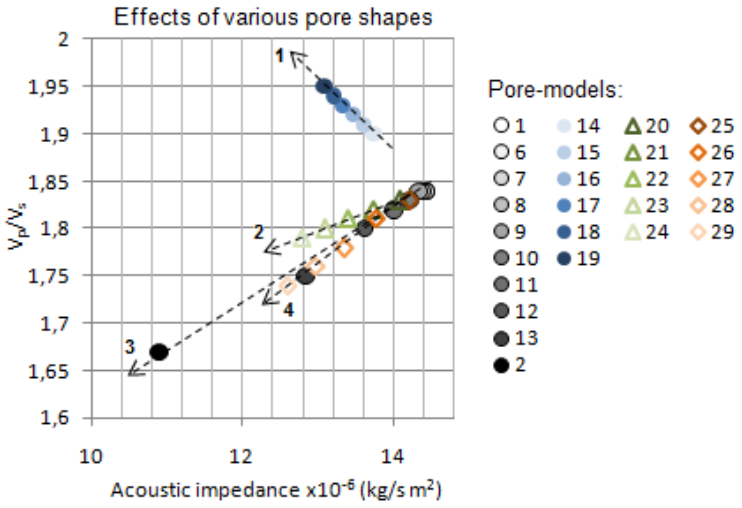

Figure 6.6 *Rock physics template showing trends for variations of different pore shapes. The illustrated trend lines refer to:* ***1****: increasing amount of 0.001 aspect ratio pores;* ***2****: increasing amount of 0.01 aspect ratio pores;* ***3****: gradual decrease in pore aspect ratios from 1.0 to 0.1;* ***4****: increasing amount of 0.1 aspect ratio pores. Definitions of the given pore-models can be found in Table 6.1 and Table 6.2.*

6.2.2 Amplitude versus offset responses

The results of the variations in pore-model and porosity can in addition to the previous evaluations be evaluated according to the effects on the amplitude versus offset responses. Figure 6.7 shows such responses for the boundary between facies 4 overlaid by facies 5 in a reflection coefficient versus incidence angle cross-plot, for pore-models 1-5 assigned to facies 4, in addition to its original pore-model. Facies 5 keeps its original values. In Figure 6.9 similar results for the same boundary are shown, when different porosities are assigned to facies 4, keeping its original pore-model. Seismic one-dimensional (1D) AVO results for Well A are shown in Figure 6.8 for varying pore-model and Figure 6.10 for varying porosity.

Facies 4 is completely enclosed by Facies 5, so that reflection coefficients for the upper boundary of facies 4 are similar in magnitude, but of opposite sign (+/-) as the coefficients for the lower boundary. Both upper- and lower-boundary responses are marked (yellow square) in Figure 6.8 and 6.10.

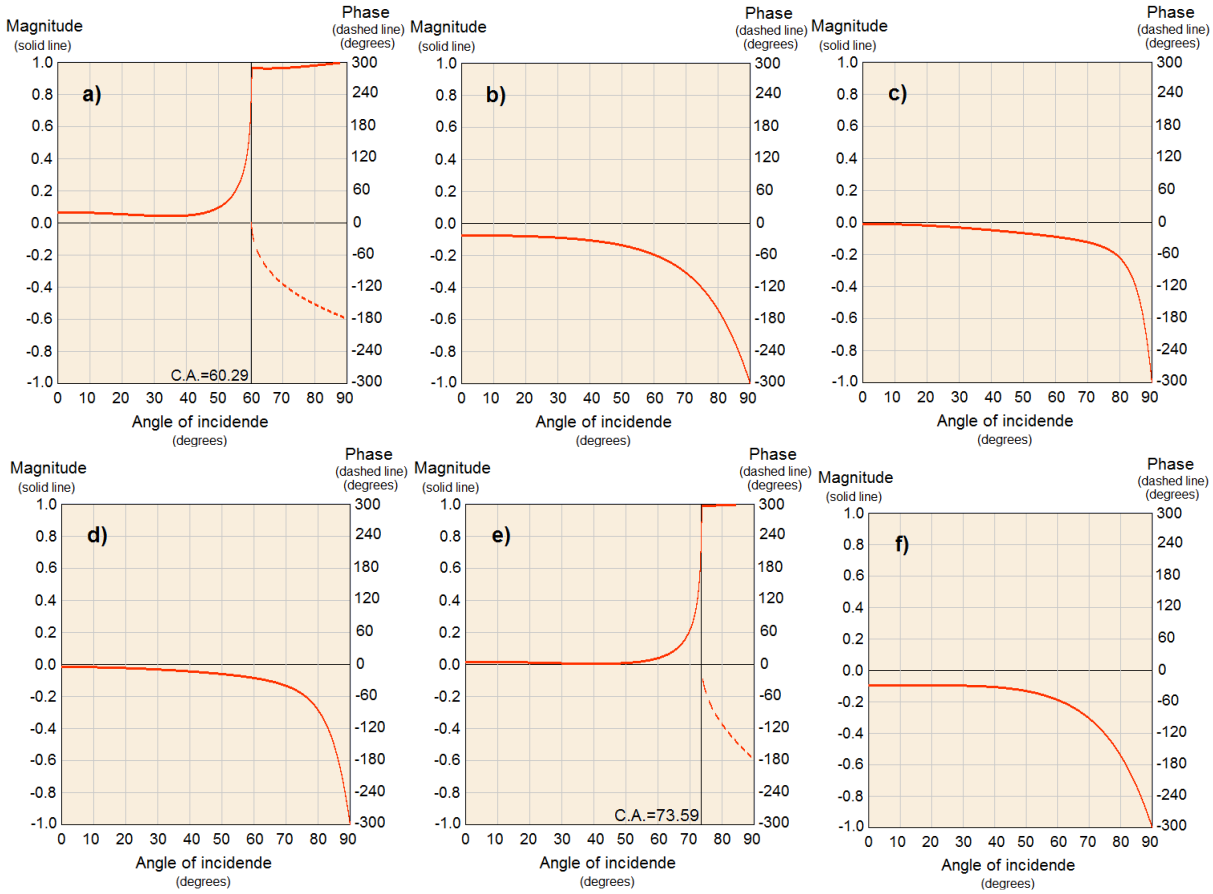

Figure 6.7 *Reflection coefficients versus angle of incidence for the interface between facies 5 (upper) and 4 (lower), when facies 4 has been assigned different pore-models (p.m.):* ***a****) p.m. 1;* ***b****) p.m. 2;* ***c****) p.m. 3;* ***d****) p.m. 4;* ***e****) p.m. 5; and* ***f****) original p.m. (F-4). C.A. is abbreviation for critical angle.*

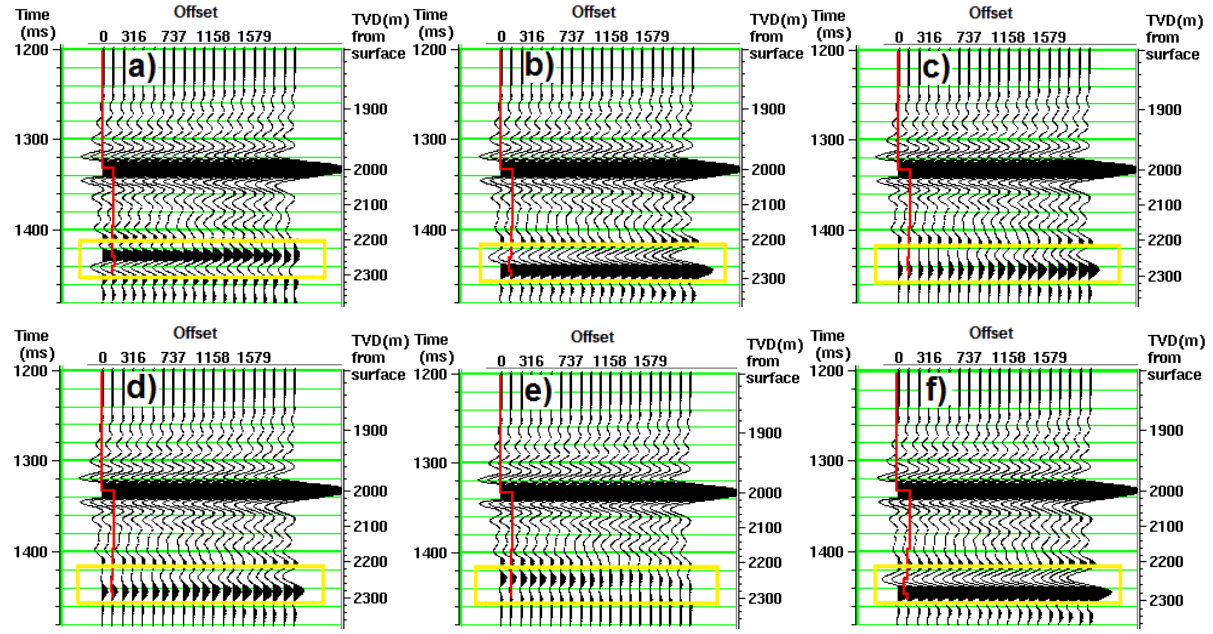

Figure 6.8 *AVO responses for the interface between facies 4 and 5, when facies 4 has been assigned different pore-models (p.m.):* ***a****) p.m. 1;* ***b****) p.m. 2;* ***c****) p.m. 3;* ***d****) p.m. 4;* ***e****) p.m. 5; and* ***f****) original p.m. (F-4). Red curve is P-wave acoustic impedance log. Square marks the interfaces between facies 4 and 5.*

Looking at the responses for the upper boundary of Facies 4 (Figures 6.7, 6.8, 6.9, and 6.10) it can be seen that changes in pore-model and in porosity result in quite similar AVO responses. It can for example be observed that pore-model1 gives nearly similar result as 4 % porosity, and the same is true for pore-model 4 and 8 % porosity. For pore-model 1 and 5, amplitudes decrease as offset increases, while the other pore-models result in an increase. Porosities 4, 15, and 17 % result in decreasing AVO, while 8 and 11 % porosity give increasing AVO. The original porosity (13.4 %) and pore model (F-4) show an unchanged AVO response up to incidence angle 30 °.

All AVO responses which have positive reflection coefficients at zero offset, have decreasing coefficients with increasing offset, and will reach a critical angle at a given offset. Near this angle, and for post-critical-angle-offsets, calculated amplitudes increase severely. Thus even though these amplitudes decrease with increasing offset, it may look like they increase due to this distortion for wide offsets.

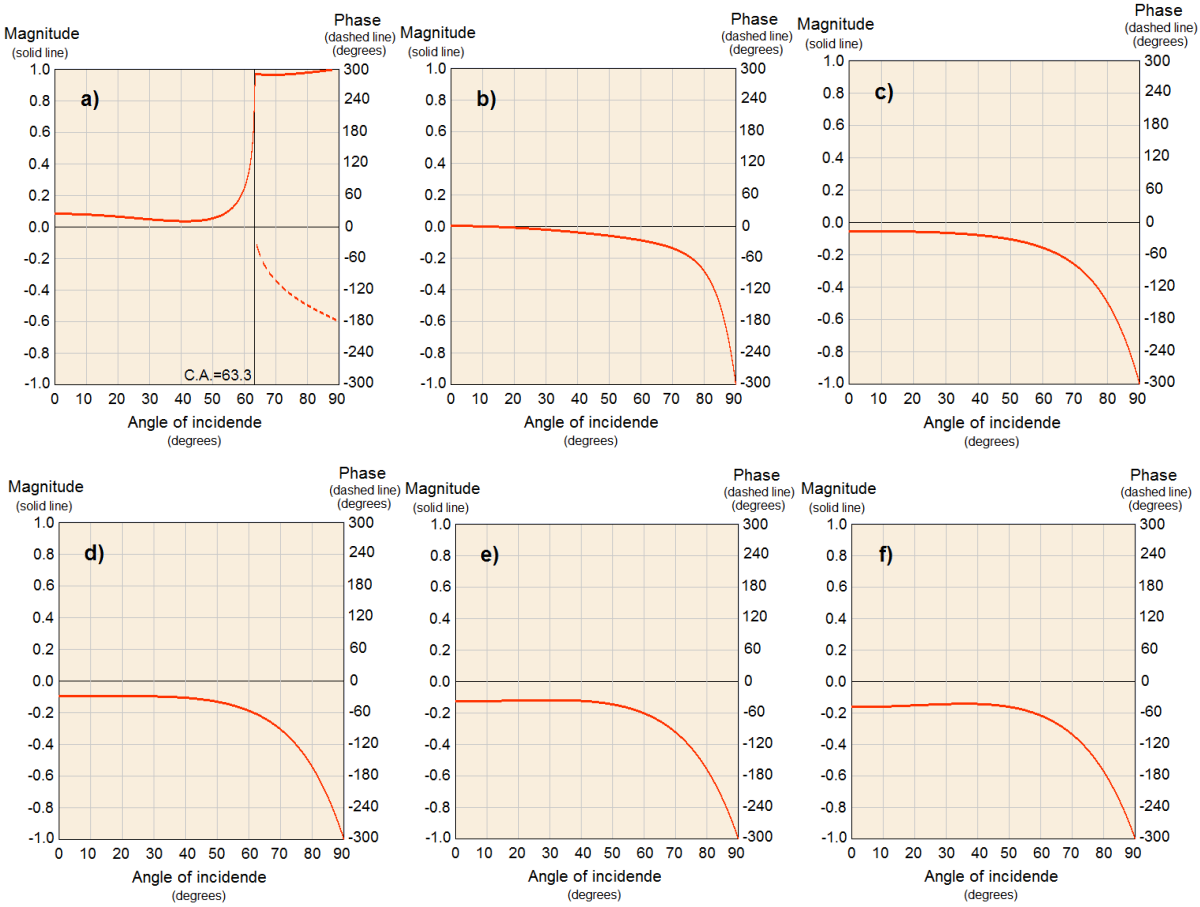

Figure 6.9 *Reflection coefficient versus angle of incidence for the interface between facies 5 (upper) and 4 (lower), when facies 4 have been assigned different porosities (φ):* ***a)*** *φ = 4 %;* ***b)*** *φ = 8 %;* ***c)*** *φ = 11 %;* ***d)*** *φ = 13.4 % (original value);* ***e)*** *φ = 15 %; and* ***f)*** *φ = 17 %. C.A. is abbreviation for critical angle.*

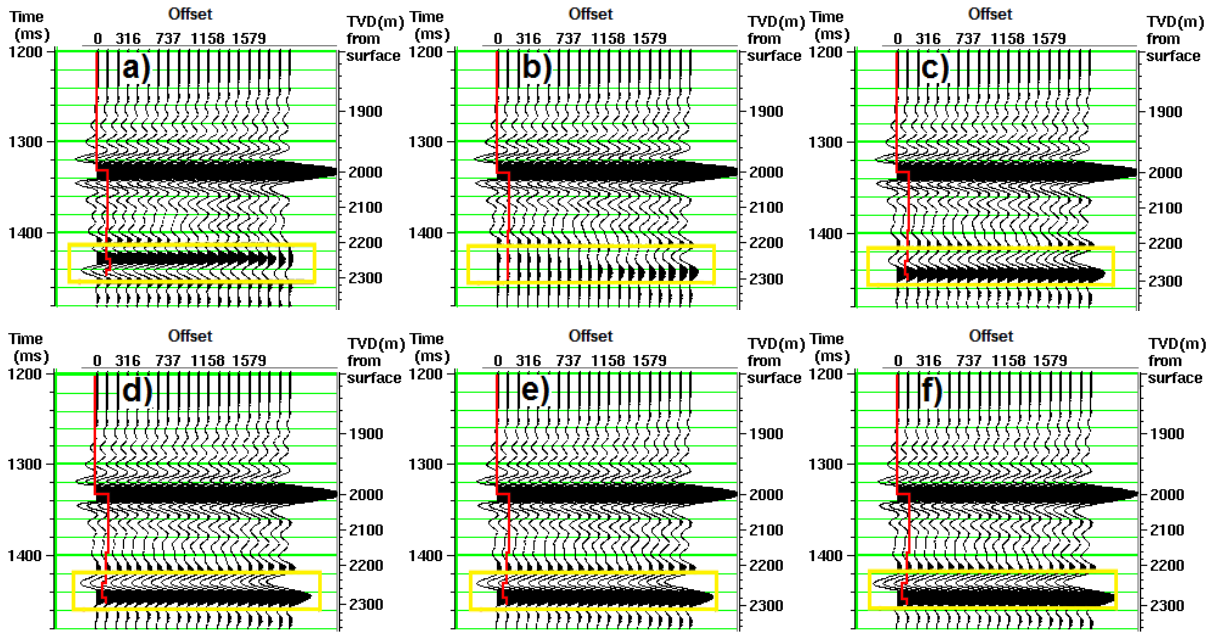

Figure 6.10 *AVO responses for boundary between facies 4 and 5, when different porosities (φ) are assigned to facies 4:* ***a****) φ = 4 %;* ***b****) φ = 8 %;* ***c****) φ = 11 %;* ***d****) φ = 13.4 % (original value);* ***e****) φ = 15 %; and* ***f****) φ = 17 %. Red curve is P-wave acoustic impedance log. Square marks the interfaces between facies 4 and 5.*

The original porosity and pore model for facies 4 give an AVO response which according to Figures 4.2 and 4.3 can be defined as a class III response (although Castagna and Swan (1997) recommend that such grouping into classes should be done in the context of looking for deviations from an expected background response). In the same manner, the results for pore models (p.m.) 1-5 can be grouped as class I (p.m. 1), class II (p.m. 3, 4 and 5), and class III (p.m. 2). The results for the different porosities can be grouped as AVO classes I (φ = 4 %), II (φ = 8 %), III (φ = 11 %, 13.4 %, 15 %), and IV (φ = 17 %). Thus variation of porosities may change the class of the AVO response to any of the four classes.

6.3 Mineralogy Effects

6.3.1 Velocities and acoustic impedances

Due to the fact that aragonite is an unstable mineral, it is generally not found in significant amounts in carbonate rocks due to conversion to calcite. Thus, most carbonates consist of calcite and/or dolomite, and varying amounts of non-carbonate minerals like quartz and clay. Since minerals have different properties, varying the

mineralogy of a rock will alter its properties. To investigate the extent of modifications on seismic rock properties caused by varying mineralogy, mineralogies for facies 2 and 4 will be altered. Both facies originally consist of 95 % calcite and 5 % quartz. Effects on velocities when introducing 5-20% non-calcite minerals (quartz and clay), and carbonate minerals (dolomite and aragonite) in the calcite matrixes of these facies (without the original 5 % quartz content) are illustrated in Figure 6.11. In addition, velocities for the facies consisting of pure calcite and pure quartz, clay, dolomite and aragonite are shown. Elastic moduli, densities, velocities and velocity ratios for the different minerals investigated are listed in Table 6.3.

Table 6.3 *Velocities and velocity ratios for minerals commonly present in carbonate rocks*

Material	K (GPa)	μ (GPa)	ρ (g/cm^3)	V_p (m/s)	V_s (m/s)	V_p/V_s
Calcite	76.80	32.00	2.710	6640	3436	1.93
Dolomite	94.90	45.00	2.870	7347	3960	1.86
Aragonite	44.80	38.80	2.920	5750	3645	1.58
Quartz	37.00	44.00	2.650	6008	4075	1.47
Clay	13.43	5.90	2.457	2944	1550	1.90

When adding dolomite to the matrix, moderate increases in V_p and V_s for both facies are observed (Figure 6.11 a)). Contrary, increasing aragonite content causes velocities to decrease moderately (Figure 6.11 b)).

P-wave velocity is higher for calcite than for quartz, while the opposite is true for S-wave velocity (Table 6.3). Thus, one could expect that increasing the quartz content in a rock would reduce V_p, while increase V_s. However, the results in Figure 6.11 c) show that this is not necessarily the case. For facies 2, V_p increases when increasing the quartz content from 0-20 %, although the changes are minor. For facies 4, looking at the same mineral variation, V_p remains approximately unchanged when introducing quartz in the calcite matrix. V_s increases for both facies as more quartz is added, although these changes also are minor.

Clay has significantly lower velocities than calcite. Thus, introducing clay in the calcite matrix reduces velocities for facies 2 and 4 considerably (Figure 6.11 d)). Adding 20 % clay lowers the P-wave velocities with about 500 m/s compared to when only calcite is present. Shear velocities are lowered slightly less.

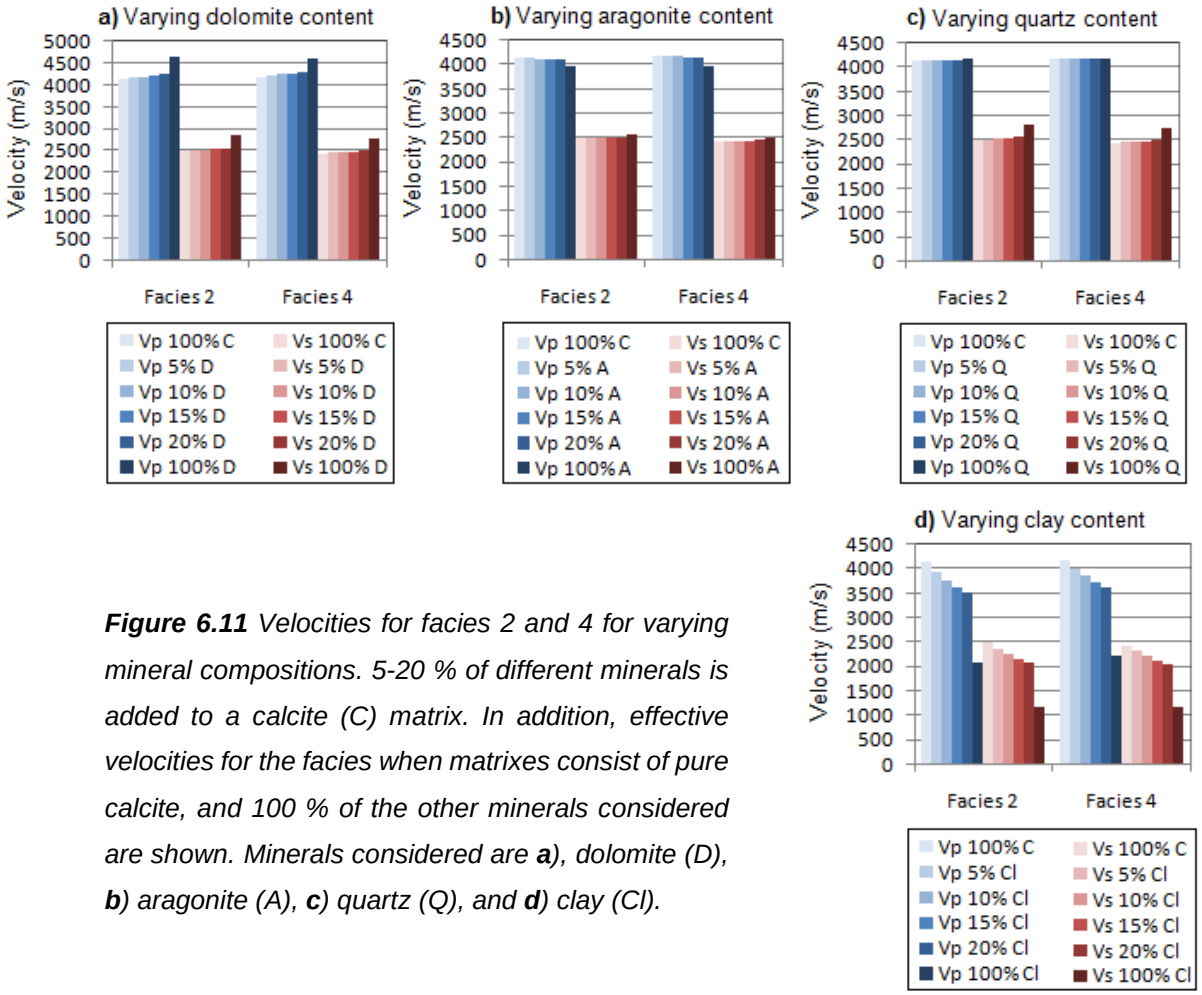

Figure 6.11 *Velocities for facies 2 and 4 for varying mineral compositions. 5-20 % of different minerals is added to a calcite (C) matrix. In addition, effective velocities for the facies when matrixes consist of pure calcite, and 100 % of the other minerals considered are shown. Minerals considered are* ***a****), dolomite (D),* ***b****) aragonite (A),* ***c****) quartz (Q), and* ***d****) clay (Cl).*

Figure 6.12 extends the results in Figure 6.11, showing velocities and V_p/V_s ratio for facies 2 when matrix is varied gradually from calcite to dolomite, quartz, aragonite, and clay, separately. The results have slight variations compared to Figure 6.11 because they are calculated with Kuster-Toksöz rather than DEM approach for practical reasons. It can be seen that quartz slightly reduces V_p, rather than increasing it. Other than this, velocity results are approximately the same in the two Figures.

V_p/V_s ratios decrease when including dolomite, quartz or aragonite in the calcite matrix, and the values are lower than corresponding results for clay. These results are as expected from the mineral values listed in Table 6.3. However, a more surprising result is the increase in V_p/V_s ratio when going from a pure calcite matrix to a pure clay matrix. Applying to the minerals themselves, calcite has slightly higher velocity ratio than clay. Thus the increase in the ratio, considering effective rock values, when more clay is introduced in the matrix, clearly is an effect of other rock properties, like porosity, pore shapes, or fluid properties. As seen in the previous section (6.2), pore

shapes greatly affect V_p/V_s ratios. Thus, it is reasonable to believe that pore shapes may affect the effects of mineralogy, like they affect porosity results as seen in Figure 6.5 b). The pore-model of facies 2 consists mostly of 0.1 aspect ratio pores, which is shown to cause low V_p/V_s ratio (Figure 6.5 b) and d), and Figure 6.6). Clay has low elastic moduli and density compared to the other minerals studied (Table 6.3) and, thus is considerably softer. This may explain a possible lower effect of V_p/V_s-lowering pore shapes on elastic behavior of a rock consisting partly or entirely of clay, than of the other minerals investigated.

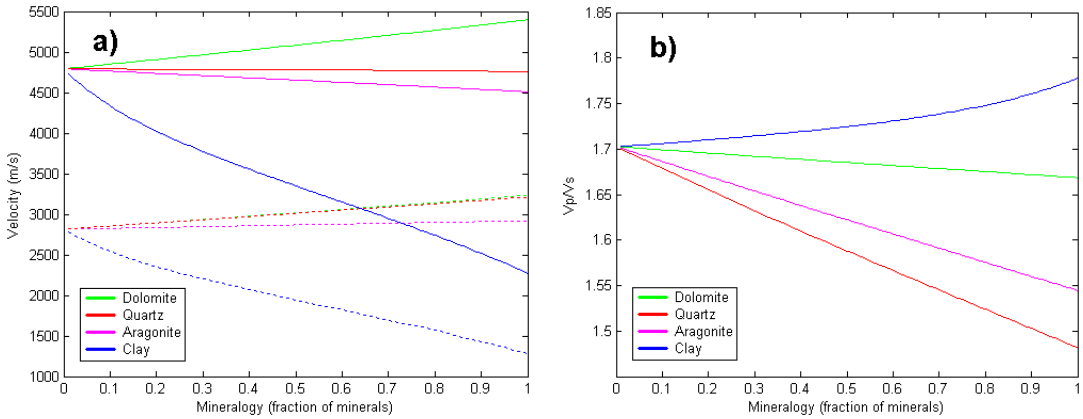

Figure 6.12 *Velocity (**a**) and velocity ratio (**b**) for facies 2 when matrix is varied gradually from calcite to dolomite, quartz, aragonite, and clay, separately. Fraction of minerals refers to the fractions of the mentioned minerals, while the remaining content is calcite. Dashed lines refer to S-waves.*

An important process altering the mineralogy of carbonates is dolomitization, which may change the mineralogy entirely from calcite (or aragonite) to dolomite (Eberli et al., 2003), and may increase or reduce the porosity. Figure 6.13 shows velocities for dolomitization of facies 2. The dolomitization is simulated by increasing the amount of dolomite, and reduce calcite content. Results for conversion of all calcite to dolomite (keeping 5 % quartz) are shown, with different porosities: 25 %; 22 %; 17.8 % (original value); and 12 %. Thus both increase and decrease in porosity have been considered. In addition, results for a mineralogy consisting of 50 % dolomite, 45 % calcite, and 5 % quartz, with original porosity, and with 21 % porosity are shown.

When porosity is unchanged, V_p and V_s increase as dolomite content increase. When in addition porosity is increased to 25 %, when all calcite is converted to dolomite, both velocities decrease compared to the original facies. Increasing porosity to 22 % for the same mineralogy, give approximately similar velocities as original

values, although slightly increased. When porosity is reduced to 12 %, and all calcite is converted to dolomite, V_p and V_s increase notably. When the rock consists of 50 % dolomite, the velocities increase compared to original ones when keeping the porosity constant, while decrease when increasing the porosity to 21 %.

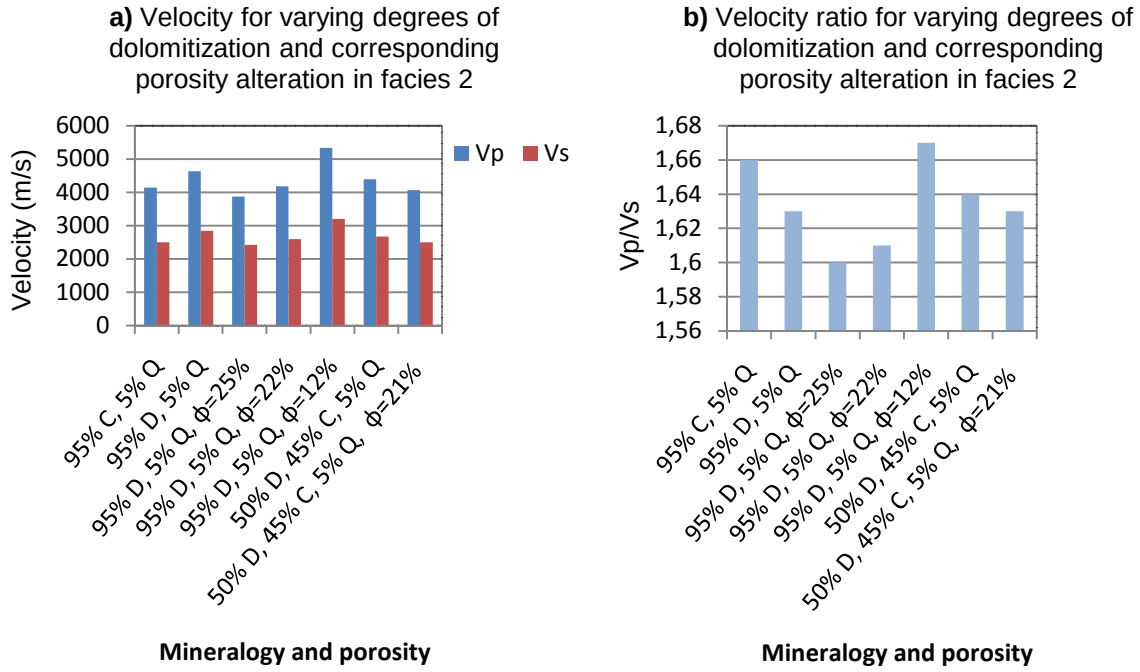

Figure 6.13 *Velocities (**a**) and velocity ratios (**b**) for facies 2 for different mineral compositions and porosities, corresponding to varying degrees of dolomitization, with and without porosity increase or reduction. Letters refer to: C: calcite; D: dolomite; and Q: quartz.*

It is obvious from these results that the increase in velocity resulting from increasing the dolomite content of a rock can get balanced by a following increase in porosity, reducing the velocities. That is, varying dolomite content may not result in notably velocity variations when the porosity is increased sufficiently.

Velocity ratios are shown in Figure 6.13 b). As expected V_p/V_s ratio decrease when more dolomite is introduced to the rock. It decreases further when porosity is increased. Thus, velocity ratio, like the individual velocities, can be balanced by porosity variations when adding more dolomite to the matrix.

Figure 6.14 shows a rock physics template including most of the mineralogy (and corresponding porosity) variations for facies 2 showed in Figures 6.11 and 6.13. It can be seen that increasing quarts content decreases the velocity ratio, while acoustic impedance remains approximately unchanged. Results for aragonite are

approximately the same. When exchanging the increasing quartz or aragonite content with increasing dolomite content, V_p/V_s ratio decreases, although less than for increasing amount of quartz, and AI increases. The different dolomitization scenarios create a wide range of velocity ratios and acoustic impedances. When dolomitizing facies 2 completely (keeping 5 % quartz) without changing porosity, velocity ratio decreases and acoustic impedance increases, compared to the original values. When porosity is altered, both V_p/V_s and AI decrease for increasing porosity. The same relation is true when only 50 % of the matrix consists of dolomite. Thus, it seems possible to separate the different dolomitization scenarios in a rock physics template.

Addition of clay, as already seen (Figure 6.12), increases velocity ratio. AI does also increase, and the range is clearly greater than those achieved for the other minerals when 0-20 % of the given minerals is added to calcite.

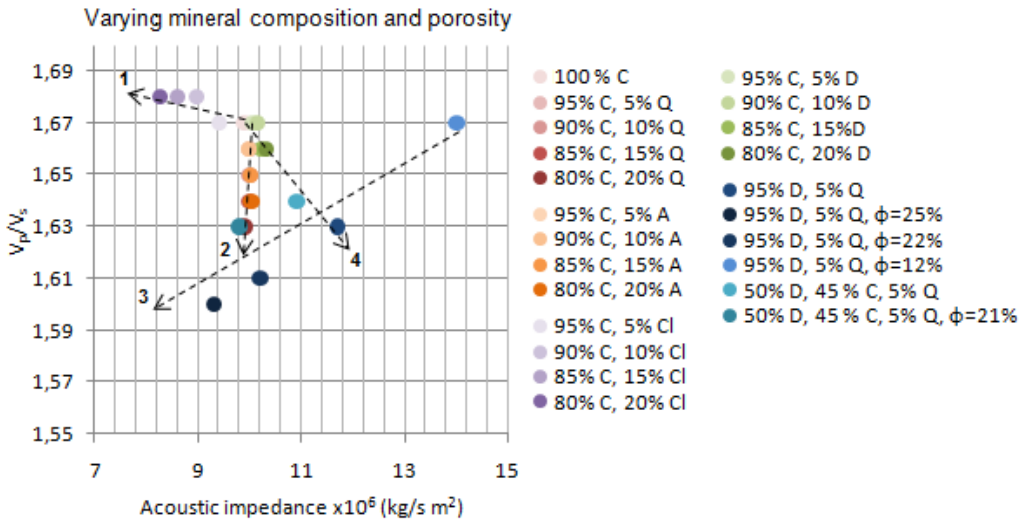

Figure 6.14 *Velocity ratio and acoustic impedance variations for varying mineralogy and porosities. Trendlines refers to:* ***1****: increasing clay content;* ***2****: increasing aragonite or quartz content;* ***3****: increasing porosity, and* ***4****: increasing dolomite content. Letters refer to: A: aragonite; C: calcite; Cl: clay; D: dolomite; and Q: quartz.*

6.3.2 Amplitude versus offset responses

To evaluate mineralogy effects on AVO responses, responses for alterations simulating results of dolomitization processes will be studied. The interface between facies 1 and 2 seen in Well B is considered. Dolomitization of facies 2, without porosity change (Figure 6.15 b) and c)) increases the reflection coefficient to a less negative value, compared with the original facies (a). A porosity increase related to the

dolomitization, reduces the reflection coefficient (d, e), while the decrease in porosity increases the coefficient to a positive value (f). AVO gradients are seen to be positive for the initial case, and when the facies is fully dolomitized with porosity increased to 25 %. All other gradients are negative. Thus, class II, III, and weak class IV AVO responses are resulting from these mineralogy and porosity changes.

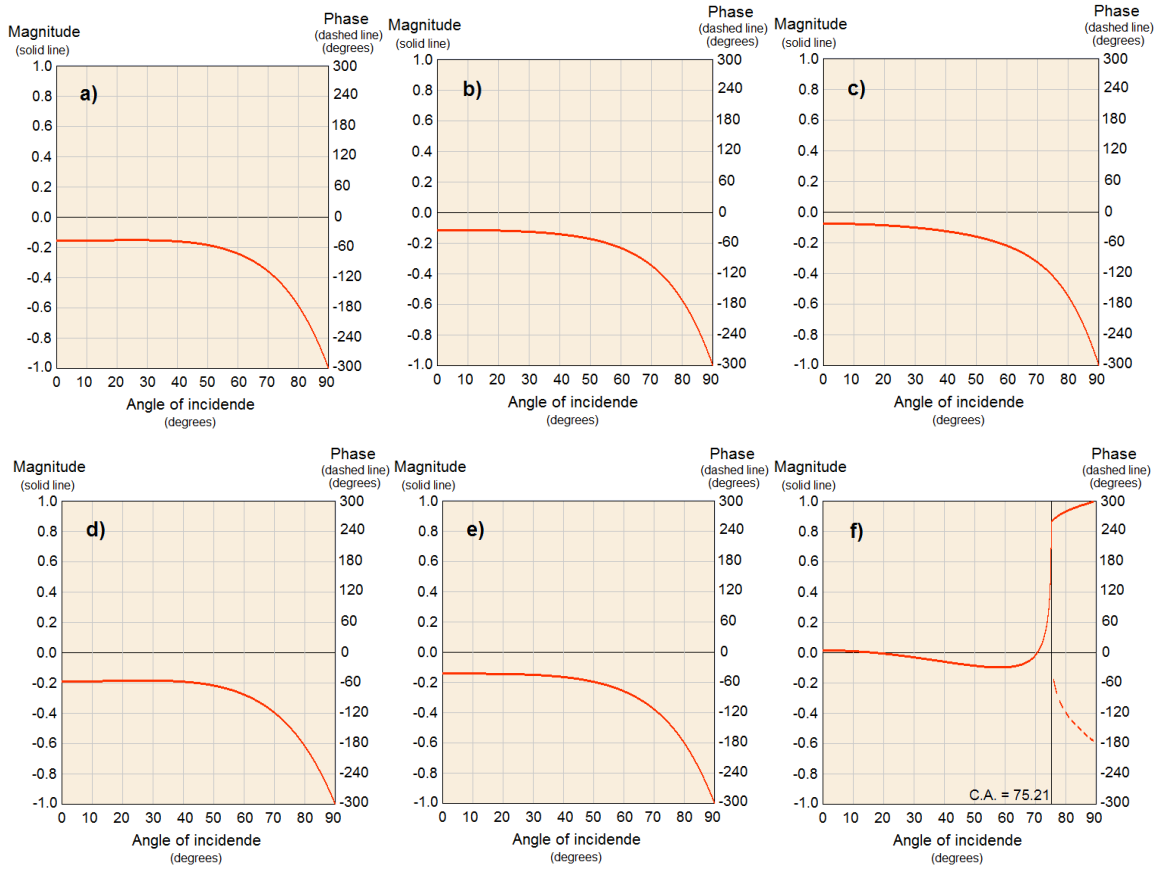

Figure 6.15 *Reflection coefficient versus angle of incidence for the interface between facies 1 and 2 for increasing different cases of dolomitization scenarios and related porosity alteration in facies 2:* ***a****) original facies;* ***b****) 50 % dolomite;* ***c****) 95 % dolomite;* ***d****) 95 % dolomite and 25 %;* ***e****) 95 % dolomite and 22 % porosity; and* ***f****) 95 % dolomite and 12 % porosity. C.A. is abbreviation for critical angle.*

6.4 Fluid effects

In the petroleum industry the main goal when investigating real seismic data is to determine what kinds of fluids are saturating the studied lithologies. As seen in the previous sections, different rock parameters can affect seismic signatures of rocks in

different ways. Thus, one has to be able to separate effects of fluids from effects caused by other parameters to determine what kind of fluid saturates a rock. That is why studying various rock parameters effects on seismic responses is important; if certain links between given rock parameters and their effects on seismic responses can be established, this will help determining the various properties of a given rock. However, establishing such links is not always straightforward, due to the fact that some properties may affect the responses of other properties. In this section, in which fluid responses are investigated, the responses caused by various fluid compositions will be studied related to different cases of some of the previously discussed variables. As seen in Figure 5.1, there is a trap in well B, and facies will thus be studied in detail as a reservoir saturated with various fluids.

6.4.1 Velocities and acoustic impedances

Figure 6.16 a) shows bulk modulus for different fluids and fluid compositions, while densities are showed in b). Fluid properties are calculated assuming temperatures and pore pressures representing 0.5, 2, and 4 km depth assuming normal pore pressures, and the case of overpressure at 4 km depth (overpressure refers to higher than normal pore pressures, and will be discussed in section 6.5). The oil is a medium oil (defined as oil having API between 22.3 and 31.1 (Gelius and Johansen, 2007)) with 25.7°API, while salinity for brine, and specific gravity for gas are the same as defined earlier (chapter 5). Gas has a clearly lower modulus than brine and oil, and for fluid mixtures composed of brine and gas, and oil and gas, only small fractions of gas are required to

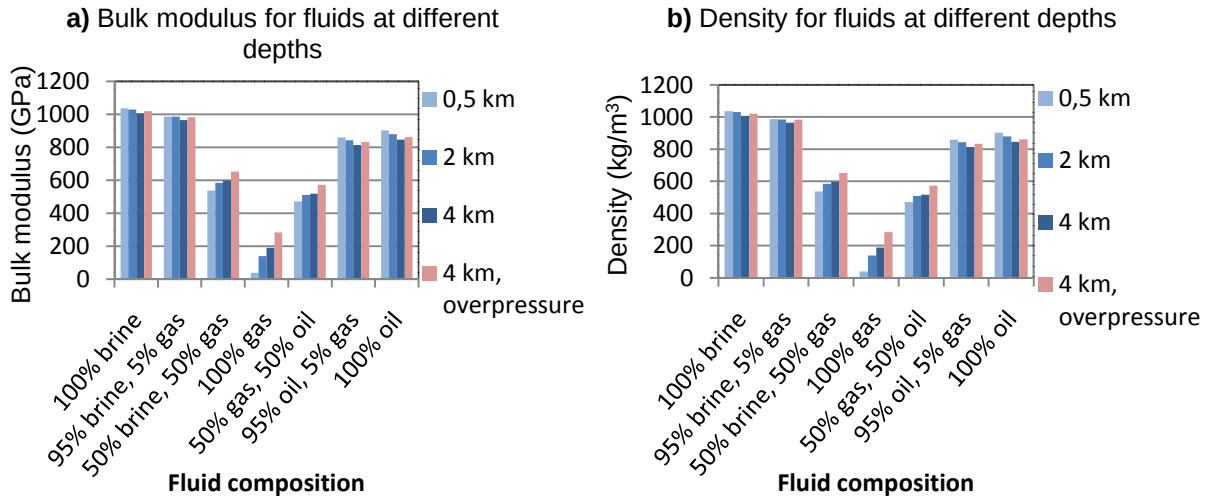

Figure 6.16 *Bulk modulus (**a**) and density (**b**) for different fluid compositions at different depths.*

reduce the modulus significantly. Density of gas is also clearly lower than for brine and oil. However, small fractions of gas (~5 %) in brine or oil compositions do only alter densities slightly. Thus, bulk modulus for fluid mixtures is more influenced by gas content than density is. Both bulk modulus and density is higher for brine than for oil.

The specific temperatures and pore pressures defined for each depth, in addition to the given specifications for fluid properties, result in increasing bulk modulus for increasing depth, and further increase for a case of overpressure (described in section 6.5), for all fluid compositions except for oil. Modulus decreases with increasing depth for oil, although increasing to the highest value for overpressure at 4 km depth. Density decreases for increasing depth for both brine and oil (slightly more for oil), which means that the temperature increase affects the brine and oil density more than increasing pore pressure (for the given temperatures and pore pressures defined for each depth). Gas, on the other hand, gets an increasing density when depth is increased. For all fluid compositions, density is higher at 4 km depth when there is overpressure in the pores than for normal pore pressure.

When the model is saturated with the various fluid compositions showed in Figure 6.16, the resulting velocities are as shown in Figure 6.17.

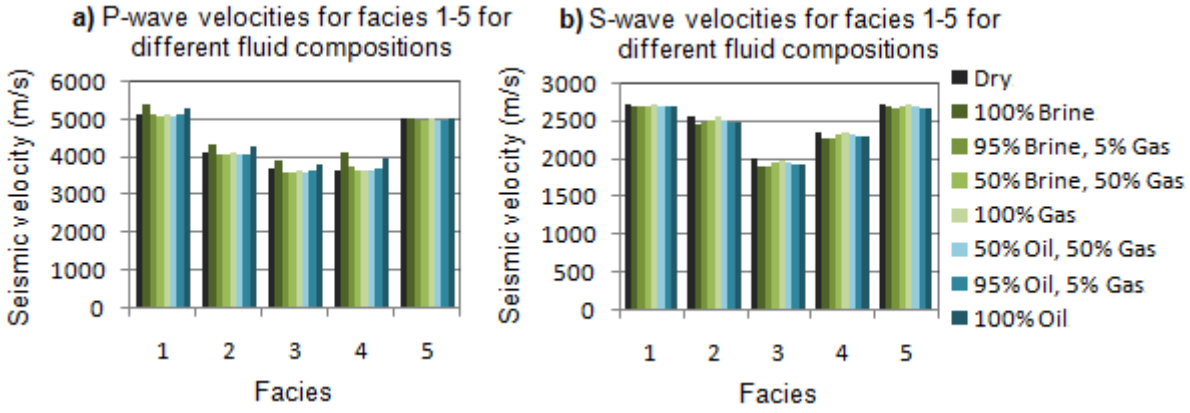

Figure 6.17 *Seismic velocities for facies 1-5 saturated with various fluid compositions, in addition to dry values.*

It can be seen that all facies have highest P-wave velocity when brine saturated, therenext when oil saturated. When portions of gas are introduced to the fluid, velocities decrease. There is a clear decrease when only 5 % gas is introduced. However, introducing 50 % gas in the fluid, compared to 5 %, results in only slight

further decreases in velocities. For pure gas saturation velocities are higher than when only 5 or 50 % of the fluid consists of gas. This means that for saturation of mixtures of brine and gas, and oil and gas, bulk modulus decrease is more significant than density decrease for the velocities, for the apperance of gas, so that the velocities decrease compared to pure brine or oil saturated facies. On the other hand, when the facies are saturated with pure gas, there are only slight decreases in bulk modulus compared to when saturated with 50 % gas and 50 % brine or oil, while the density have more prominent decrease, thus increasing the velocity.

S-wave velcocities show a different trend for varying saturation fluids than P-wave velocities. Since effective shear modulus remains constant for saturation of each of the fluids, only density determines the variations in velociy. Denser saturation fluids give lower velocities, and highest velocities are thus attained for gas saturation. In contrast to V_p, V_s show little decrease when only a small fraction of gas (5 %) is apparent, while the difference in velocities for 5 and 50 % gas content is higher.

All facies shows similar velocity trends for variation of saturating fluid, although the variations are more prominent for some facies than for other. Concerning dry facies, S-waves got higher velocities than when saturated, which is obvious since density is lower, while shear modulus is similar, compared to dry values. For P-waves one might expect dry velocities to be lower than saturated ones, but as seen, this is not necessarily the case. For all facies, dry velocities are higher than velocities for saturation of gas and/or fluid compositions containing some fraction of gas.

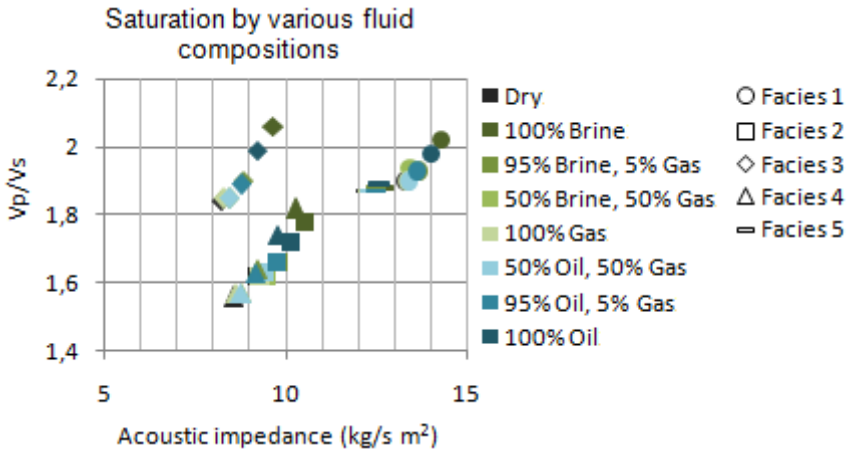

Figure 6.18 *Velocity ratio and acoustic impedance for facies 1-5 saturated with various fluid compositions, in addition to dry values.*

In Figure 6.18 the velocity ratios and acoustic impedances resulting from saturating facies with different fluids are shown. A clear trend is observed. Both velocity ratio and acoustic impedance increase for denser saturation fluids. The different facies are separated in the plot, although some are closely spaced, and the gradients for increase in V_p/V_s as AI increases, seem to be approximately similar for every facies, so that none of the fluid compositions give values for a given facies that coincides with values for other facies, except for facies 2 and 4, which have almost coincident values for each saturation fluid. These two facies do not have porosities or pore-models that are more similar than for other facies, but they do have exact similar mineralogies. Thus, it can be assumed that the mineralogy is the reason why these to facies show such similar results.

To more clearly see the effects of mineralogy on saturation fluid trend in a rock physics template, facies 2 (with porosity increased to 25 %) are saturated with the varying fluids, keeping its original mineralogy, and for a new mineralogy, where all calcite is exchanged with dolomite.

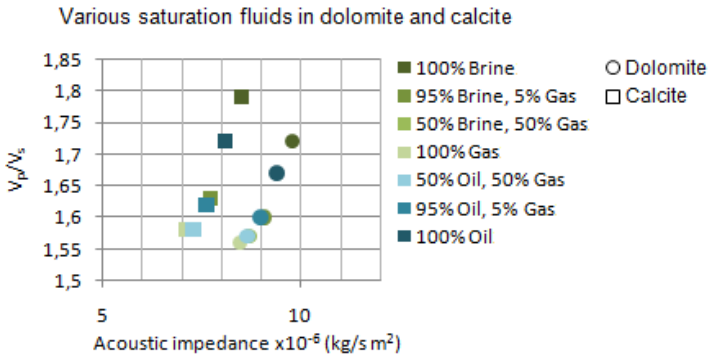

Figure 6.19 *Rock physics template for facies 2 with 25 % porosity and original mineralogy, and when calcite is exchanged with dolomite.*

The results are shown in Figure 6.19. The observations are similar as for the preceding figure, and the two mineralogies show approximately similar gradients in the plot. Although the trend resulting from saturation of different fluids seems to be the same for each facies in Figure 6.18, and for both mineralogies in Figure 6.19, with an approximately constant gradient with an increase of about 0.1 V_p/V_s per 0.5 x 10^6 kg/s m^2 for increasing fluid density, the range of increasing velocity ratio and impedance varies for the different facies and mineralogies. Facies 5 shows notably smaller variations than the other facies. In addition, V_p/V_s ratio for dolomite varies less than for

calcite for the different saturating fluids, which imply that mineralogy at least partly determine the range of the variations of V_p/V_s and AI caused by varying saturation fluid.

Since a rock with higher porosity contains more fluid than a rock of lower porosity, porosity is also expected to be a determining factor for the range of these variations. Figure 6.20 shows velocity, velocity ratio, bulk modulus, density, and acoustic impedance for facies 2 with different porosities when saturation is varied from gas to brine. It can be seen in this figure that each of the parameters (velocity, velocity ratio, bulk modulus, density, and acoustic impedance) varies more for higher porosity, although not significantly. In addition, it is obvious that porosity is a more crucial factor for velocities than saturation fluid for fluids consisting of more than about 10 % gas.

While densities increase stably towards higher brine content, the other parameters show a more rapid increase from about 90 to 100 % brine. Velocities differ from the other parameters, which increase all the way from gas to brine, in that V_p decreases up to 90 % brine, and increase further up to 100 %, while V_s decreases stably all the way to full brine saturation.

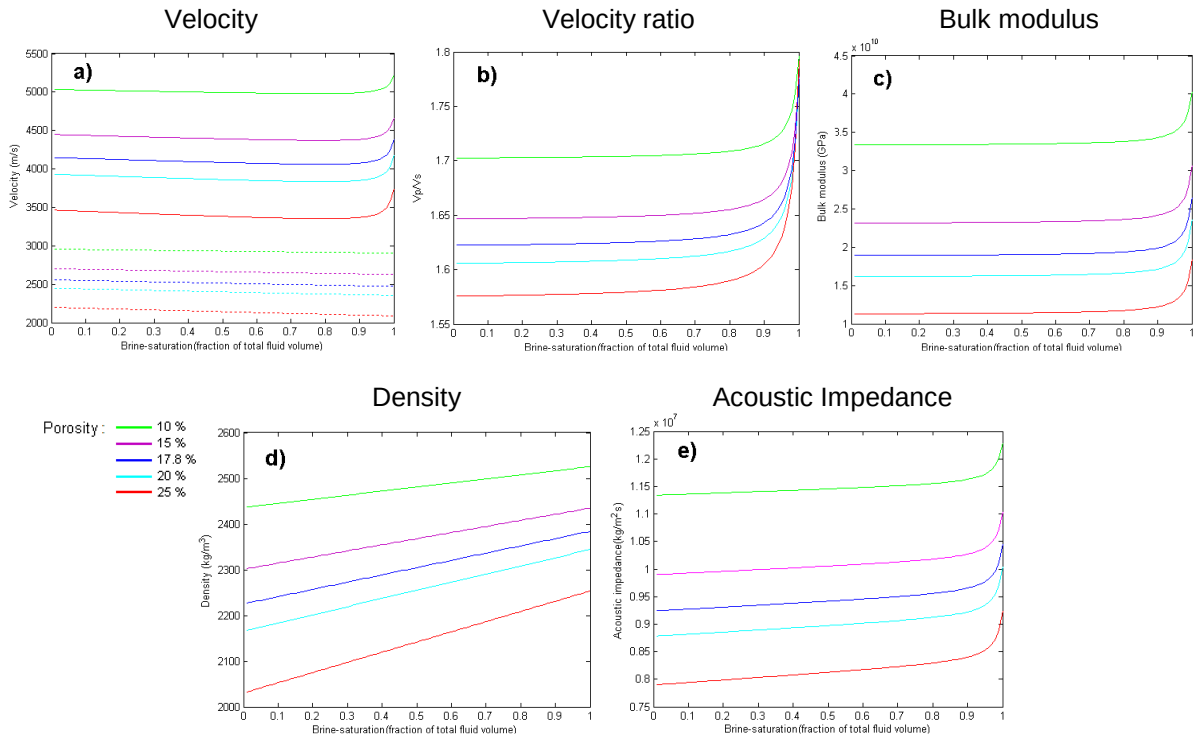

Figure 6.20 *Velocities (**a**), velocity ratio (**b**), bulk modulus (**c**), density (**d**), and acoustic impedance (**e**) for facies 2 with different porosities saturated with a fluid composition consisting of varying amounts of gas and brine, ranging from 100 % gas to 100 % brine.*

6.4.2 Amplitude versus offset responses

AVO analysis is widely used for fluid detection purposes, due to different fluids varying effects on AVO responses. Such responses for well B, when the whole carbonate model is saturated with the different fluids from Figure 6.16, are shown in Figure 6.21. Porosity for facies 2 is increased to 25 %, to enhance reservoir quality and fluid effects.

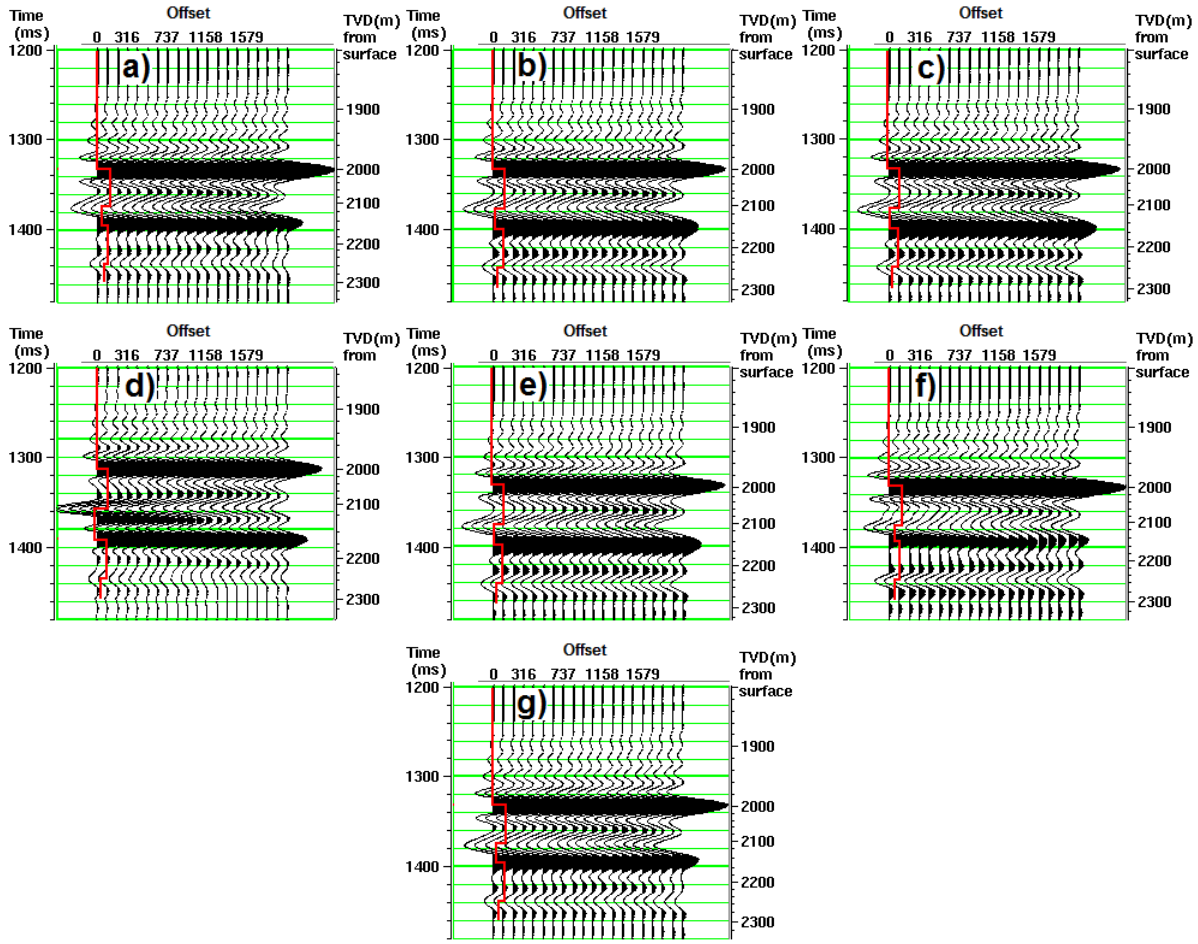

Figure 6.21 *AVO responses for well B for varying saturation fluids. Overlying sandstone is saturated with 95 % brine and 5 % gas. Porosity for facies 2 is increased to 25 %. The carbonate model is saturated with* ***a****) brine;* ***b****) 95 % brine, 5 % gas;* ***c****) 50 % brine, 50 % gas;* ***d****) gas;* ***e****) 50 % oil, 50 % gas;* ***f****) 95 % oil, 5 % gas; and* ***g****) oil. Red curve is P-wave acoustic impedance log.*

There is no significant divergence between the cases of brine saturation (a), and saturation of mixtures of gas and brine (b, c), although amplitudes increase when more gas is present, except for amplitudes of the interface between sandstone (saturated with 95 % brine and 5 % gas in all cases) and carbonate, which decrease. The explanation for the increasing amplitudes is the fact that the decrease in acoustic

impedance due to increasing gas content is more prominent for more porous facies, which makes the contrasts between the facies in well B greater, due to the specific stacking of the different facies (Figure 6.1). When the model is saturated with different portions of oil and gas, the results are quite similar as for brine and gas.

AVO classes present are class I for interfaces between sandstone and facies 1, and between facies 2 and 5, and class IV for interfaces between facies 1 and 2, and 5 and 4. Variation of saturation fluids does not change any of the AVO classes for this well when the whole carbonate model is saturated with the same fluid.

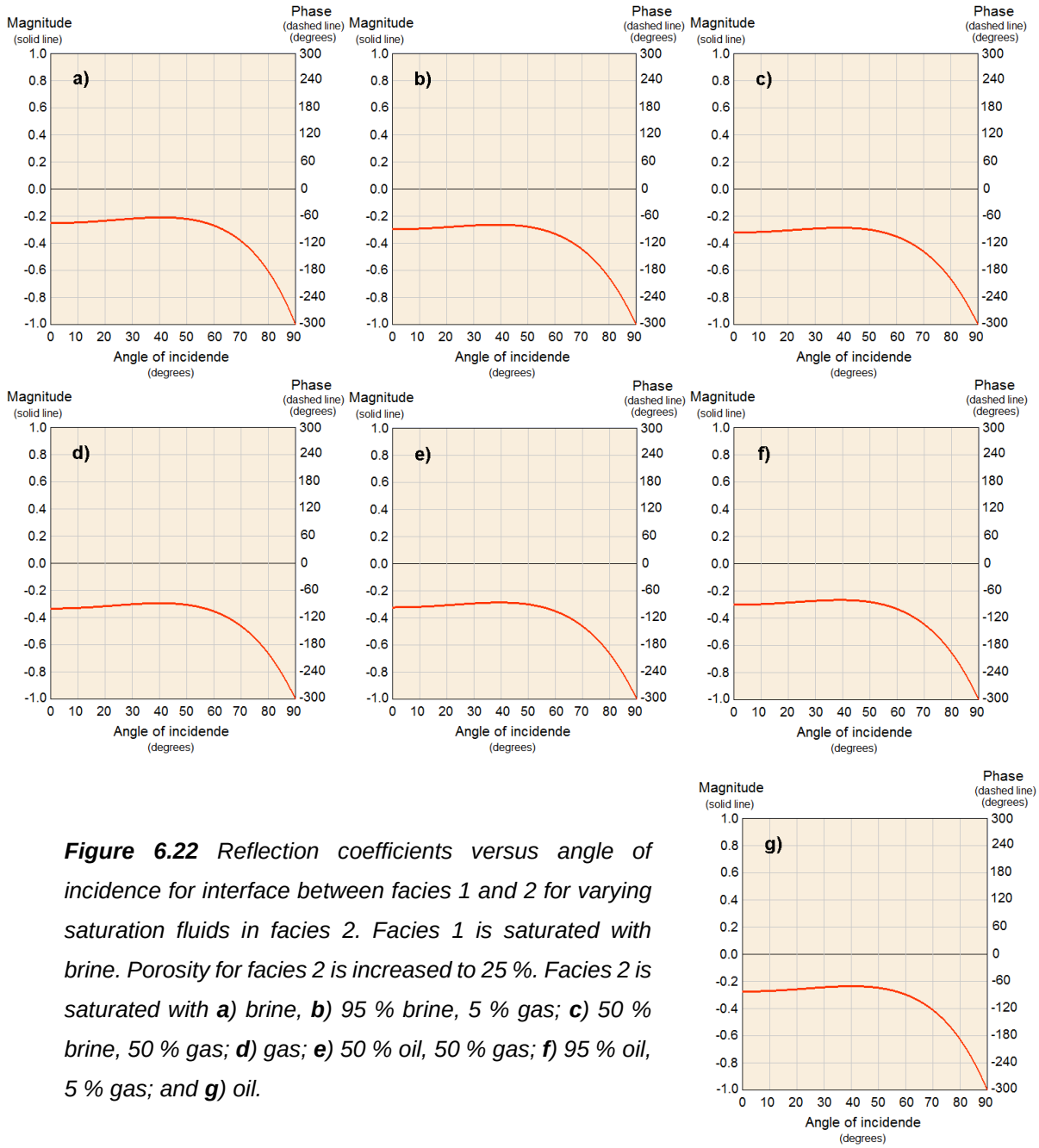

Figure 6.22 *Reflection coefficients versus angle of incidence for interface between facies 1 and 2 for varying saturation fluids in facies 2. Facies 1 is saturated with brine. Porosity for facies 2 is increased to 25 %. Facies 2 is saturated with* ***a****) brine,* ***b****) 95 % brine, 5 % gas;* ***c****) 50 % brine, 50 % gas;* ***d****) gas;* ***e****) 50 % oil, 50 % gas;* ***f****) 95 % oil, 5 % gas; and* ***g****) oil.*

Figures 6.22 and 6.23 show AVO responses for the same well, when fluid is varied only in facies 2, while the rest of the model is saturated with brine (porosity for facies 2 is increased to 25 % to enhance to effects of saturation fluids). The AVO responses can be classified as class IV responses for all saturations. The variations caused by the different fluids are minimal. However, amplitude increases when fluids with more gas content are present. The AVO gradient increases slightly for gas and increasing gas content in brine, compared to fully brine saturation. The opposite is true for oil saturation; the gradient is higher when no gas is added to the oil.

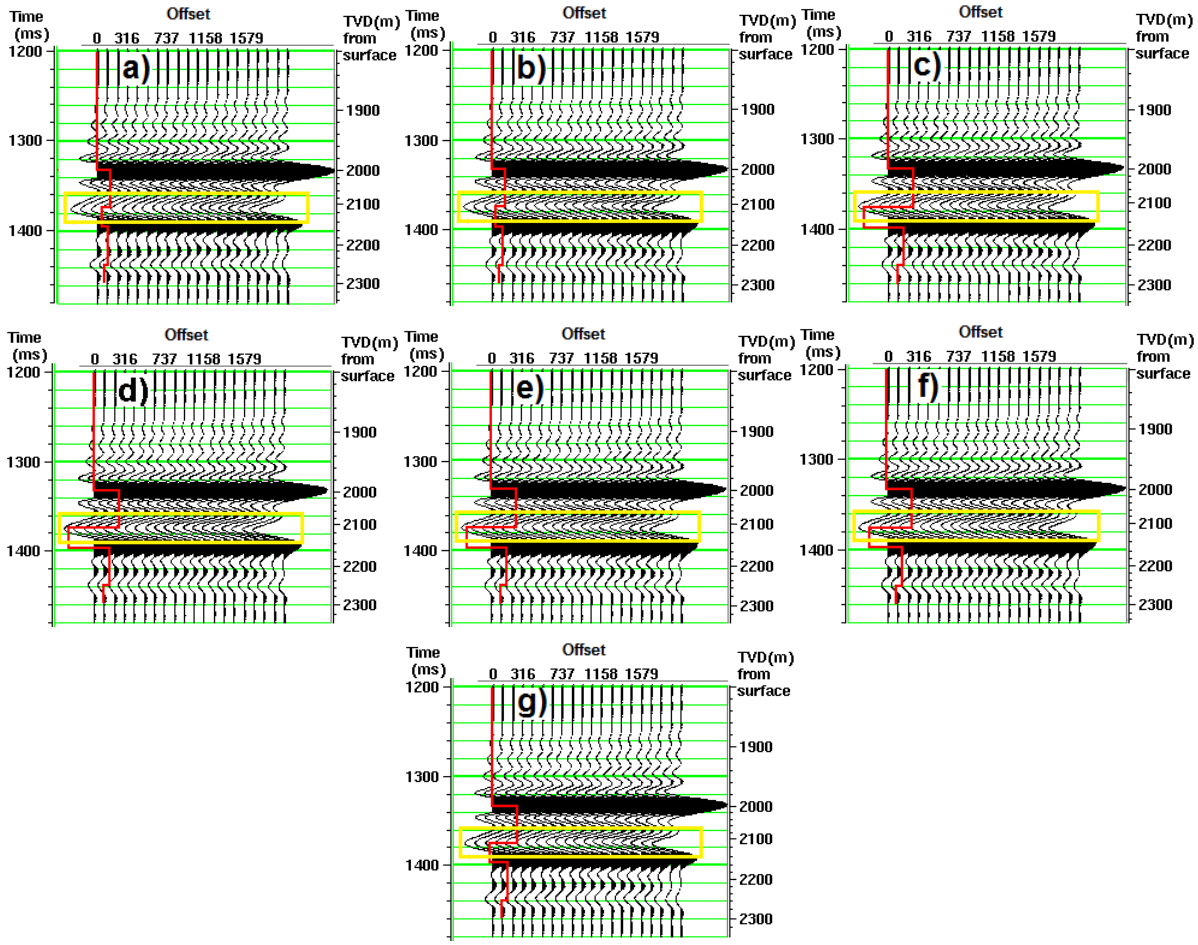

Figure 6.23 *AVO responses for interface between facies 1 and 2 for varying saturation fluids in facies 2. Facies 1 is saturated with 95 % brine and 5 % gas. Porosity for facies 2 is increased to 25 %. Facies 2 is saturated with* ***a****) brine,* ***b****) 95 % brine, 5 % gas;* ***c****) 50 % brine, 50 % gas;* ***d****) gas;* ***e****) 50 % oil, 50 % gas;* ***f****) 95 % oil, 5 % gas; and* ***g****) oil. Red curve is P-wave acoustic impedance log. Square marks upper interface of facies 2.*

6.5 Pressure and Depth Effects

All intrinsic rock factors previously examined may in different extents get altered by extrinsic factors like pressure and depth, and such alterations will be investigated in this section.

When burial depth increases, the weight of overlying lithology, and hence the lithostatic or overburden pressure will increase, as well as the hydrostatic pressure or pore pressure. Burial depths of 0.5, and 4 km will be simulated and compared to the initial depth of 2 km. The model at 500 m depth can be seen as an earlier stage of the evolution than when buried at 2 km depth, with higher porosities due to an earlier stage of cementation of original pore space. Or it can be seen as the model being uplifted from 2 to 0.5 km, with dissolution of matrix material, increasing the porosity. For this reason, new porosities have been calculated for the model simulating 500 m depth, assuming higher porosities. New porosities are calculated based on empirical equations (6.1 and 6.2) relating porosities to burial depth (Schmoker and Halley, 1982):

$$\varphi_c = 51.34e^{-z/1929}, \tag{6.1}$$

$$\varphi_d = 30.36e^{-z/4618}. \tag{6.2}$$

Φ is porosity and *z* is depth in meters. Indices *c* and *d* refers to rocks composed of 75 % or more of calcite and dolomite, respectively. Thus equation 6.2 is used for facies 3, while equation 6.1 is used for the rest of the facies. These equations imply initial porosities at zero depth to be 51.34 % for calcite and 30.36 % for dolomite, and they will give the same porosity for every calcite or dolomite facies at a given depth. Thus, the equations are rather used to calculate a ratio between porosity at 0.5 km and 2 km depth, to find new porosities for 500 m depth (Table 6.4). Due to the lower gradient for porosity reduction in dolomite, facies 2 rather than facies 3, has the highest porosity at 500 m depth.

Table 6.4 *Porosities for facies 1-5 at 500 m depth.*

Facies	Porosity
1	12.0 %
2	38.7 %
3	29.8 %
4	29.2 %
5	19.6 %

Table 6.5 *Mineralogy and matrix properties for facies 1-5 at 500 m depth. Letters indicate the following minerals:* ***C****: calcite;* ***D****: dolomite;* ***Q****: quartz; and* ***Cl****: clay.*

	1	2	3	4	5
Mineralogy	0.753 C	0.933 C	0.986 D	0.939 C	0.785 C
(volume fraction)	0.247 D	0.067 Q	0.014 C	0.061 Q	0.215 Cl
K_m *(GPa)*	80.93	72.89	94.62	73.22	50.65
μ_m *(GPa)*	34.83	32.70	44.78	32.64	21.39
ρ_m *(kg/m^3)*	2750	2706	2868	2706	2656

Assuming that porosity alterations at the different depths are due to dissolution/cementation of the pore space, and that the cement consists of calcite, original mineral compositions defined for the facies change, although the changes are small. New compositions and matrix properties for 500 m depth are given in Table 6.5.

Due to the lower pressure and temperature at 500 m depth compared to 2 km depth, pore-fluid properties changes. Temperature and pore pressure at 500 m depth is set to be 20℃ and 5 MPa, respectively, accordin g to the gradients listed in chapter 5. Thus, the fluid bulk modulus for this depth is 0.14 GPa, and density is 987 kg/m^3.

To further investigate depth and pressure effects on the facies-model, calculations simulating a depth of 4 km have been made. Equations (3.31-3.35) for pore shape alterations and the following pore volume reduction described in chapter 3, have been used to investigate closing of cracks, and to establish new pore-models for 4 km depth (Table 6.6). All cracks (aspect ratio lower than 0.01) in facies 1, 3 and 5 have been closed. The porosity reductions due to these changes in pore shapes are minimal. Assuming cementation of the original porosities (for 2 km depth), and that the cement consists of calcite, new porosities are calculated based on equations 6.1 and

Table 6.6 *Porosities, pore aspect ratios and their fractions of total porosity for facies 1-5 at 4 km depth.*

Facies	Percentage of total porosity	Aspect ratio	Porosity (%)
1	100 %	0.159	1.9
2	79.7 %	0.1	6.3
	20.3 %	1.0	
3	63.19 %	1.0	13.9
	36.81 %	0.1	
4	81.11 %	1.0	4.7
	18.89 %	0.015	
5	100 %	1.0	3.2

6.2, and new compositions and properties for the matrixes of each facies at 4 km depth (Table 6.7) are computed in the same manner as for 500 m depth. According to the gradients in Figure 5.2, pore pressure and overburden pressure at 4 km depth are 38 MPa and 90 MPa, respectively, and temperature is 111℃. Bulk modulus and density for the pore-fluid at this pressure are K_f = 1.10 GPa and ρ_f = 966 kg/m^3, respectively.

Table 6.7 *Mineralogy and matrix properties for facies 1-5 at 4 km depth. Letters indicate the following minerals:* ***C****: calcite;* ***D****: dolomite;* ***Q****: quartz; and* ***Cl****: clay.*

	1	2	3	4	5
Mineralogy	0.778 C	0.956 C	0.804 D	0.955 C	0.821 C
(volume fraction)	0.222 D	0.044 Q	0.196 C	0.045 Q	0.179 Cl
K_m *(GPa)*	80.51	74.19	91.03	74.13	53.55
μ_m *(GPa)*	34.54	32.46	42.07	32.47	22.59
ρ_m *(kg/m^3)*	2746	2707	2839	2707	2665

Increasing depth may alter a rock in different ways, and in complex ways. For example, fracturing, compaction, or cementation may take place. Sufficiently high overburden pressures, may compact the rock, reducing its porosity. Pore-fluids, then escape through the pore network. This process will reduce the stress, or pressure, in the rock. For an impermeable rock, or a sealed rock, the fluid will not be able to escape in this manner, and the pore pressure will get higher than normal (when fluids are free to escape). For this case there is overpressure in the rock (Figure 5.2). If the fluid saturating such an impermeable or sealed rock is completely incompressible, it will inhibit porosity decrease and compaction of the rock as a function of pressure. In addition, high pore pressures may inhibit cementation of the pore space. As previously stated (chapter 2), carbonate minerals generally precipitate under low pressures and dissolve under high pressures. Thus, overpressured rocks may have higher porosities than adjacent rocks.

6.5.1 Seismic velocities and acoustic impedances

Seismic velocities for all facies at different depths (0.5 km, 2.0 km, and 4.0 km) are showed in Figure 6.24. In addition, velocities for overpressure at 4 km depth are shown. Rather than a 38 MPa pore-pressure, 80 MPa are chosen for the overpressured rocks. The pore-fluid properties for this pressure and depth are ρ_f = 983

kg/m^3, and K_f = 1.88 GPa. Porosities, pore-models and mineralogy are set to be the same as for 2 km depth, simulating that the pore pressure inhibit porosity reduction.

It can be seen that both P- and S-wave velocities increase as burial depth increases. When there is overpressure at 4 km depth, the velocities are lower than for normal pressure at the same depth, and V_p are only slightly higher than for 2 km depth, while V_s is approximately unchanged. This is due to the fact that the facies with overpressure, in these calculations, have no porosity reduction compared to porosities at 2 km depth, and thus no mineral or pore shape alterations. Consequently, the only factor differentiating velocities at 2 km depth and at 4 km depth when there is overpressure is the fluid properties, which only shows minor changes for the two depths.

Velocity changes due to depth, and overpressure, are clearly smaller for facies 5, than the rest of the facies. This seems to be explained by the spherical pores of facies 5, which in the previous sections was found to restrict the velocity changes caused by other factors (e.g., Figures 6.3 and 6.5 for porosity alterations).

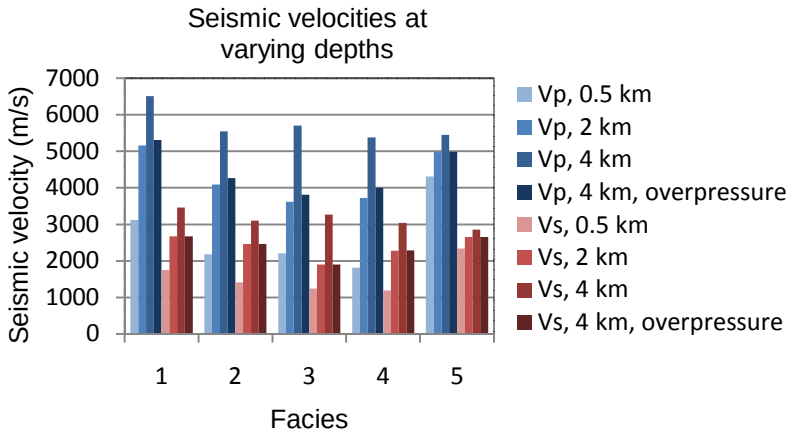

Figure 6.24 *Seismic velocities for facies 1-5 at 0.5, 2, and 4 km depth, for normal pore pressures, and at 4 km depth for overpressure.*

Depth, and overpressure, effects on velocity ratio and acoustic impedance is shown in Figures 6.25, and 6.26. It seems to be a grouping in the rock physics template of the facies at different depths, rather grouping of the individual facies. This means that a depth trend is observable in such a template for different lithologies. The trend is increasing impedances and velocity ratios for increasing depth. However, facies 1 and 3 shows a decrease in V_p/V_s at 4 km depth for normal pore pressure, in contrast to the

other facies which get their highest velocity ratios for this case. These deviations might be due to the deviations observed for these two facies in chapter 5 (Figure 5.3). For the case of overpressure, the velocity ratios seem to follow the same trend for all facies, and are increased compared to 2 km depth (normal pressure). However, due to the deviating results mentioned for normal pressure at this depth, the velocity ratio for overpressure are higher than for normal pressure for facies 1 and 3, while lower for facies 2, 4, and 5.

Although there seems to be a grouping (mostly in acoustic impedance) for the different depths, except for overpressure values which show more variance, all impedance values for facies 1 are clearly higher than for the other facies at any given depth, and are closer to the next “depth-group”, rather than the group for the actual given depth. This is also true for facies 5, except at 4 km depth at normal pore pressure. These deviations are caused by the initial high velocities for these two facies, resulting mostly from low porosities. In spite of these deviations in AI values, the trend for all facies is increasing AI for increasing depth. However, the resulting AI values for the case of overpressure, are lower than at normal pressure, and approximately the same as for 2 km depth (normal pressure).

Another observation is the fact that all facies, except for facies 1, have more similar impedance values at 4 km depth, when pressure is normal, than for the other cases.

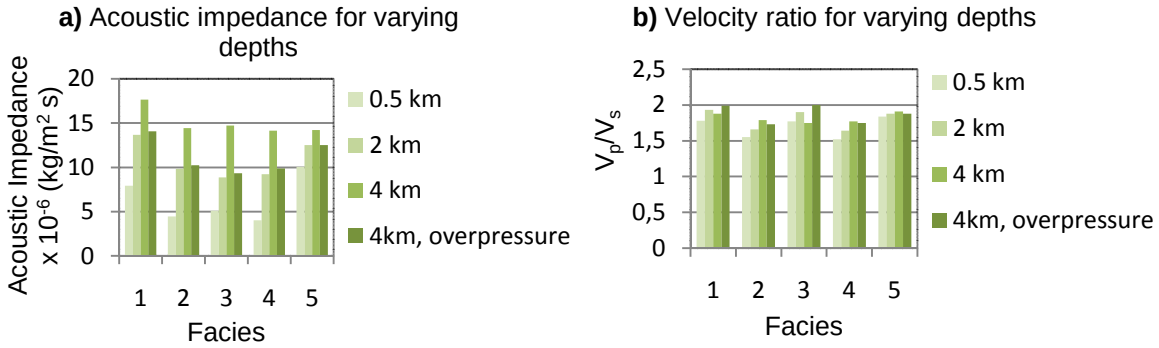

Figure 6.25 *Acoustic impedance variations (**a**), and velocity ratio variations (**b**) as function of depth for facies 1-5 for normal pore pressures, and for overpressure at 4 km depth.*

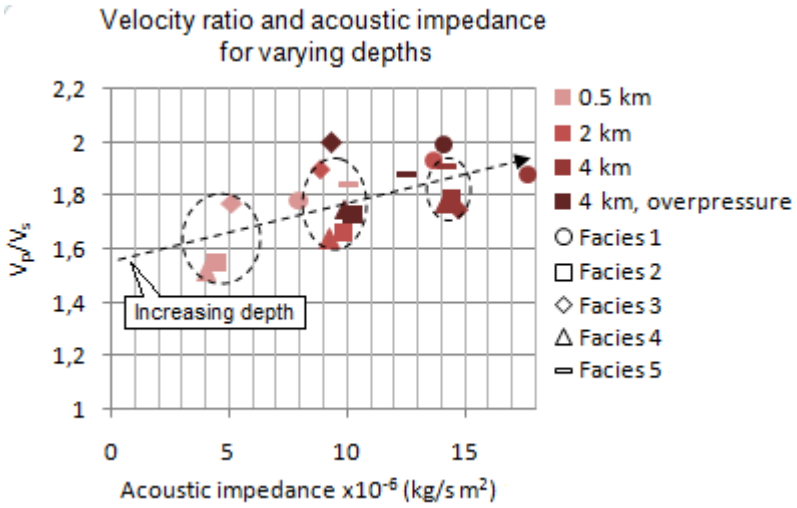

Figure 6.26 *Velocity ratio and acoustic impedance variations with depth for facies 1-5 for normal pore pressure, and for overpressure at 4 km depth.*

The variations in rock properties at the different depths examined, are due to altering porosities, pore-models, mineralogy, and saturation fluid properties, all caused by increasing pressure with depth. All these factors are varying at the same time in the simulation of different depths performed here. To investigate the effects of increased pore pressure on velocities separately, velocities are calculated for the facies with original properties for 2 km depth, saturated with fluids corresponding to pore pressures from 20-40 MPa (Figure 6.27). Velocity variations due to increasing pore pressure are negligible for S-waves, and slightly increasing for P-waves.

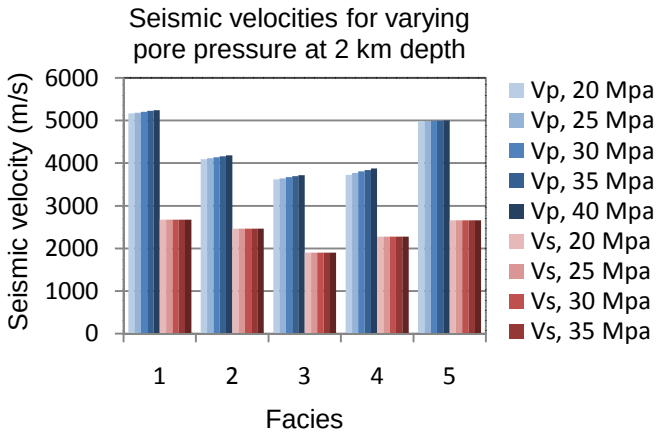

Figure 6.27 *Seismic velocities for facies 1-5 at 2 km burial depth for pore pressures ranging from 20-40 MPa, calculated with 5 MPa intervals.*

6.5.2 Amplitude versus offset responses

AVO responses for the three different depths studied are shown for well B in Figure 6.28. The isolated part of facies 2 penetrated by this well is enclosed by facies 1 and 5, which have low porosities, and are thus chosen to be the one to have an overpressure at 4 km depth, while the other facies in the well have normal pore pressures.

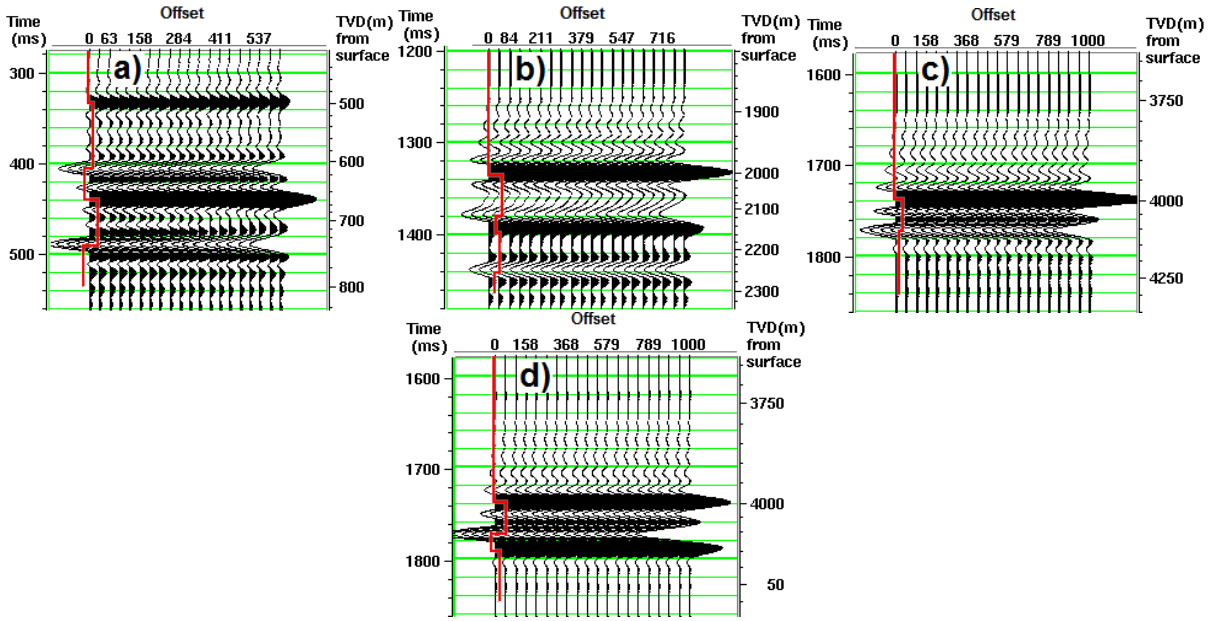

Figure 6.28 *AVO results for well B at 0.5 km depth (**a**), 2 km depth (**b**), 4 km depth for normal pore pressure (**c**), and 4 km depth for overpressure in facies 2 (**d**). Red curve is P-wave acoustic impedance log.*

The boundary between the overlying sandstone and facies 1 gives a positive reflection coefficient (*R*) and a negative AVO gradient (class I), thus showing decreasing amplitude as offset increases, for all depths. The next boundary downwards, between facies 1 and 2, results in a negative *R* at all depths. For 0.5 and 2 km depth, amplitudes decrease for larger offsets (positive gradient), which classify the responses as class IV. At 4 km depth the gradient for the same boundary is negative, giving increasing AVO, and a class III response. However, when overpressure is present in facies 2 at this depth, the boundary between facies 1 and 2 makes a class IV response, as for the other depths.

The boundary between facies 2 and 5 gives a class I AVO response, with a positive *R*, and a negative gradient, for 0.5 and 2 km depth, and at 4 km dept when overpressure is present. Again, the result for normal pressure at 4 km depth deviates

from the other cases, and the reflections from the boundary can be classified as a class II AVO response, which means that *R* is close to zero, and the boundary is hard to detect at any offsets as seen in Figure 6.28 c).

The lowermost boundary in this well, between facies 5 and 4, have a negative reflection coefficient and a decreasing AVO, corresponding to a class IV response, at the two lowest depths considered. At 4 km depth this boundary is hard to detect and the AVO signature is a class 2 response.

The concluding observations from the AVO responses for well B at varying depths, is that responses is the same at 0.5 and at 2 km depth, while all responses except for responses from the boundary between the overlying sandstone and the first facies of the carbonate model, are changed at 4 km depth. However, in the case of overpressure in facies 2 at the same depth, the interfaces above and below it show the same AVO responses as for the other depths considered.

6.6 Relative Comparison of Factors

All factors examined in the previous sections alter seismic responses in different ways and with different magnitudes. Figure 6.29 shows most of the factors studied above calculated for facies 2. In a) a rock physics template shows the directions for variations of porosity, pore shapes, mineralogy, and saturation fluid. Depth calculations are not incorporated, since depth where modeled altering all of the other factors, while this figure is simply to show the relative trends of each factors. It can be seen that adding different minerals to a pure calcite matrix can result in both increasing and decreasing V_p/V_s ratio, and increasing or decreasing acoustic impedance. Further, it is seen that although quartz and aragonite shows similar paths, the effect of adding quartz to facies is greater than for aragonite. Highest V_p/V_s ratios are achieved when introducing clay to the rock, and for a very low porosity (5.31 %), and for pore model 1. However, while clay reduces the acoustic impedance, it is high for low porosity and pore model 1. Lowest velocity ratios are clearly achieved when introducing some amount of gas to a saturation fluid consisting of brine or oil. The different pore models plot quite randomly, since there are no gradual or continuous variations in pore shapes from model 1 to 5. However, it is obvious that porosity and pore shapes can have quite similar effects on seismic responses, and an RPT may not be the best tool for differentiating them.

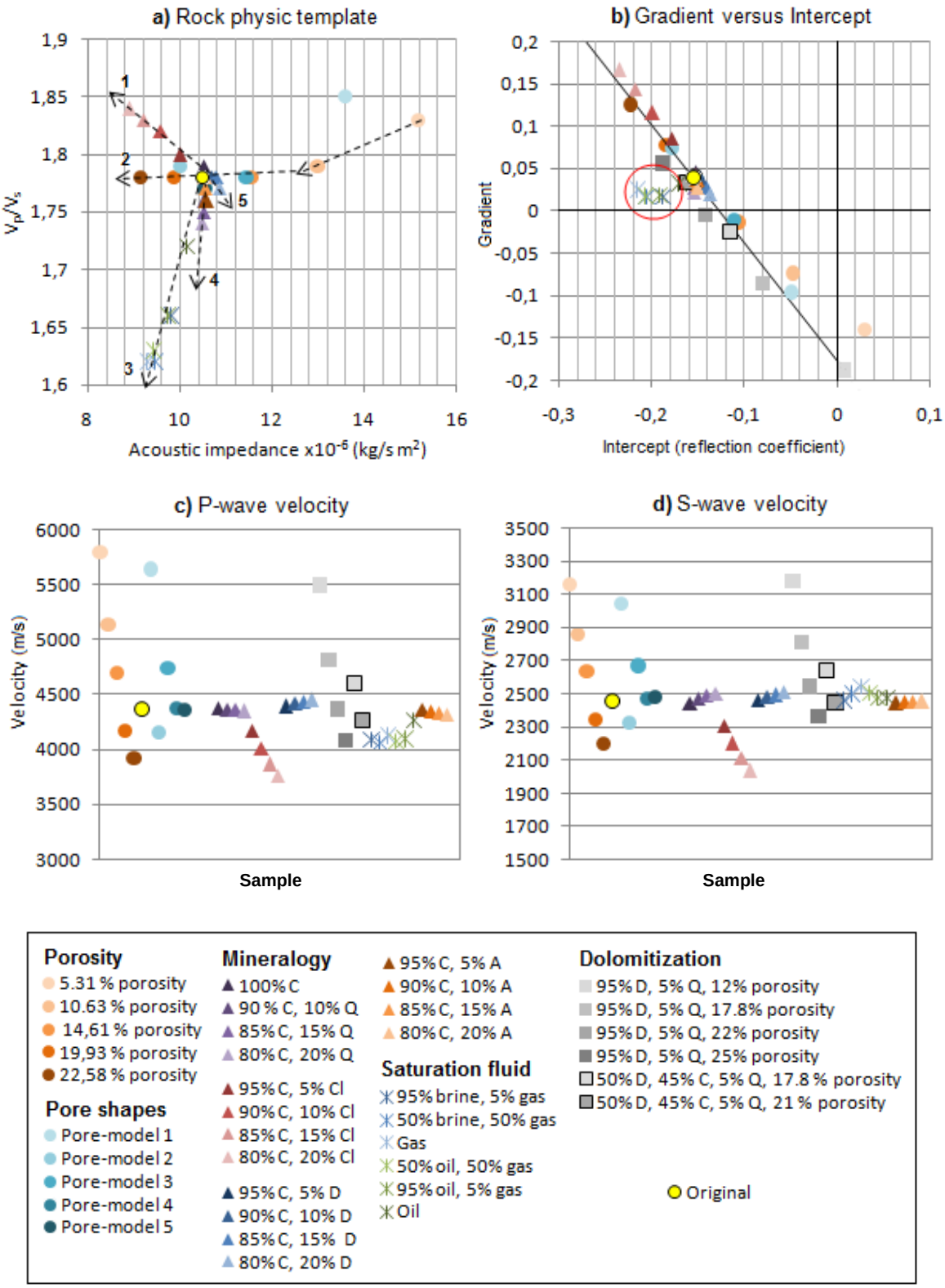

Figure 6.29 *Rock physics template (**a**), gradient versus intercept plot (**b**), P-wave velocities (**c**), and S-wave velocities (**d**) for variations of porosity, pore shapes, mineralogy, and saturation fluid in facies 2, overlaid by facies 1. All values other than for fluid variations correspond to brine saturated facies, calculated by use of Gassmann. Numbers in **a**) corresponds to increasing: **1**: clay content; **2**: porosity; **4**: aragonite or quartz content; **5**: dolomite content; and decreasing: **3**: fluid density. Letters refer to: A: aragonite; C: calcite; Cl: clay; D: dolomite; and Q: quartz. Pore-models are specified in Table 6.1.*

Figure 6.29 b) shows a gradient versus intercept (GI) plot for the same factors as showed in a). Calculations are performed for the interface between facies 1 and 2 (well B), and the alterations are done in facies 2. Facies 1 have original values and are brine saturated. This plot reveals a clear trend line for all alterations in facies 2. Exceptions to this line are values for the two lowest porosities examined, and values for all saturation fluids (marked by circle) except for saturations of pure brine and 95 % brine and 5 % gas. While the deviating porosity points have higher intercepts than the trend line, deviating points for varying saturations have lower intercepts than the trend. According to these observations fluid detection seems possible both in an RTP and in a gradient versus intercept plot for a carbonate reservoir, where overlying rock also is a carbonate, despite all other variables studied, which can alter the rock. Figure 6.29 c) and d) shows P- and S-wave velocities, respectively, for the same variations of factors as studied in a) and b). It can be seen that most of the V_p values falls in the range 4000-4500 m/s, and for S-waves the range is around 2200-2600 m/s. All values for varying saturation fluids falls into these ranges, which means that examining P- and S-wave velocities alone cannot differentiate fluid effects from other factors. This clearly reveals the advantages of RTP and GI plots.

Another fact to point out is the benefits of a GI plot compared to simply dividing AVO responses into classes. Most of the data in Figure 6.29 b) fall into a class 4. However, all points in this class follow the trend line, except for points corresponding to variations in saturation fluid. Thus, since all four classes (as stated earlier, and seen in the figure) can be found in carbonate-carbonate interfaces due to complexity of such rocks, and the corresponding wide ranges of lithologic properties, the deviations from the background trend seems more essential to investigate, than the classes alone.

6.7 Resolution

All of the seismic responses showed in this chapter are calculated corresponding to the Zoeppritz equations. These equations compute the “perfect” amplitude results for rays travelling through a layered model. That is, no energy loss due to geometrical spreading and absorption is concerned. In addition, only primary reflection events have been modeled. Such perfect seismic images are useful to study the effects different variables may have on seismic signatures. However, when studying real seismic

images, energy loss and noise will alter such optimal signatures. Figure 6.30 shows seismic responses including geometrical spreading and transmission losses from well B at different depths. Compared with Figure 6.28 a-c, showing the same images without energy losses, the images below can be seen to include more noise. A result of increasing depth is “compaction” of the seismic responses. This effect is a result of reflection events being plotted in time, rather than depth. Thus, at 500 m depth (a), where velocities are lower, more time passes from the ray reaches one interface to the next, than at 2 km depth (b), or 4 km depth (c), where less time passes due to higher velocities. Not all interfaces in the well can be seen at 4 km dept. This is because velocities calculated for this depth have all increased compared to original values at 2 km depth, and have become more similar in values, thus giving comparable acoustic impedances, and low reflection coefficients. Thus the interface between facies 5 and 4 cannot be seen at 4 km depth.

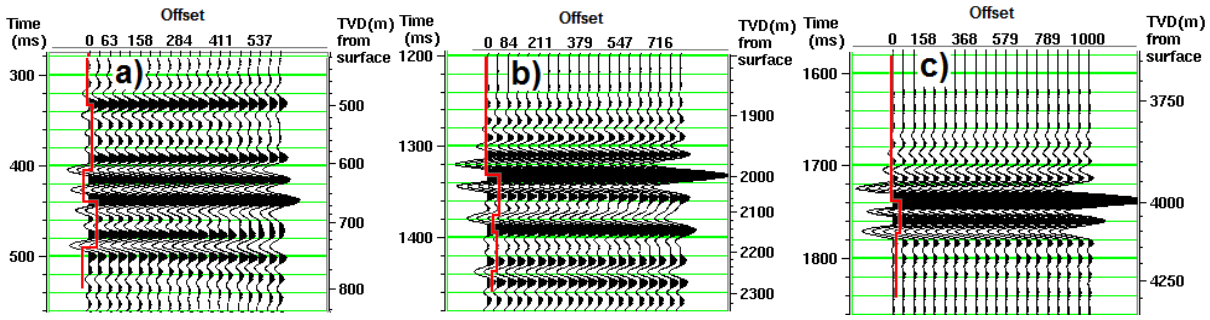

Figure 6.30 *Seismic responses well D at **a**) 0.5 km depth; **b**) 2 km depth; and **c**) 4 km depth, when energy losses are concerned. Red curve is P-wave acoustic impedance log.*

A common seismic problem for imaging deep structures, is low amplitudes caused by energy losses. In Figure 6.30 the reflections seen at 4 km depth are as bright as for the two shallower depths. However, more energy loss would be present if the carbonate model where buried beneath varying lithologies, giving rise to reflections and transmissions, rather than a uniform sandstone with no internal reflectors.

Chapter 7: Discussion

This thesis has focused on exploring resulting seismic responses from variation of common rock properties, seeking to demonstrate possible links between rock properties and seismic signatures. In addition to try to reveal such links, another aim has been to establish possible approaches on how to differentiate between seismic responses of various variables. Data from real measurements (performed by other authors), and additional assumptions made according to these, have been used as input for synthetic modeling to ensure the validity of the model defined. This established synthetic model has been the basis for exploring the results of variation of various rock parameters determining the elastic behavior of rocks. The discussion of the overall outcome of this modeling, will focus on the different trends observed, emphasizing to reveal valuable information on how to invert information about rocks from seismic data. In addition the results will be discussed in light of observations made by other authors, and the effects of assumptions incorporated in the utilized rock physics models, and their validity, will also be a focus. Last, thoughts concerning further work will be presented.

7.1 Observations

7.1.1 Porosity and pore shapes

Porosity has been stated by various authors to be the main controlling factor for velocities in rocks (e.g., Wang, 1997). Velocity variations caused by varying porosity have in this study been observed to be as large as about 2000 m/s for P-waves for a porosity range from 4-17 % (Figure 6.3). For S-waves, variations for the same range were about 1000 m/s. The resulting V_p/V_s ratio, and acoustic impedance (AI), have been observed to decrease as porosity increases (e.g., Figure 6.4), although velocity ratio alterations are not as noteworthy as variations in AI. This is in accordance with observations by Anselmetti and Eberli (1993, 1997), which have observed that the velocity ratios for Maiella limestones decrease as porosity increases. However, in addition they observed that the V_p/V_s range for carbonates from various locations, increased for lower porosities.

The observed effects on seismic parameters for porosity variations are influenced by pore shapes. Figure 6.5 shows that the P-wave velocity at 25 % porosity varied as much as nearly 1500 m/s due to different pore models, while for S-waves the range was over 500 m/s. At the same porosity V_p/V_s ratio had a range near 0.20, and the acoustic impedance varied with about 3.0 x 10^6 kg/s m^2. These ranges were calculated for various pore models established in order to try to reveal effects of different pore shapes in different amounts on velocity, velocity ratio, and acoustic impedance. Thus, end members for these theoretically defined pore models may not be likely to find in nature, so that the ranges in seismic parameters caused by varying pore models, are probably smaller than maximum ranges observed from this study. However, important information can be derived from these observations. Velocities of rocks consisting of mostly spherical pores were influenced less by porosity variations than rocks with lower aspect ratio pores. This was also true for acoustic impedance and V_p/V_s ratio. Actually, facies 5, which consists almost entirely of spherical pores, has been observed throughout the study be less affected by other factors.
When significant amounts of pores with aspect ratios 0.1 or 0.01 were present, velocities, velocity ratio, and acoustic impedance clearly decreased, and the variations due to increasing porosity were greater than when larger amounts of spherical pores were present. Figure 6.6 showed that small fractions of 0.001 aspect ratio pores, in contrast to 0.01 pores or pores with higher aspect ratios, greatly increased the V_p/V_s ratio. This tendency is supported by observations by Guéguen et al. (2009), which have found cracks to increase the velocity ratio for sandstones, and also by Tatham (1982), who in addition states that dolomite velocity ratios are controlled by dominant aspect ratios in the range 10^{-2} to 10^{-1}, and the velocity ratios of dense limestones of generally low porosity, are controlled by aspect ratios in the range 10^{-3} to 10^{-2}.

Observations in this study support the statement that pore shapes are of almost equal importance as porosity for carbonates (Anselmetti and Eberli, 1993, 1997).

Concerning the pore models assigned to the facies, facies 1 and 3 have small, although significant, amounts of very low aspect ratio pores. Thus these pore-models may not be totally realistic to be found in nature. Nevertheless, these pore models have been assigned the facies to fit the measured data and the assumed mineralogies (based on measured data), and can be seen as general elastic effects of all factors that may have an impact on elastic behavior, which are not incorporated in other ways, like

cement type and sites of cementation in the pores, in addition to effects of pore shapes.

7.1.2 Mineralogy

Effects of varying amounts of different minerals included in a calcite matrix have been studied to reveal possible seismic effects of variations in carbonate mineralogy. Increasing quartz content up to 20 % was observed to have little effect on seismic velocities for the facies considered (Figure 6.11 and 6.12). The same was true for acoustic impedance (Figure 6.14). However, V_p/V_s ratio was more affected, and decreased as quartz content increased (Figure 6.12 and 6.14). Results for aragonite were relatively comparable as for quartz, and in a rock physics template, results for these two minerals were observed to coincide and were not possible to separate.

When dolomite was added to the calcite matrix, P-wave velocities increased (Figure 6.11 and 6.12), while the increases in V_s were observed to be insignificant for matrix compositions containing up to 20 % dolomite. A dolomitizaion process may increase or reduce porosity in a rock. This process has been modeled for facies 2 for full dolomitization (all calcite are converted to dolomite) and for partly dolomitization (50 % of the matrix consists of dolomite), concerning both increasing, decreasing, and unaltered porosity. Figure 6.13 showed that velocities can be quite similar for different dolomitization scenarios. Increasing dolomite content, increased velocities, while increasing porosity had a reverse effect. However, it was seen that in a rock physics template, increasing porosity and increasing dolomite content have opposing trends (Figure 6.14). Although both parameters caused decreasing V_p/V_s ratio when increased, the effects on acoustic impedance differed. While adding more dolomite to the matrix was observed to increase the impedance, increasing porosity reduced it.

Pore shape effects were not incorporated when investigating dolomitization, due to a lack of information concerning quantification of pore shape effects due to solution and cementation. Thus, the results do not fully reveal effects of dolomitization.

Increasing clay content was observed to be a more influencing factor than the other minerals studied. Velocities decreased notably from 0-20 % clay content (Figure 6.11). Both P- and S-wave velocities decreased with about 500 m/s. On the other hand, V_p/V_s ratio were observed to increase when adding clay to the calcite matrix, and in addition the ratio was higher than for compositions of the other minerals studied

(Figure 6.12 and 6.14). Acoustic impedance showed a significant decrease due to the decreasing velocities and density.

Eberli et al. (2003) have stated that insolubles, mainly clay, lower velocities in carbonates, and that fast velocities (> 4000 m/s P-wave velocity) are only to be reached if the clay content is below 5 %. This statement seems to be in accordance with the observations made in this project, although facies 5 has been defined to consist of 19 % clay, and has a P-wave velocity of 5062 m/s. However, this matrix was assumed based on the low density and high velocity measurements for this facies, without any information about the mineralogy itself. In addition, a pore model consisting of mostly spherical pores has been assigned this facies to fit the measurements and the defined matrix properties. Thus, this facies is probably not totally reliable for the evaluation of effects of clay-content on velocities, since spherical pores give high velocities, and in addition is observed to reduce effects of other parameters.

Compared to porosity and pore shapes (Figure 6.3 and 6.5), mineralogy was shown to have less impact on velocities for carbonates. Varying amounts of the three carbonate minerals (calcite, dolomite, and aragonite), gave only slight variations in velocities. Of common non-carbonate minerals which may be present in carbonate rocks, quartz had an insignificant effect on velocities, while clay caused the greatest effects of the minerals considered. Thus, mineralogy seems to be a less important factor determining velocities in pure carbonates. This is supported by observations from other authors. Eberli et al. (2003) and Anselmetti and Eberli (1993, 2003) states that the mineralogic composition of carbonates has little direct influence on seismic properties, and that amount of dolomite has little correlation with velocity. However, the dolomite type, and the dolomitization process, which can be fabric destructive or fabric preserving, can yield extremely high or very low velocities. Also, the processes that alter mineralogy may have a strong influence on velocities, by altering porosity and pore shapes (Anselmetti and Eberli 1993, 2003).

Tatham (1982) points to the affection of pore shapes on V_p/V_s ratio, which makes lithology detection from this factor uncertain for carbonates.

7.1.3 Fluids

Fluid effects on velocity are different for P- and for S-waves. The general observations in this study were that V_p decreased for lower-density saturation fluids, except a slight

increase for pure gas saturation, while V_S decreased for denser saturation fluids. Velocity variations for all fluids and facies studied were smaller than 500 m/s.

In a rock physics template increasing V_P/V_S and AI were observed for saturation of higher-density fluids (Figure 6.18). The V_P/V_S-AI gradients were approximately the same for each facies, although the exact values were varying. The amounts of variations are dependent on lithology. Figure 6.20 showed that in the range of 0-10% gas in the fluid, P-wave velocities had a rapid increase as gas content decreased. When gas content was lower than about 10 %, further increase in gas content had insignificant impact on velocities. It was also seen that porosity was more significant for velocities than saturation fluid.

Fluid substitutions are performed by the Gassmann equations, and the reliability of the results will be discussed later in this section.

7.1.4 Pressure and depth

Depth and pressure can alter a rock significantly, and in various ways. Thus it may be difficult to predict alterations in a rock due to increasing depth and pressure. Generally porosity decreases with increasing burial depth, while pore pressure increases. This is the basis for depth modeling in this study. Porosities at different depths have been predicted based on empirical gradients from Schmoker and Halley (1982). Matrix composition has been changed assuming that reduction of pore space is due to calcite cementation. From 2 to 4 km depth, pore models have been altered assuming closing of cracks. In addition, a case of overpressure at 4 km depth was modeled assuming the same rock properties as at 2 km depth, but a higher pore pressure. With these assumptions, velocities were observed to increase significantly with depth, however the increases from 2 to 4 km for the case of overpressure, were only slight (Figure 6.24). In a rock physics template, increasing depth was observed to increase both acoustic impedance and velocity ratio, although deviations to this trend exist (Figure 6.26). Facies 1 and 3 showed higher velocity ratios at 2 km than at 4 km burial depth. As pore space got cemented by calcite for increased depth, matrix compositions for facies 1 and 3, consisting of calcite and dolomite, got higher fractions of calcite, which increased V_P/V_S ratio of the matrix. In addition, the velocity ratio was observed to increase as porosity decreased. These facts oppose the observed decrease in velocity ratio for facies 1 and 3 at 4 km depth. The explanation may thus be the effect of closing

of cracks in these two facies. Closing cracks also appeared in facies 5, but the amount of cracks initially present was significantly smaller in this facies than in facies 1 and 3.

This deviation might also be due to calculation method, since these to facies are originally saturated, while facies 2 and 4 are originally dry. Facies 5 which also is originally saturated do not show this deviation, but is seen to have less variation than the other facies in all cases. Deviations for these two facies are also observed in chapter 5 when comparing Gassmann and DEM results, supporting the assumption that calculation method may be causing the deviation.

The observed depth responses may be reliable, since compaction and cementation generally increase with depth. However, due to carbonates diagenetic potential, it is shown that neither burial depth nor age has a major control on velocity evolution (Anselmetti and Eberli, 2003). Compaction alone is not the main process causing increasing velocities as burial depth increases. Porosity reduction due to cementing is of major importance, and porosity is stated to be the most important physical factor influencing velocity (Anselmetti and Eberli, 2003). However, a positive relation between velocity and depth is not necessarily the case. Velocity inversions may occur due to different diagenetic potentials of rocks. Different facies may have different evolutions (Figure 3.5). Velocity inversions occur in the model defined for this project, due to stacking of different facies with varying velocities. In fact, carbonates deposited at shallow water generally have higher porosities than carbonates from deeper shelf, slope or basin, due to higher diagenetic potential of shallow-water carbonates (Anselmetti and Eberli, 1993). This is true for the original values for facies concerned in this project; the lagoon facies are of the highest velocities.

For the depth simulation carried out in this study, cracks were closed due to increasing pressure at 4 km depth. On the other hand, fracturing could also occur when pressure increases, which will decrease velocities. Thus there can be great variations in velocities for carbonate rocks at a given depth, and predicting exact evolution of a rock as it get buried is not straightforward. Porosity- and velocity-evolution from time of deposition through burial history are controlled by initial lithology and diagenetic alterations together (Eberli et al., 2003). However, the depth modeling in this project could represent a general case, since cementation and porosity reduction, and closing of cracks, are processes which may take place in increasing amount as burial depth

increases. But it is important to keep in mind that great deviations to this trend may occur.

The case of overpressure at 4km depth was simulated by increasing pore pressure, keeping porosities constant compared to at 2 km burial depth. Resulting velocities were higher than at 2 km depth, and lower than at 4 km depth when pore pressure was normal. Such lowering in velocities due to abnormal high porosities in overpressured rocks may appear in real settings, but is certainly not necessarily the case. High porosities as result of “undercompaction” are not required for cases of overpressure. Teige et al. (1999) have observed that porosity is not elevated in overpressured North Sea shales, and states that only if compaction is completely mechanical, higher than normal porosities can be expected in overpressured rocks. When compaction is mainly due to diagenesis, porosities can be normal despite the presence of overpressure. Thus, for carbonates there may be a lack of relationship between overpressure and elevated porosities, due to carbonates great diagenetic potential. However, Conybeare and Shaw (2000) have proposed excess pressure release associated with rock failure as a prominent mechanism for initiating carbonate cementation, meaning that cementation is inhibited for overpressured rocks, which is consistent with the general fact that carbonates precipitate at low pressures and dissolve at high pressures. Thus, there might be higher-than-normal porosities in overpressured carbonates even though they are highly susceptible to diagenetic processes, since high pressures may inhibit the porosity-reducing diagenetic processes.

For increasing pore pressure, from 20 to 40 MPa, slight increases in P-wave velocities were observed, while the effects on S-wave velocities were negligible (Figure 6.27). These effects were calculated by changing fluid properties according to the given pressures, which made the saturated rocks stiffer when pressure was increased. Thus, pore shape alterations due to varying pore pressure are not considered.

Kitamura et al. (2005) have observed that velocities are controlled by lithology under low pore pressure conditions, while at pressures over hydrostatic pressure conditions (10-20 MPa) velocities show no clear relation to lithology. These observations are opposing the results from this study, where pore pressure variations from hydrostatic (20 MPa, at 2 km burial depth) to 40 MPa resulted in only small increases in V_p, while V_s was unchanged. Significant velocity variations for the different

facies were seen at all pore pressures in the given range. This result indicate that simulating increasing pore pressures by substituting fluids calculated for higher pressure conditions, utilizing Gassmann theory, may not be fully appropriate. This is probably due to the fact that fracturing as a result of increasing pore pressure is not incorporated in the study.

7.1.5 AVO responses

All variables studied have been observed to affect AVO responses, and all four AVO classes are observed for carbonate-carbonate interfaces. This observation is supported by observations of Li et al. (2003), which also have found that all classes can be present in limestone/dolomite interfaces.

Even though a class 4 response frequently is associated with gas saturation (e.g., Castagna and Swan, 1997), this study has shown that this response can also be achieved as a result of other rock properties. However, when results were plotted in an intercept-gradient plot, this revealed a trend-line which fits all data points for variations of the considered factors quite accurately, except for values for fluid substitution, and values for pore model 1, and for very low porosity (Figure 6.29 b)). When more gas was present in the saturating fluid, intercept and gradient values deviated more from the trend-line, caused by reduced gradients and intercepts compared to full brine saturation. Thus, even though the interface studied felled into a class 4 both when fully brine saturated with original intrinsic rock properties, and when saturated with other fluid compositions, and for variations of other parameters, saturation by fluid compositions containing amounts of gas and/or oil could be separated from brine saturation, and from other factors. Thus, AVO studies may be valuable for fluid detection in carbonates, even though their complexity is high, which may give rise to considerable velocity variations. This is supported by observations of other authors. Li et al. (2003) have stated that fluids do affect carbonate rock properties with significant magnitude, and have found class 3 and 4 AVO effects to correspond to good quality reservoirs. Eissa et al. (2003) have observed a smaller intercept for gas-saturated dolomite than for tight limestone, and a small positive gradient for gas-dolomite, while tight limestone exhibits a larger negative gradient. Gas saturation of facies 2 gave a low intercept and a small positive gradient.

The importance of looking for deviations from an expected background response, rather than simply group responses into different classes is pointed out by

Castagna and Swan (1997). They claim that such grouping should be done in the context of deviations, meaning the given class of a response only is important for the deviating responses.

7.1.6 Relative effects of different variables

As observed, different rock variables can alter seismic properties in various ways. Thus, an aim is to be able to differentiate between responses caused by different rock properties. As seen in Figure 6.29 a) effects of variable parameters can be differentiated in a rock physics template, due to their distinctive trends, even though they may cause velocities of quite similar magnitudes. Gas saturation clearly resulted in the lowest V_p/V_s ratio of all variations, while highest ratio was achieved for the cases of very low porosities, spherical pores, or fractions of clay introduced to the rock. Further it was seen that such high-ratio responses could be separated due to their acoustic impedance values, since clay caused a low value in contrast to the two other parameters.

Although variations of different parameters seem to be possible to differentiate in an RTP, the effects of pore shapes can give various results due to the wide ranges of possible combinations of different pore shapes, and may thus plot quite randomly, even though given pore shapes affects seismic parameters in certain ways (Figure 6.5 and 66).

Concerning porosities, there were almost no variations in velocity ratio for variations in porosity for acoustic impedances below about $13*10^7$ m/s*kg/m^3, although clear variations in AI was observed (Figure 6.29 a)).

The quite coincident values which may result from porosities and pore shapes, once more point to the assumption that pore shapes are of almost equal importance as porosity in carbonates, and it is of great importance for seismic inversion to be able to differentiate them.

Seismic parameters for facies 5 are observed to vary less than for other facies for variations of all factors, except pore shapes. The pore model assigned to facies 5, consisting almost entirely of spherical pores is assumed to be the reason for this deviating behavior of facies 5.

7.2 Reliability of Observations

Since this study has been a synthetic modeling project, although based on real measurements, an important question is if the results are reliable and thus may be expanded as general information, rather than just results of this specific study. This question is raised due to the fact that all rock physics models have incorporated assumptions and limitations. Calculations have been performed using DEM approach, and Gassmann equations have been used for fluid substitutions. DEM calculations are based on the Kuster-Toksöz equations, which assume isolated pores, whereas Gassmann theory assumes a connected pore structure. Pore-space in carbonates may be connected or isolated. DEM incorporate pore-to-pore interactions due to higher order scattering. Thus, there are some important differences between these methods. Of great importance is fluid substitution. This is especially important in this study since both initially wet and dry rock measurements have been used. In chapter 5 it was seen that originally wet and originally dry facies got different results when comparing Gassmann and DEM. Gassmann gave lower fluid effects than DEM. Rossebø et al. (2005) have observed that Gassmann overestimates fluid effect for low porosities, and underestimates it for high porosities. In addition, Gassmann may give too low saturated velocities for rocks containing cracks or fractures, due to the assumptions of connected pore space, and pressure equalization for seismic frequencies (Shiyu and Payne, 2009).

Although validity of Gassmann calculations for carbonates has been debated, Rasolofosaon et al. (2008) suggests that it may be measuring techniques rather than Gassmann calculations which give erroneous values, and Adam et al. (2005) have observed that when including uncertainties for measurements, Gassmann predicted values fall within the confidence interval of the experimental data. Thus, it is hard to estimate how close to reality velocities calculated in this project are. However, even though the calculation methods probably do not give the exact correct velocities, the deviations may not be significant. In addition, fluids are seen to not be the major velocity determent factor in carbonates. Pore forms, which have been showed by many authors to be of great importance for carbonate velocities, have been defined prior to calculations, so that the effects of these are incorporated in calculated velocities by DEM.

Although the calculation methods may not fully predict elastic behavior of all

rock systems, the overall resulting trends in this project have mostly been seen to coincide with well-known geological and seismic relations, and trends observed by other authors. Thus, it is reasonable to believe that the results obtained are reliable.

7.3 Further work

Although seismic effects of various rock properties have been examined in this study, there are still many more aspects that could be investigated. The difficulties for predicting depth effects have been discussed, so this issue would certainly be of interest to investigate further. Thus, further work could include an investigation of real data from various depths. Thin sections would reveal pore shapes, mineralogy and information about cementation, while porosities, densities and velocities could be measured. With such data at hand, an aim could be a quantification of general trends in order to improve predicting results for rock physics modeling.

Another topic to further investigate could be diagenetic processes, due to their significance for carbonates. Cement effects other than porosity reduction have not been considered in this study, and could be interesting to study in depth, since both cement type and site in the pore space can affect elastic behavior of rocks.

In addition, an evaluation of DEM and Gassmann validity for fluid effects could be performed related to real data, and fluid-matrix interactions, and consequent fluid effect on shear modulus, would certainly be an interesting topic.

Chapter 8: Conclusions

Carbonate geology

- Carbonates are complex rocks which can have a great range of properties due to the variations in formation processes, and later rock-affecting processes, especially diagenesis.
- These rocks may be good reservoirs, or they can form source rock or seal.
- Mineralogy variations in carbonates are small since only three carbonate minerals exist.
- Porosity variations can have a wide ranges, and show little correlation with depth.
- Various pore shapes can be formed in carbonates.

Porosity and pore shape effects

- Porosity has great impact on seismic velocities, and a general observation is that increasing porosity reduces velocities and the V_p/V_s ratio.
- Pore shape effects have been observed to be of almost equal importance as porosity for velocities. Pores of lower aspect ratios are less rigid and easier to deform than pores of higher aspect ratios, and thus reduce velocities. V_p/V_s ratio is seen to be high for spherical pores, and low for pores of aspect ratio 0.1. However, small fractions of pores with aspect ratios 0.001 increase the velocity ratio.
- Differentiation of porosity and pore shape effects on seismic responses is seen to be difficult, which makes this a non-uniqueness problem when revealing pore volume and texture properties from seismic data.

Depth effects

- Depth effects are not straightforward to model for carbonates, due to diagenetic processes. As a general case, velocities and velocity ratio are seen to increase as burial depth increases, due to mechanical and diagenetic compaction, which reduces porosity. However, great deviations from this trend could occur due to diagenetic processes as cementation and dissolution.

- Modeled results of closing of cracks as a consequence of increasing mechanical compaction have revealed increasing velocities.
- Overpressure can result in elevated porosities due to trapping of incompressible fluids. High pore pressure may in addition inhibit cementation. This situation has been showed to lower seismic velocities.
- Simulation of increasing pore pressure by accordingly alter pore fluid effects, is seen to have little impact on velocities.

Mineralogy effects

- Variations of amounts of calcite, dolomite, and/or aragonite in a carbonate matrix, have been showed to be of minor significance for velocities.
- Fractions of quartz were observed to have negligible effects on velocities, while introducing small amounts of clay in the matrix composition clearly reduced velocities and V_p/V_s ratio.
- Dolomitization may increase or reduce velocities, thus this process can affect velocities significantly. On the other hand, since adding dolomite to a calcite composition slightly increases velocities, while increasing porosity decreases velocities, these two factors can counteract each other and show little effect on velocities.
- Dolomite and porosity effects are observed to have opposing trends in a rock physics template. While V_p/V_s ratio was observed to decrease for both increasing dolomite content and porosity, increasing porosity caused a lowering in acoustic impedance, while the opposite was the case for increasing dolomite content.

Fluid effects

- Gas saturation reduces velocities and results in considerable reduction in V_p/V_s ratio compared to rocks saturated with brine.
- Brine and oil produce comparable velocities and V_p/V_s ratios, although slightly lower for oil.

Differentiation of effects of various factors

- It has been observed that various rock property affecting factors produce distinctive trends in a rock physics template.
- AVO responses for carbonate-carbonate interfaces can fall into all four AVO classes.
- Although variations of porosity, pore shapes, and mineralogy can change the AVO class, the results for such variations in a gradient versus intercept plot are shown to follow a trend line, while variations in saturation fluid plot outside this line.

References

Adam, L., and Batzle, M., 2008. Elastic properties of carbonates from laboratory measurements at seismic and ultrasonic frequencies. The Leading Edge, Vol. 27, No. 8, p. 1026-1032.

Adam, L., Batzle M., and Brevik, I., 2005. Gassmann's fluid substitution paradox on carbonates: seismic and ultrasonic frequencies. Society of Exploration Geophysicists Expanded Abstracts, Vol. 24, p. 1521-1524.

Anselmetti, F. S., and Eberli, G. P., 1993. Controls on sonic velocity in carbonates. Pure and Applied Geophysics, Vol. 141, No. 2-4, p. 287-323.

Anselmetti, F.S., and Eberli, G. P., 1997. Sonic velocity in carbonate sediments and rocks, in Palaz, I. and Marfurt, K. J., eds., Carbonate seismology, Society of Exploration Geophysicists: Geophysical developments series, Vol. 6, p. 53-74.

Batzle, M., and Wang, Z., 1992. Seismic properties of pore fluids. Geophysics, Vol. 57, No. 11, p. 1396-1408.

Boggs Jr., S., 2006. Principles of sedimentology and stratigraphy 4th ed. Pearson Prentice Hall, 662 p.

Bourbié, T., Coussy, O., and Zinszner, B., 1987, Acoustique des Milieux Poreu. Gulf Publishing Company. 334 p.

Box, R., and Doss, E., 2008. Typical AVO response as a function of depth and fluid pressure gradient: Gulf of Mexico shelf. The Leading Edge, Vol. 27, No. 10, p. 1252-1262.

Bruce, B., and Bowers, G., 2002. Pore pressure terminology. The leading Edge, Vol. 21, No. 2, p. 170-173.

Castagna, J. P., and Swan, H. W., 1997. Principles of AVO crossplotting. The Leading Edge, Vol. 16, No. 4, p. 337-344.

Choquette, P. W., Pray, L. C., 1970. Geologic nomenclature and classification of porosity in Sedimentary carbonates. American Association of Petroleum Geologists Bulletin, Vol. 54, No. 2, p. 207-250.

Conybeare, D. M., and Shaw, H. F., 2000. Fracturing, overpressure release and carbonate cementation in the Everest Complex, North Sea. Clay Minerals, Vol. 35, No. 1, p. 135-149.

CREWES, Zoeppritz explorer applet, 2009. www.crewes.org/ResearchLinks/ExplorerPrograms/ZE/ZEcrewes [accessed: 20th of May, 2009].

Davies, G.R., Smith Jr., L.B., 2006. Structurally controlled hydrothermal dolomite reservoir facies: an overview. American Association of Petroleum Geologists Bulletin, Vol. 90, No. 11, p. 1641-1690.

Droste, H., Van Steenwinkel, M., 2004. Stratal geometries and patterns of platform carbonates: the Cretaceous of Oman, in Eberli, G. P., Masaferro, J. L., and Sarg, J. F., (eds.), Seismic imaging of carbonate reservoirs and systems: American Association of Petroleum Geologists Memoir Vol. 81, p. 185-206.

Dunham, R. J., 1962. Classification of carbonate rocks according to depositional texture, in Ham, W. E. (ed.), Classification of carbonate rocks. American Association of Petroleum Geologists Memoir 1, p. 108-121.

Dvorkin J. P., 2008. Yet another *Vs* equation. Society of Exploration Geophysicists Expanded Abstracts 26, Vol. 26, p.1570-1574.

Eberli, G. P., Baechle, G. T., Anselmetti, F. S., and Incze, M. L., 2003. Factors controlling elastic properties in carbonate sediments and rocks. The Leading Edge, Vol. 22, No. 7, p. 654-660.

Eissa, M. A., Castagna, J. P., and Alan L., 2003. AVO detection of gas-producing dolomite trends in nonproducing limestone. The Leading Edge, Vol. 22, No. 5, p. 462-468.

Embry, A. F., and Klovan, J. E., 1971. A late Devonian reef tract on northeastern Banks Island Northwest Territories. Canadian Petroleum Geologists Bulletin, Vol. 19, p. 730-781.

Fischer, K. C., Möller, U., and Marschall, R., 1997. Development of an exploration concept for the Shuaiba Formation using seismic sequence and facies analysis with forward modeling, in Palaz, I., Marfurt, K.J. (eds.), Carbonate Seismology, Society of Exploration Geophysicists: Geophysical developments series, Vol. 6, p. 407-416.

Folk, R. L., 1959**.** Practical petrographic classification of limestones. American Association of Petroleum Geologists Bulletin, Vol. 43, p. 1-38.

Folk, R. L., 1962. Spectral subdivision of limestone types, in Ham, W. E. (ed.), Classification of Carbonate Rocks. American Association of Petroleum Geologists Memoir 1, p. 62-85.

Folk, R. L., 1965. Some aspects of recrystallization in ancient limestones, in Pray, L. C., and Murray, R. S. (eds.), Dolomoitization and limestone diagenesis. SEPM Special Publication No. 13, p. 14-48.

Foster, D. J, Keys, R. G., and Reilly, J. M., 1997. Another perspective on AVO crossplotting. The Leading Edge, Vol. 16, No. 9, p. 1233-1239.

Gassmann, F., 1951. Elastic waves through a packing of spheres. Geophysics, Vol. 16, No. 4, p. 673-685.

Gelfand, V., Ng, P., Nguyen, H., and Larner, K., 1986. Seismic lithologic modeling of amplitude-versus-offset data. Society of Exploration Geophysicists Expanded Abstracts, Vol. 5, p. 334-337.

Gelius, L. J., and Johansen, T. A., 2007. Rock physics of porous materials. GeoCLASS. www.learninggeo.com [accessed: 10th of December, 2007]

Gomez, J. P., Rai, C. S. and Sondergeld, C. H., 2007. Effect of microstructure and pore fluid on the elastic properties of carbonates. Society of Exploration Geophysicists Expanded Abstracts, Vol. 26, p. 1565-1569.

Guéguen, Y., and Palciauskas, V., 1994. Introduction to the physics of rocks. Princeton UniversityPress, 392 p.

Guéguen, Y., Sarout, J., Fortinn, J., and Schubnel, A., 2009. Cracks in porous rocks: tiny defects, strong effects. The Leading Edge, Vol. 28, No. 1, p. 40-47.

Han, D.-H., 1986. Effects of porosity and clay content on acoustic properties of sandstones and unconsolidated sediments. Ph. D. thesis, Stanford University.

Hill, R., 1952. The elastic behavior of a crystalline aggregate. Proceedings of the Physical Society, Section A, Vol. 65, No. 5, p. 349-354.

James, R., 2005. Marine biogeochemical cycles 2nd ed., in Bearman, G. (ed.), S330 Oceanography, Vol. 5, Butterworth-Heinemann, 130 p.

Kearey, P., Brooks, M., and Hill, I., 2002. An introduction to geophysical exploration, 3rd ed. Blackwell Publishing, 262 p.

Kitamura, K., Takahashi, M., Masuda, K., Ito, H., Song, S., and Wang, C., 2005. The relationship between pore-pressure and the elastic-wave velocities of TCDP-cores. American Geophysical Union, Fall Meeting 2005, abstract No. T51A-1326.

Kumar, M., and Han, D., 2005. Pore shape effect on elastic properties of carbonate rocks. Society of Exploration Geophysicists Technical Program Expanded Abstracts, p. 1477-1480.

Kuster, G. T., and Toksöz, M. N., 1974. Velocity and attenuation of seismic waves in two-phase media: Part I. Theoretical Formulations. Geophysics, Vol. 39, No. 5, p. 587-606.

Li, Y., Downton, J., and Goodway, B., 2003. Recent applications of AVO to carbonate reservoirs in the Western Canadian Sedimentary Basin. The Leading Edge, Vol. 22, No. 7, p. 670-674.

Lucia, F. J., and Major, R. P., 1993. Is dolomitization a porosity-generating or a porosity-destroying diagenetic process? (abs.): American Association of Petroleum Geologists 1993 Annual Convention Program, p. 141.

Marion, D., and Jizba, D., 1997. Acoustic properties of carbonate rocks: use in quantitative interpretation of sonic and seismic measurements, in Palaz, I. and Marfurt, K. J., (eds.), Carbonate seismology, Society of Exploration Geophysicists: Geophysical developments series, Vol. 6, p. 75-94.

Mavko, G., Mukerji, T., and Dvorkin, J., 1998. The rock physics handbook: tools for seismic analysis in porous media. Cambridge University Press, 329 p.

Mjelde, R., 2009. Seismic acquisition: Geophysical principles. www.learninggeoscience.net [accessed: 25th of March, 2009].

Moore, C. H., 1989. Carbonate diagenesis and porosity. Developments in Sedimentology, Vol. 46, Elsevier, 338 p.

Palaz, I., and Marfurt, K. J., 1997. Carbonate seismology: an overview, in Palaz, I., Marfurt, K.J. (eds.), Carbonate Seismology, Society of Exploration Geophysicists: Geophysical developments series, Vol. 6, p. 1-7.

Rafavich, F., Kendall, C. H. St. C., and Todd, T. P., 1984. The relationship between acoustic properties and the petrographic character of carbonate rocks. Geophysics, Vol. 49, No. 10, p. 1622-1636.

Rasolofosaon, P., Lucet, N., Zinszner, B., 2008. Petroacoustics of carbonate reservoir rocks. The Leading Edge, Vol. 27, No. 8, p. 1034-1039.

Reuss, A., 1929. Berechnung der Fliessgrenzen von Mischkristallen auf Grund der Plastizitätsbedingung für Einkristalle. Zeitschrift für Angewandte Mathematik und Mechanik, Vol. 9, p. 49-58.

Rossebø, Ø. H., Brevik, I., Ahmadi, G., R., and Adam, L., 2005. Modeling of acoustic properties in carbonate rocks. Society of Exploration Geophysicists Technical Program Expanded Abstracts, Vol. 24, No. 1, p. 1505-1508.

Rutherford, S. R, and Williams, R. H., 1989. Amplitude-versus-offset variations in gas sands. Geophysics, Vol. 54, No. 6, p. 680-688.

Sayers, C. M., 2008. The Elastic Properties of Carbonates. The Leading Edge, Vol. 27, No. 8, p. 1020-1024.

Schlager, W., 1992. Sedimentology and sequence stratigraphy of reefs and carbonate platforms. The American Association of Petroleum Geologists Continuing education course notes Vol. 34, 71 p.

Schmoker, J. W., and Halley, R. B., 1982. Carbonate porosity versus depth: a predictable relation for South Florida. The American Association of Petroleum Geologists Bulletin, V. 66, No. 12, p. 2561-2570.

Scholle, P. A., 1978. A color illustrated guide to carbonate rock constituents, textures, cements, and porosities. The American Association of Petroleum Geologists Memoir 27, 241 p.

Selley, R. C., 1998. Elements of petroleum geology 2nd ed. Academic Press, 470 p.

Sheriff, R.E., 1989. Geophysical methods. Prentice Hall, 605 p.

Sheriff, R.E., 1991. Encyclopedic dictionary of exploration geophysics, 3rd ed. Society of Exploration Geophysicists, 384 p.

Shiyu, X., and Payne, M. A., 2009. Modeling elastic properties in carbonate rocks. The Leading Edge, Vol. 28, No. 1, p. 66-74.

Soltveit, K., 2007. Geological and seismic characterization of Miocene temperate Carbonates, Moratalla, S-E Spain. M. Sc. Thesis, Department of Earth Science. Bergen, University of Bergen. 118 p.

Stanley, S. M., 2005. Earth system history 2nd ed. W. H. Freeman, 567 p.

Sun, Y. F., 2004. Pore structure effects on elastic wave propagation in rocks: AVO modeling. Journal of Geophysics and Engineering, Vol. 1, No. 4, p. 268–276.

Tatham, R. H., 1982. V_p/V_s and lithology. Geophysics, Vol. 47, No. 3, p. 336-344.

Teige, G. M. G., Hermanrud, C., Wensaas, L., and Nordgård Bolås, H. M., 1999. The lack of relationship between overpressure and porosity in North Sea and Haltenbanken shales. Marine and Petroleum Geology, Vol. 16, No. 4, p. 321-335.

Tucker, M. E., Wright V. P., 1990. Carbonate sedimentology. Blackwell Scientific Publications, 482 p.

Walsh, J. B., 1965. The effect of cracks on the compressibility of rocks. Journal of Geophysical Research, Vol. 70, p. 381-89.

Wang, Z., 1997. Seismic properties of carbonate rocks, in Palaz, I., Marfurt, K.J. (eds.), Carbonate Seismology, Society of Exploration Geophysicists: Geophysical developments series, Vol. 6, p. 29-52.

Wilson, J. L., 1975. Carbonate facies in geologic history. Springer-Verlag, Berlin, 471 p.

Wilson, J. L., 1997. Carbonate depositional environments and diagenesis, in Palaz, I., Marfurt, K. J. (eds.), Carbonate seismology, Society of Exploration Geophysicists: Geophysical developments series, Vol. 6, p. 9-28.

Wood, A. W., 1955. A textbook of sound. The MacMillan Co., 360 p.

Wyllie, M. R. J., Gregory, A. R., and Gardner, G. H. F., 1958. An experimental investigation of factors affecting elastic wave velocities in porous media. Geophysics, Vol. 23, No. 3, p. 459-493.

Ødegaard, E., and Avseth, P., 2004. Well log and seismic data analysis using rock physics templates. First Break, Vol. 23, No. 10, p. 37-43.

Apendix

Kuster-Toksöz Model:

Definitions of tensor components T_{ijij} and T_{ijij} in equations 3.27 and 3.28:

$$T_{iijj} = \frac{3F_1}{F_2}, \tag{1}$$

and

$$T_{ijij} - \frac{1}{3}T_{iijj} = \frac{2}{F_3} + \frac{1}{F_4} + \frac{F_4F_5 + F_6F_7 - F_8F_9}{F_2F_4}\ , \tag{2}$$

where

$$F_1 = 1 - \left[\frac{3}{2}(g+\theta) - R\left(\frac{3}{2}g + \frac{5}{2}\theta - \frac{4}{3}\right)\right], \tag{3}$$

$$F_2 = 1 - \left[\frac{3}{2}(g+\theta) - R\left(\frac{3}{2}g + \frac{5}{2}\theta - \frac{4}{3}\right)\right]$$
$$-\tfrac{1}{2}(3B-1)(3-4R)[g+\theta - R(g-\theta+2\theta^2)]\ , \tag{4}$$

$$F_3 = 1 - \frac{1}{2}\left[R(2-\theta) + \frac{1+\alpha^2}{\alpha^2}g(R-1)\right]\ , \tag{5}$$

$$F_4 = 1 - \frac{1}{4}[3\theta + g - R(g-\theta)]\ , \tag{6}$$

$$F_5 = B\theta(3-4R) - R\left(g+\theta-\frac{4}{3}\right) + g\ , \tag{7}$$

$$F_6 = B(1-\theta)(3-4R) - g + R(g+\theta)\ , \tag{8}$$

$$F_7 = 2 - \frac{1}{4}[9\theta + 3g - R(5\theta+3g)] + B\theta(3-4R)\ , \tag{9}$$

$$F_8 = B(1-\theta)(3-4R) - 1 + 2R - \frac{g}{2}(R-1) - \frac{\theta}{2}(5R-3)\,, \tag{10}$$

$$F_9 = B\theta(3-4R) - g(R-1) + R\theta\,, \tag{11}$$

where

$$B = \frac{K_f}{3K_m}\,, \tag{12}$$

$$R = \frac{3\mu_m}{3K_m + 4\mu_m} = \left(\frac{V_s}{V_p}\right)_m^2\,, \tag{13}$$

$$g = \frac{\alpha^2}{1-\alpha^2}(3\theta - 2)\,, \tag{14}$$

$$\theta = \frac{\alpha}{(1-\alpha^2)^{3/2}}\left[cos^{-1}\alpha - \alpha(1-\alpha^2)^{1/2}\right], \tag{15}$$

Zoeppritz equations:

PP-reflection coefficient:

$$R_{pp} = \left[\left(b\frac{cos\theta_1}{V_{p1}} - c\frac{cos\theta_2}{V_{p2}}\right)F - \left(a + d\frac{cos\theta_1}{V_{p1}}\frac{cos\varphi_2}{V_{s2}}\right)Hp^2\right]/D\,, \tag{16}$$

where θ and φ are incident angles for P- and S-waves, respectively, and indexes 1 and 2 refers to properties for upper and lower layer, respectively, and

$$a = \rho_2(1 - 2V_{s2}^2p^2) - \rho_1(1 - 2V_{s1}^2p^2)\,, \tag{17}$$

$$b = \rho_2(1 - 2V_{s2}^2p^2) + 2\rho_1V_{s1}^2p^2\,, \tag{18}$$

$$c = \rho_1(1 - 2V_{s1}^2p^2) + 2\rho_2V_{s2}^2p^2\,, \tag{19}$$

$$d = 2(\rho_2 V_{s2}^2 - \rho_1 V_{s1}^2)\,, \tag{20}$$

$$F = b\frac{cos\varphi_1}{V_{s1}} + c\frac{cos\varphi_2}{V_{s2}}\,, \tag{21}$$

$$H = a - d\frac{cos\theta_2}{V_{p2}}\frac{cos\varphi_1}{V_{s1}}\,, \tag{22}$$

$$D = EF + GHp^2\,, \tag{23}$$

$$E = b\frac{cos\theta_1}{V_{p1}} + c\frac{cos\theta_2}{V_{p2}}\,, \tag{24}$$

$$G = a - d\frac{cos\theta_1}{V_{p1}}\frac{cos\varphi_2}{V_{s2}}\,, \tag{25}$$

where

$$p = \frac{sin\theta_1}{V_{p1}} = \frac{sin\theta_2}{V_{p2}} = \frac{sin\varphi_1}{V_{s1}} = \frac{sin\varphi_2}{V_{s2}}\,, \tag{26}$$

Original values from Soltveit (2007) and Droste and Van Steenwinkel (2004):

Table 1 *Facies 1, 3, and 5 (Droste and Van Steenwinkel, 2004) are saturated, while facies 2 and 4 (Soltveit, 2007).*

	1	2*	3	4*	5
V_p (m/s)	5166	4146.2	3615	3658.0	4997
V_s (m/s)	2677	2518.0	1903	2388.8	
ρ (kg/m^3)	2650	2223.7	2450	2334.1	2475
φ (%)	5.5	17.7	21.5	12.9	9.0